DEVELOPMENT OF THE MMS DREDGE PLUME MODEL

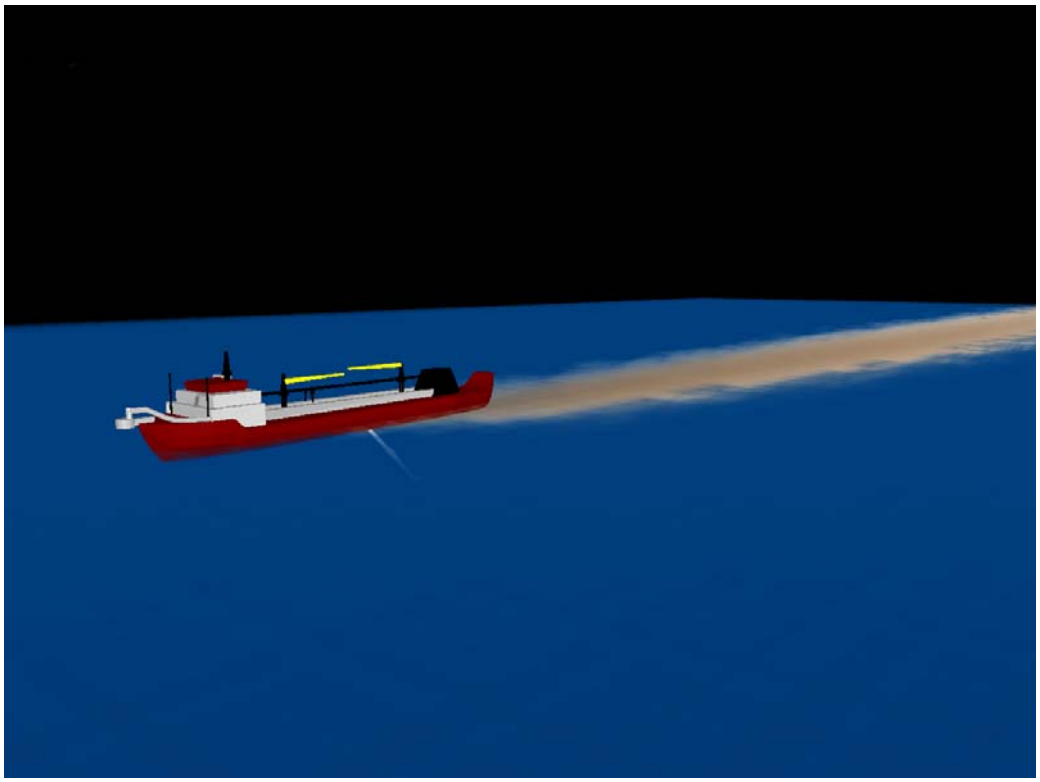

PREPARED FOR:
U.S. DEPARTMENT OF THE INTERIOR
MINERALS MANAGEMENT SERVICE
Under Contract Number No. 01-01-CT-31127

MMS U.S. Department of the Interior
Minerals Management Service

March 2004

DEVELOPMENT OF THE MMS DREDGE PLUME MODEL

Prepared for:

Leasing Division, Sand and Gravel Unit
Minerals Management Service
U.S. Department of Interior
Herndon, Virginia

Prepared by:

W.F. Baird & Associates Ltd.
Madison, Wisconsin

March 2004

DISCLAIMER

This report has been reviewed by the Minerals Management Service and approved for publication. Approval does not signify that the contents necessarily reflect the views and policies of the Service, nor does mention of trade names or commercial products constitute endorsement or recommendation for use.

TABLE OF CONTENTS

LIST OF FIGURES

LIST OF FIGURES (cont'd)

LIST OF TABLES

ACKNOWLEDGEMENTS

This report was prepared under contract to the Sand and Gravel Unit, Leasing Division, Minerals Management Service, Contract No. 01-02-CT-85139. Barry Drucker was the MMS Project Manager and contributed significantly to the project objectives and the overall success of the project. Dr. Rob Nairn of Baird and Associates was the Project Manager. The senior authors were Douglas Scott and Michael Fullarton of Baird & Associates, Jeremy Spearman of HR Wallingford and Nick Bray of Dredging Research Ltd.

1.0 INTRODUCTION

1.1 Project Background

The U.S. Minerals Management Service (MMS) Leasing Division has the responsibility for administering the Department of the Interior's role in mineral resource development other than oil, gas, and sulfur on the U.S. outer continental shelf (OCS). MMS does not develop and maintain a schedule of lease offering for OCS sand resources. Rather, the leasing process for OCS sand must begin by a request from potential users of the sand. Only recently have OCS sand resources been considered as feasible sources of sand for beach nourishment. Between 1995 and 2001, MMS conveyed 14,600,000 cubic yards of OCS sand for ten projects.

MMS expects that the OCS sand resources will be long-term sources of sand borrow material for coastal erosion management because of:

- The general diminishing supply of onshore and nearshore sand;
- Impact of sea level rise and other natural and human-induced factors leading to increased erosion;
- The renourishment cycles for beaches or coastal areas requiring quantities of sand not currently available from State sources; and
- Immediate/emergency repair of beaches and coastal damage from severe coastal storms.

MMS has responsibility for providing environmental analysis and assessment information enabling the responsible management of the OSC sand resources. There is a range of environmental concerns, including both direct and indirect impacts with the dredging operations necessary for sand borrow extraction. One primary concern is the direct impact of the suspended sediment plume and related bed sedimentation generated by dredging operations on the physical and biological environments.

This project has focused on the development of a comprehensive tool, known as the MMS Dredge Plume Model, to numerically simulate the plume created by a Trailing Suction Hopper Dredge (TSHD). The modeling system that was created has a number of advanced features, making it unique among the models of its type.

1.2 Study Objectives

Specific objectives of this project included:

- The development, testing and delivery of a numerical model, which can be used to predict plume and sedimentation characteristics, associated with both the overspill and draghead sediment sources developed in dredging operations. The target vessel was a Trailing Suction Hopper Dredge.

- The development of software tools to facilitate the use of the model and the interpretation of the modeling results.

- The completion of sensitivity testing to assess the plume model performance.

- Validation against an available dataset from an actual dredging operation.

The ultimate goal of the MMS program is to develop a tool to assess the sedimentation footprint generated by possible future dredging operations at the sand borrow areas in the OCS.

1.3 Study Documents

This report provides a summary of the technical characteristics of the MMS Plume Model, the sensitivity testing program and the model validation studies. A companion MMS Plume Model User's Guide provides detailed information on setup and use of the modeling system. As well, a User's Guide to the Plume Animator 3D visualization tool has been provided.

1.4 Team Organization

The project team was comprised of the following members with the identified responsibilities:

Rob Nairn, Ph.D., P.Eng. Baird & Associates – Project Manager

W.F. Baird & Associates Ltd. ("Baird")
Rob Nairn, Ph.D., P.Eng. – Sediment Dynamics
R. Douglas Scott, Ph.D., P.Eng. – Oceanographer and Hydrodynamic Modeling
Qimiao Lu, Ph.D. – Sediment Dynamics and Model Developer
Stephen Langendyk – GIS Expertise
Tim Kenny, P.E. – Dredging Specialist

H.R. Wallingford Ltd.
T. Neville Burt, B.Sc., C.Eng. – Dredging and Siltation Expertise
Mike Dearnaley, Ph.D. – Dredge Plume and Siltation Modeling
Jeremy Spearman, Ph.D. – Plume Dispersion Modeling

Dredging Research Ltd. ("DRL")
R. Nick Bray, B.A. – Dredging Specialist
John Land, B.Sc., C.Eng. – Dredging Specialist

Coastline Surveys Ltd.
David Hitchcock, Ph.D. – Dredge Monitoring Specialist

Marine Ecological Surveys Ltd.
Richard Newell, Ph.D. – Marine Ecologist

2.0 OVERVIEW OF TRAILER DREDGE PLUME BEHAVIOUR

2.1 Introduction

This section of the report provides an overview as to the nature of plumes caused by dredging operations. When such operations release sediments into ambient waters, there are two main phases:

- A *Dynamic* phase in which the plume behavior is determined largely by the nature and concentration of the overspill sediments and their release mechanisms.

- A *Passive* phase in which the plume transport is controlled by the ambient currents.

The characteristics of each phase are summarized below along with a discussion of the various sources of sediments present in dredging operations.

2.2 Sources of Sediment in TSHD Operations

There are various sources for sediment release and plume creation during trailing suction hopper dredge operations, such as:

- Draghead disturbance. TSHD's pump sediments into their hoppers by means of suction pipes lowered to the seabed. At the bottom end of the suction pipe is a draghead designed to maximize the concentration of sediments in the pump mixture. The disturbance created by the draghead can induce sediment re-suspension and plume development.

- Discharge of Overflow. Some of the sediments pumped into the hopper settle out of suspension, while the remaining sediments, generally composed of fine sands and silts, are discharged through one or more spillways. When sand is dredged, the spillways are used to "densify" the hopper load by replacing water with sand materials.

- Screening Discharge. Oversize or undersize screening can be used in aggregate dredging when only a particular size fraction range of material is desired. The reject material is discharged from the vessel.

2.3 Dynamic Phase

During trailer suction hopper dredging operations material is disturbed and introduced into the water via spillways, as water is displaced from the hopper, or via aggregate dredger screening chutes. The introduction of this sediment, which can have significant initial momentum, into the water column results in a body of water, denser

than the surrounding water, which descends towards to the seabed. This initial rapid descent of the plume is referred to as the *dynamic phase* of plume dispersion and the plume is referred to as the *dynamic plume*.

As the dynamic plume descends, ambient water is entrained into the plume, diluting the plume and slowing its downward descent. A proportion of the sediment may be "stripped" from the plume into the surrounding water column to form a passive plume while the remainder of the released material impacts upon the bed as a *density current*. Some material may be re-suspended into the water column as a result of the impact, while the rest of the material moves radially outwards across the seabed as a dense pancake-like plume, slowing with time. During this radial expansion settling of sediment occurs from the density current onto the bed. Initially, the mixing that occurs between the density current and the ambient waters is limited. However, when the concentration and thickness of the density current are sufficiently low, and if the ambient currents are sufficiently high, then significant mixing occurs and sediment is released into the water column to form a passive plume (Figure 1).

Under conditions which are sufficiently stratified, it is possible for the dynamic plume never to reach the bed. Under these conditions the dynamic plume converges on a position of neutral buoyancy and experiences internal or *dynamic* collapse pancaking outward as a density current in a similar fashion to that resulting from impact on the bed.

The zone of influence of the dynamic plume, i.e. the (moving) zone behind the dredger where the plume experiences the descent and collapse of the dynamic plume phase, can vary considerably depending on the magnitude (and direction) of the current flow, the speed of the dredger, the initial density of the sediment/water mixture (relative to the ambient waters) and the initial momentum of the mixture. The shape of this zone tends to be a long, thin corridor, and may extend over an area up to a few hundred meters wide and a few meters km long. The suspended sediment concentration within the dynamic plume is higher than that of the passive plume and can be of the order of tens of thousands of milligrams per liter near the dredger, reducing to tens or hundreds of milligrams per liter (above background) at the "downstream" extremity of the zone.

2.4 Passive Phase

Material stripped from the plume into the water column during the rapid descent of material, or as a result of the impact of the dynamic plume on the bed, or subsequently during the flow of material along the bed, will form a passive plume of material that will slowly disperse with the mixing effects of currents and waves. This effect, together with the settling of sediment particles, will reduce the concentration of the passive plume over time.

There are two main mechanisms whereby this occurs.

- *Turbulent diffusion*, the small-scale temporal and spatial variations in current flow

- *Shear dispersion*, the effect of different current velocities through the water column, which results in particles at different heights traveling in different directions and at different speeds, thus spreading the plume. This effect is much larger than turbulent diffusion except in quiescent waters.

The zone of influence of the passive plume can be very large, several kilometers or more, and is dependent on the magnitude of tidal currents and the magnitude of the sediment releases arising from the dredging operation. Suspended sediment concentrations within the plume can be in the order of hundreds of milligrams per liter (above background) in the vicinity of the dredger, reducing to tens of milligrams per liter (above background) with distance from the dredger.

2.5 Bed Re-suspension Phase

Dredge plume sediments deposited on the seabed may become re-suspended if the ambient currents exceed thresholds for sediment erosion. Thus, these sediments can become even further dispersed in time through the actions of tides, wind and waves.

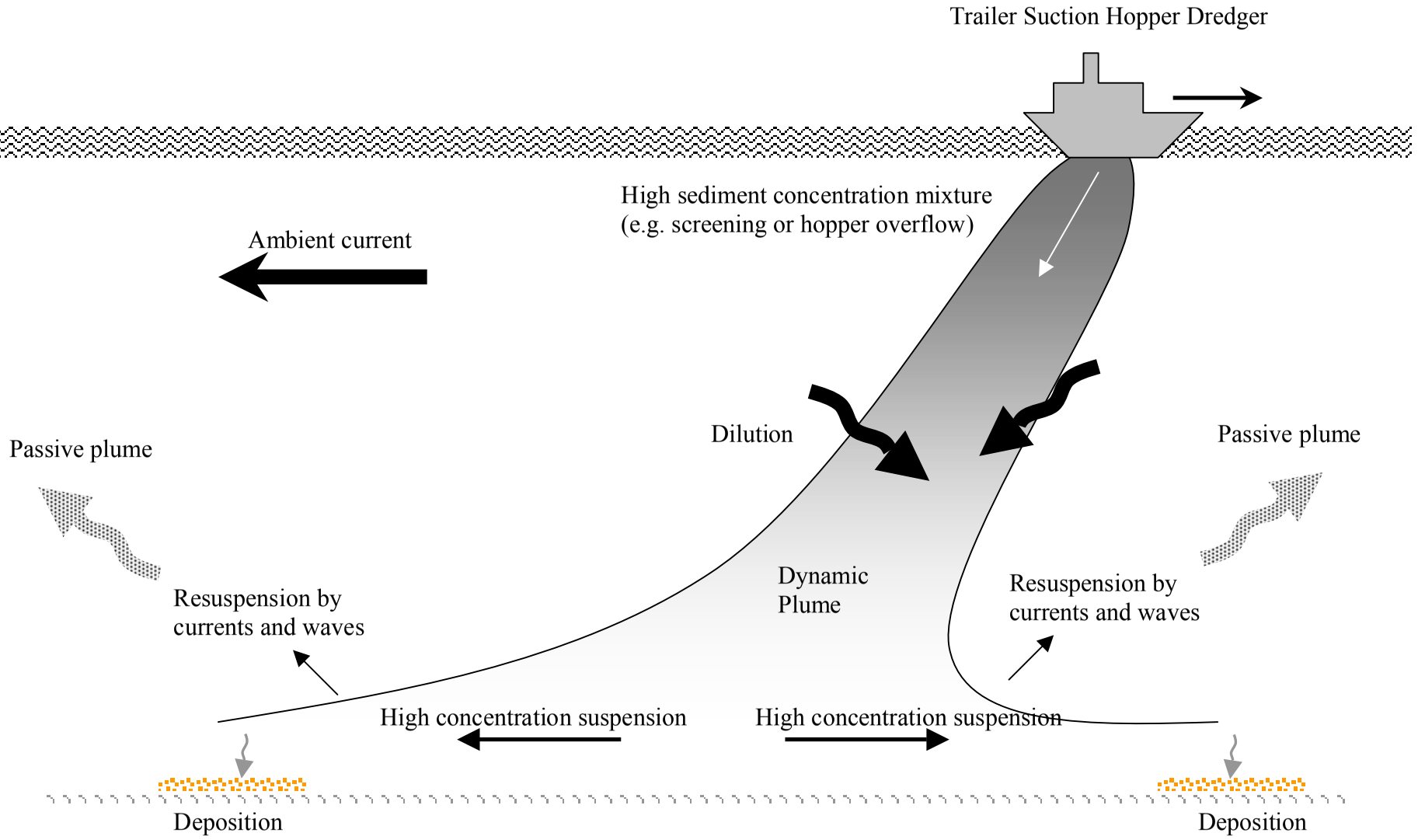

FIGURE 1. Overview of Dredge Sedimentation Processes

3.0 THE DREDGER PROCESS MODEL

3.1 Introduction

The dredger process model simulates the behavior of the various TSHD operations, and estimates the various releases and sediment disturbances that can arise from these operations.

3.2 Logic Basis for Model

The trailing suction hopper dredger is considered as having four components, which may contribute to suspension of sediment. These are:

1) Discharge of overflow water;

2) Discharge from the oversize screen;

3) Discharge from the undersize screen;

4) Draghead disturbance.

These four components are built into the model and can be turned on or off, according to the requirements of the operator.

All of the above-mentioned effects are also related to the loading cycle of the dredger, since the loading period is necessary for plume modeling and the loading rate determines the time when loading is completed. In addition, in deep water, when inboard pumps are being used, the loading rate will be affected by the immersed depth of the pumps, which in turn is determined by the laden draft of the vessel. In addition, the trailer is a self-propelled dredger and operates over a significant length of the site. Any output from the trailer process model must be input to the dynamic plume model at the correct location. A further complication is that the dredging is discontinuous, because the dredger must travel to the discharge point to unload its cargo and return to the dredging site. The point at which loading ceases and travel to the disposal point commences is determined by the loading rate and the overall cycle time. It is, therefore, necessary to examine the trailer dredging operation as a whole, rather than a number of isolated processes.

For the purposes of the current model, the movement of the vessel over the seabed and its effect on the location of any discharge does not affect the process model. However, it does affect the plume model and is taken into account in the interface between the process model and the dynamic plume model.

The processes are examined in detail below.

3.3 Overflow Discharge

Although overflow does not occur until the dredged mixture in the hopper reaches the pre-set weir level, the behavior of the material dredged prior to overflow is of significance. Fine material entering the hopper during this period may not settle in the hopper and may, thus, be available for overflowing during the subsequent part of the cycle. How much of the fine material settles and how much remains in suspension in the supernatant water (the water above the sediment) is not clearly understood. This is an area that appears to require more research. For the purposes of the current model, the operator enters an assumed percentage of this material that will be discharged in the overflow. The quantity of solids relating to this percentage is then computed during the non-overflow period. This material is then discharged during overflow at a rate proportional to the volume of the supernatant water remaining in the hopper.

The procedure adopted by the model prior to overflow is as follows:

The number of one-minute steps between turns, t_r, are computed:

$$t_r = \frac{3.222 \times 10^{-2} \times l}{K} \tag{3.1}$$

where K is the trailing speed in knots; and l is the length of trail run in meters.

The flow into the hopper, Q, in m^3/min is a function of the number of suction pipes, S; the diameter of the suction pipes, D_s; and the velocity in the suction pipes, v_s, as follows:

$$Q = 47.124 \times D_s^2 \times v_s \times S \tag{3.2}$$

The mixture concentration, C_v, is given by:

$$C_v = \frac{(\gamma_m - \gamma_w)}{(\gamma_s - \gamma_w)} \tag{3.3}$$

based on γ_w, γ_s, and γ_m, the density of water, solids and the mixture, respectively.

The time until overflow, t_0, is given by:

$$t_o = \frac{(V_h - V_p)}{Q} \tag{3.4}$$

where V_h is the hopper capacity in m^3 and V_p is the pre-load volume of water in the hopper in m^3.

The weight of solids entering the hopper per minute, W_m, is computed from:

$$W_m = \frac{Q \times \gamma_s \times (\gamma_m - \gamma_w)}{(\gamma_s - \gamma_w)} \qquad (3.5)$$

Then, the total weight of solids in the hopper at the point of overflow, W_o, is given by:

$$W_o = t_o \times W_m \qquad (3.6)$$

Most of this stays in the hopper but the proportion smaller than 20 microns stays in suspension and is available for release when overflowing begins.

When overflowing commences, the hopper acts as a settling tank. The settlement process is described in Vlasblom and Miedema (1995) and relies generally on the Camp model, with a few modifications to take account of hindered settling, scouring as the load increases and the effects of the Constant Tonnage Loading System (if installed). An existing model, developed by Dredging Research Ltd and reasonably well validated during practical usage, has been used as a reference.

The procedure adopted after overflow commences is as follows.

For each particle size (except for particles smaller than 20 microns, which are considered to always stay in suspension and flow overboard) it is necessary to compute how much stays in the hopper and how much leaves by overflowing. Therefore, the settling efficiency of the hopper has to be computed for each particle size, as follows:

The hopper load parameter (or surface loading), v_o, is computed from:

$$v_o = \frac{Q}{60 \times L \times B} \qquad (3.7)$$

where L is the hopper length and B, the hopper width.

Then the standard settling velocity for a particle, v, is computed according to its size, d. For particles smaller than 100 micron:

$$v = 424 \times (\gamma_s - \gamma_w) \times \left(\frac{d}{1000}\right)^2 \qquad (3.8)$$

For particles between 100 and 2,000 microns:

$$v = 8925 \times \left(\frac{\sqrt{1 + 95(\gamma_s - \gamma_w) \times \left(d \times 10^{-3}\right)^3} - 1}{d} \right) \qquad (3.9)$$

For particles greater than 2,000 microns:

$$v = 87 \times \sqrt{(\gamma_s - \gamma_w) \times d \times 10^{-3}} \qquad (3.10)$$

The Reynolds Number, R_e, for this settling velocity and particle size has to be computed:

$$R_e = \frac{v \times d \times 10^{-6}}{\nu} \qquad (3.11)$$

where v is the Kinematic Viscosity.

The hindrance factor, f_h, is then computed, as follows:

For $R_e < 0.2$:

$$f_h = (1 - C_v)^{4.65} \qquad (3.12)$$

For $R_e > 0.2$ and < 1.0:

$$f_h = (1 - C_v)^{\frac{4.35}{R_e^{0.03}}} \qquad (3.13)$$

For $R_e > 1.0$ and < 200:

$$f_h = (1 - C_v)^{\frac{4.45}{R_e^{0.1}}} \qquad (3.14)$$

For $R_e > 200$:

$$f_h = (1 - C_v)^{2.39} \qquad (3.15)$$

Then the hindered settling velocity, v_h, is given by:

$$v_h = f_h \times v \qquad (3.16)$$

and hindered settling efficiency, r_h, is given by:

$$r_h = \frac{v_h}{v_o} \qquad (3.17)$$

To take account of the effects of turbulence, the longitudinal velocity, v_b, in the hopper is computed. This is given by:

$$v_b = \frac{Q}{\left(B \times H_0 - \frac{W_s(\gamma_s - \gamma_w)}{\gamma_s(\gamma_h - \gamma_w) \times L} \right) \times 60} \tag{3.18}$$

where H_0 is the hopper depth and W_S, the weight of solids.

It must be noted that, for a Constant Tonnage System, H_0 will reduce after the maximum tonnage has been achieved.

The turbulence factor is then computed as follows:

For $r_h < 2.94$:

$$r_t = \left[1 - 0.2 \times r_h^{0.85} \left[1 - Tanh\left(\frac{0.75}{r_h^{1.5}} \times \left(\log\left(\frac{v}{v_b} \right) + 2.6 - r_h \right) \right) \right] \right] \tag{3.19}$$

For $r_h > 2.94$:

$$r_t = \left[0.5 - Tanh\left(\frac{0.75}{r_h^{1.5}} \left(\log\left(\frac{v}{v_b} \right) + 2.6 - r_h \right) \right) \right] \tag{3.20}$$

Then the total settling efficiency is given by:

$$r = r_h \times r_t \tag{3.21}$$

If r>1, then 100% of the grains are retained in the hopper.

If r< 1, then 100*r % of grains are retained and 100*(1-r)% of grains are lost.

The theory put forward by Vlasblom and Miedema was tested on a spreadsheet version of a preliminary settlement tank model. In general, the results are comparable with those used in the DRL model, but slightly more pessimistic with respect to settling efficiency. However, the equation for scour, derived by Camp (1946), seems to give rather low values for scouring velocity and it is considered (as Vlasblom and Miedema also state in their paper) that this equation ought to be investigated in more detail. The expression given in Soulsby and Whitehouse (1997) has been used as a basis for the scour effect. The procedure is as follows:

First, the dimensionless grain size, D_*, is computed from:

$$D_* = \left[\frac{g(s-1)}{\nu^2} \right]^{0.33} \times d \times 10^{-6} \tag{3.22}$$

where, $s = \frac{\gamma_s}{\gamma_w}$, v is the Kinematic Viscosity, and g is the accelerator due to gravity.

Then, the Threshold Shield's Parameter, θ_{cr}, is computed from:

$$\theta_{cr} = \frac{0.30}{(1+1.2\times D_*)} + 0.055[1 - Exp(-.020\times D_*)] \qquad (3.23)$$

and, from this the Threshold Bed Shear Stress, T_{cr},

$$T_{cr} = \theta_{cr} \times g \times (\gamma_s - \gamma_w) \times d \times 10^{-3} \qquad (3.24)$$

This allows the Threshold Depth-Averaged Velocity, U, to be determined from:

$$U = 7 \times \left(\frac{T_{cr}}{\gamma_w}\right)^{0.5} \times \left(\frac{d}{H_h}\right)^{-0.143} \qquad (3.25)$$

For a Constant Volume System, the depth of water in the hopper, H_h, is given by:

$$H_h = H_0 - \frac{W_s \times (\gamma_s - \gamma_w)}{\gamma_s \times (\gamma_h - \gamma_w) \times B \times L} \qquad (3.26)$$

For a constant tonnage system, H_h is affected by the lowering of the weir when the maximum tonnage is reached. Under these circumstances, H_h is given by:

$$H_h = \left(\frac{T_h}{\gamma_w \times B \times L}\right) - \frac{W_s \times (\gamma_s - \gamma_w) \times \gamma_h}{\gamma_s \times \gamma_w \times (\gamma_h - \gamma_w) \times B \times L} \qquad (3.27)$$

with T_h being the maximum tonnage in the hopper.

So, when the longitudinal velocity in the hopper exceeds the threshold depth-averaged velocity, no particles of the size being considered will settle and all will go over the overflow.

Now that a method of determining how much of a certain size of particle remains in the hopper has been established, and how much goes overboard, a running total can be kept of the weight of solids in the hopper (for each particle size) and the amount overflowed (also for each particle). These totals can be reviewed at the end of each trail run and at the end of the loading process.

To find out when loading finishes, it is necessary to determine the overall loading rate. This is done by dividing the total load of solids in the hopper, W_s, by the total cycle time (loading, turning, transporting and disposal). Loading finishes when this rate is at its maximum.

$$Loading - rate = \frac{W_s}{\left(t_c + n \times \left(t_r + t_t\right) + t_p\right)} \tag{3.28}$$

where t_c is the time to travel to the disposal site, dispose and return; t_r is the trailing run time; t_t, the turning time; t_p the loading time; and n the number of complete trail runs.

3.4 Discharge Due to Screening

3.4.1 Oversize Screening

For each grain size category, the model computes how much of the mixture material is larger than the oversize screen size (m_o). Then the mixture lost in the oversize screening process, W_o, is computed from the following expression:

$$W_o = Q_m - C_o \times r_o \times a_o \times b_o \times \left[\frac{a_o \times g}{2 \times V_m} + \sin(\alpha_o) \times V_m\right] \tag{3.29}$$

where Q_m is the mixture flow (discharge of the fluid); C_o, a mixture loss constant; r_o, the ratio of voids to total area; a_o, the screen length; b_o, the screen width; V_m, the mixture velocity; and α_o, the screen angle with the horizontal; and g, the acceleration due to gravity.

The percentage of incoming mixture lost, W_o%, is then given by:

$$W_o\% = \frac{W_o}{Q_m} \times 100 \tag{3.30}$$

It is assumed that the amount of material rejected by the oversize screen, O_1%, for a particle of size d_1 is computed from the aperature size in microns and the suction pipe diameter, D_s, in meters:

$$O_1\% = W_o\% + \left(\frac{d_1}{S_o}\right)^w \times m_o{}^x \times \left(\frac{Q_m}{4.32 D_s^2}\right)^y \times \left(\frac{\gamma_m}{1.2}\right)^z \times 100 \tag{3.31}$$

where S_o is the oversize screening aperature opening in microns.

This can then be expressed as a percentage of the *in situ* material coming up the suction pipe, I_{o1}%, by:

$$I_{o1}\% = \frac{O_1\% \times d_{m1}\%}{100} \tag{3.32}$$

And these may be summed to find the total % of solids rejected by the oversize screen, I_o%:

$$I_o\% = \sum_1^n I_{o1}\% + I_{o2}\% + etc. \tag{3.33}$$

The solids of each size fraction remaining in the stream must now be expressed as a percentage of the total solids remaining in the stream (d_1%, d_2%, etc.) as follows:

$$d_1\% = \left(\frac{d_{m1}\% - I_{o1}\%}{100 - I_o\%} \right) \times 100 \tag{3.34}$$

This then builds up the particle size distribution for the material passing to the hopper or to the undersize screening process. In addition, it is necessary to know the mixture flow, Q_o, and the density of the new mixture, γ_o. These are given by the following expressions:

$$Q_o = Q_m - W_o \tag{3.35}$$

and,

$$\gamma_o = \left(\frac{Q_m}{Q_o} \right) \times \left(\frac{100 - I_o\%}{100} \right) \times (\gamma_m - \gamma_w) + \gamma_w \tag{3.36}$$

3.4.2 Undersize Screening

The undersize screening is either fed by the main suction pipe, in which case the mixture parameters are the original Q_m, γ_m and PSD, or the material has been through the oversize screening and the mixture parameters are Q_o, γ_o and the new PSD derived from the over size screen, by the process described above. The algorithms given below assume that oversize screening has taken place.

First, the fraction of material greater than the under size screen, m_u is computed. Then, the mixture passing through the undersize screening process, W_u, is computed from:

$$W_u = C_u \times r_u \times a_u \times b_u \times \left[\frac{a_u \times g}{2 \times V_{m/o}} + \sin(\alpha_u) \times V_{m/o} \right] \tag{3.37}$$

where the equation symbols have similar meaning to those of equation 3.29 except that they now pertain to undersize screening.

The percentage of incoming mixture passing through, W_u%, is then given by:

$$W_u\% = \frac{W_u}{Q_o} \times 100 \tag{3.38}$$

Then the amount of material collected (passing over) by the undersize screen, $O_1\%$, for a particle of size d_1 is given by:

$$O_1\% = 100 - W_u\% + \left(\frac{d_1}{S_u}\right)^w \times m_u{}^x \times \left(\frac{Q_o}{4.32D_s^2}\right)^y \times \left(\frac{\gamma_o}{1.2}\right)^z \times 100 \qquad (3.39)$$

where S_u is the undersize screening aperature opening in microns.

This can then be expressed as a percentage of the *in situ* material coming up the suction pipe, $I_{u1}\%$, by:

$$I_{u1}\% = \frac{O_1\% \times (d_{m1}\% - I_{o1}\%)}{100} \qquad (3.40)$$

And these may be summed to find the total % of solids collected by the undersize screen, $I_u\%$:

$$I_u\% = \sum_1^n I_{u1}\% + I_{u2}\% + etc. \qquad (3.41)$$

The solids of each size fraction remaining in the stream must now be expressed as a percentage of the totals solids remaining in the stream ($d_1\%$, $d_2\%$, etc.) as follows:

$$d_1\% = \left(\frac{I_{u1}\%}{I_u\%}\right) \times 100 \qquad (3.42)$$

This then builds up the particle size distribution for the material passing to the hopper. In addition, it is necessary to know the water flow, Q_u, and the density of the new mixture, γ_u. These are given by the following expressions:

$$Q_u = Q_{(o)} - W_u \qquad (3.43)$$

and,

$$\gamma_u = \left(\frac{Q}{Q_u}\right) \times \left(\frac{I_u\%}{100}\right) \times (\gamma_m - \gamma_w) + \gamma_w \qquad (3.44)$$

3.5 Draghead Effects

The dredgemaster will try to dredge at a relatively high average density to obtain the maximum hopper load without overflow. The draghead will be lowered sufficiently far into the sand to ensure that it is not starved of material to be dredged. In such circumstances, the amount dredged will generally be less than the amount of material disturbed by the draghead. Material disturbed by the draghead, but not dredged, will be available for re-suspension, subject to a soil disaggregation index.

The rate of sediment re-suspension from the draghead, in kg/s, whilst it is in the seabed, is given by the following:

$$Loss = DI \times f_{dr} \times \frac{[0.5172 \times K \times B_d \times h \times (\gamma_n - \gamma_w) - Q \times (\gamma_m - \gamma_w)] \times \gamma_s}{(\gamma_s - \gamma_w)} \qquad (3.45)$$

Where DI is the soil disaggregation index, and f_{dr} is a "draghead factor" which will need to be determined from measurements on site and is likely to depend on the size and type of draghead and the site characteristics. K is the trailing speed; B_d, the width of the draghead; and h, the depth of the draghead immersion.

The soil disaggregation index, DI, will be a maximum when jet water is being used to fluidize the seabed. In this case, the DI will represent, at maximum, the amount of material in the bed which is suspended (usually sediment less than 63 microns in size).

The losses derived from this algorithm are then applied to the duration of the trailing run, i.e. from commencement of loading until the draghead is lifted at the end of the run.

4.0 OVERVIEW OF SEDIMENT RELEASE REPRESENTED IN PLUME DISPERSION MODEL

4.1 Introduction

Trailer suction hopper dredgers consist of vessels containing a large hopper into which dredged sediment can be pumped. Dredging occurs using suction. One or two dragheads are lowered onto (or partially into) the bed and sediment and water are sucked from the bed through the draghead via a pipe into the hopper. The sediment/water mixture is of the order of 20% sediment (by volume) and so as the hopper is filled most of the load is water. In order to achieve a greater load, pumping is allowed to continue after the hopper is filled. This results in the water in the hopper overflowing (either over the side of the ship or through a central spillway) and being released into the water column. As this water overflows, it contains a proportion of sediment which is then released into the water column to form a plume.

Trailer suction hopper dredgers differ in some respects depending on the type of dredging that they are primarily used for. Dredgers used primarily for aggregates can have the capacity to screen out fractions of sediment to achieve the right particle size distribution for a particular market. Such dredgers release sediment into the water column both over the ship side through a specially designed screening chute and through the overflow described above. Dredgers used for a variety of uses – maintenance, capital, aggregate, beach recharge, etc, do not usually have this capacity. The variety of dredger design essentially means that there are two main sources of plumes from TSHD's – screening and overflow – and that either or both of these releases can occur either over the ship side or through the bottom of the hull.

As well as the two main sources of sediment release, screening and overflow, the procession of the draghead either on the surface of, or through, the bed causes disturbance of the bed and resuspension into the water column. Though the field data relating to this effect is limited, the evidence from the few existing studies is that the release of sediment from the action of the draghead is small in comparison with the releases of sediment from screening and overflow.

All three of these dredger releases are predicted by the Dredger Process model (See Chapter 3). In the case of the overflow and screening releases, however, the density of the sediment/water mixture discharged can be significantly greater than the ambient waters and moreover, especially in the case of the screened discharge, the discharged mixture has an initial momentum. The density difference and momentum result in a dynamic plume. The representation of the dynamic plume is discussed further in Chapter 5.

4.2 Overflow and Screening Release

The overflow and screening releases from the trailer dredger are independently predicted by the Dredger Process Model (Chapter 3) and their initial behavior (the dynamic plume phase) is independently modeled by the Dynamic Plume Model. At any point in the simulation of dredger plume dispersion there will be a dynamic plume resulting from screening and a different dynamic plume resulting from overflow. The exception to this is at the start of the dredging when the hopper is still filling. At this point there is release from screening but none from

overflowing. The dynamic plume model is used to predict how much of each sediment fraction remains in suspension (and how it is distributed spatially) and how much deposited onto the bed at the point where the dynamic phase ends and the passive phase starts.

The user is able to state if the screening and/or overflow is discharged through the hull of the dredger and the release of the dynamic plume is adjusted accordingly. Note that where both screening and overflow are released through the hull together, only one dynamic plume is produced.

Where dredgers have multiple ship side weirs, the resulting releases are modeled as one individual release of initial discharge and cross-section equal to the sum of the individual discharges and cross-section.

4.3 Draghead Release

The dredger process model (Chapter 3) calculates the draghead release as the difference between the amount of material disturbed and the amount of material sucked up by the draghead. It is considered that only the finest fractions (less than 62 microns) will be re-suspended into the water column in this way as the coarser fractions will almost immediately settle back onto the bed.

4.4 Surface Release

The phenomenon of air entrainment has been noted where the overflow and screening plumes impinge on the water surface when discharged from the dredger. The impact of bubbles of air being initially entrained into the plume is not well described by science but it causes an upward current as the air escapes and rises to the surface and drags some of the finer sediment particles to the surface. This creates a surface plume of the finer sediment fractions, although the mass contained in this type of plume is considered to be small compared to the mass of the plume involved in the downward dynamic descent. The model allows for a user-defined proportion of the mass released from the dredger to be released at the surface. It is suggested that this is set to “a few” percent where no specific information is available.

4.5 Settling of Sediment Particles out of the Dynamic Plume

As the dynamic plumes from screening and overflow entrain ambient fluid and momentum their vertical speed reduces, in some conditions to speeds less than the settling velocity of fractions contained within the plume. In this case sediment particles will start to settle out of the plume.

The contribution of the sediment settling out of the dynamic plume to passive plume dispersion is likely to be of little interest since although there may be a considerable proportion of the coarse sediment being released into the water column in this way, such sediment will rapidly fall onto the bed and will not contribute to increases in suspended sediment concentrations in the water column after the first few minutes of release.

To simplify the representation of this mechanism the total amount of sediment settling out is calculated for each fraction. This sediment is then distributed randomly over the entire path of the dynamic plume, in this case, schematized as a linear path.

4.6 Particle Release in the Passive Plume Model

In all, the passive plume model simulates the release of material from eight possible sources.

1. The sediment released into the water column from the overflow plume.

2. The sediment release onto the bed from the overflow plume.

3. The sediment settling out of the overflow plume as it slows in speed.

4. The sediment released into the water column from the screening plume.

5. The sediment release onto the bed from the screening plume.

6. The sediment settling out of the screening plume as it slows in speed.

7. The sediment released at the surface.

8. The sediment released by the draghead.

Sources 1 to 6 are calculated by the Dynamic Plume model (using calculated release rates provided by the Dredger Process Model). Source 7 is user defined while Source 8 is calculated directly by the Dredger Process model. The nature of the different sources is illustrated in Figure 2.

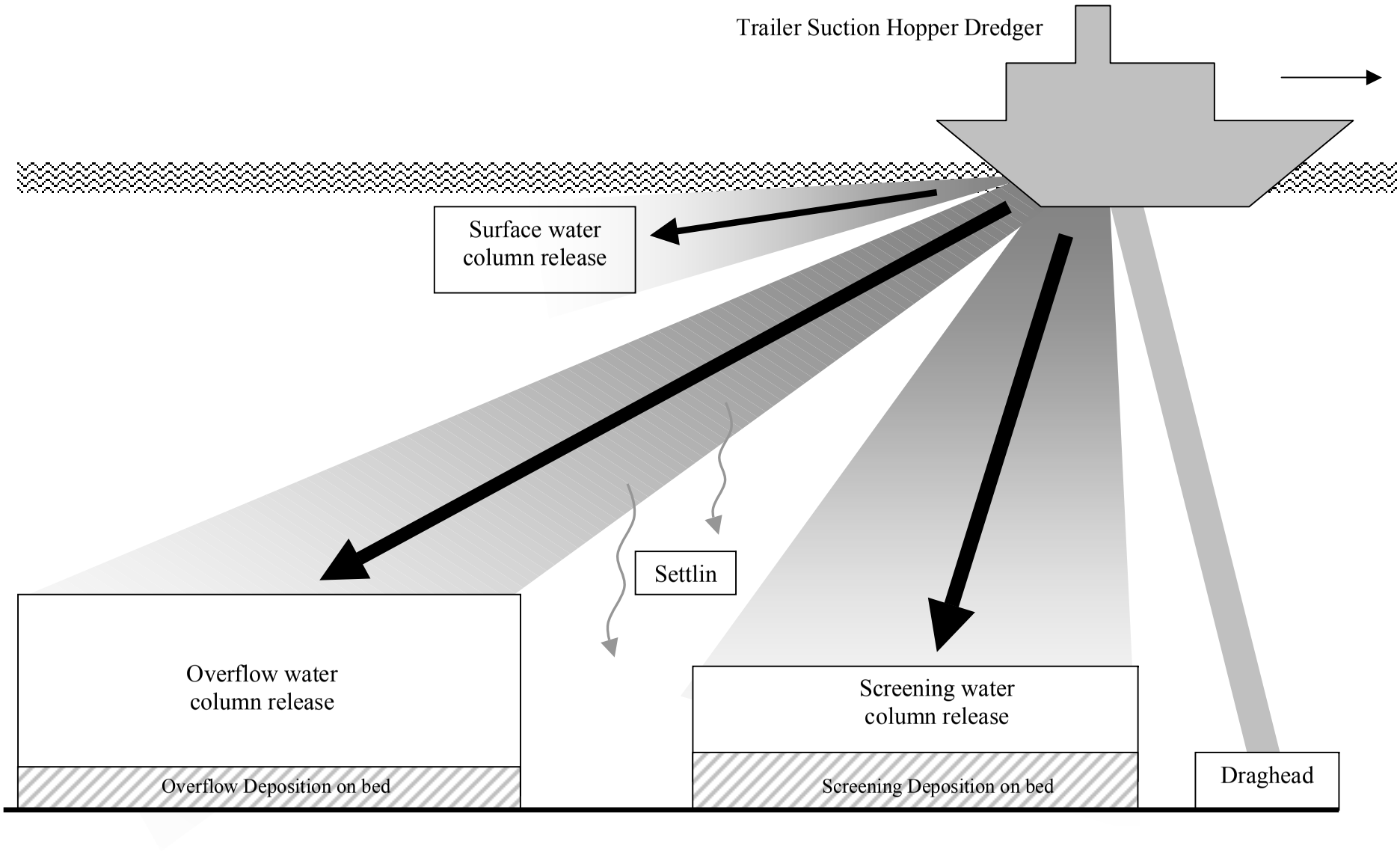

FIGURE 2. Nature of Different Sediment Sources

In addition, for completeness and recognizing the uncertainty surrounding dynamic plume mixing, a further source of release is provided. This allows for additional detrainment from the dynamic plume (through mechanism(s) different to those above) into the ambient waters along the length of the dynamic plume path. It is not intended that this source should be used, as detrainment is likely to be very small, except where there is some evidence for this process being significant.

On each release time step the passive plume model releases a user specified number of particles (each with mass decided by the Process model, the Dynamic Plume model and/or the user). These particles are randomly assigned to each of the above sources, depending on the relative mass release of each, and randomly throughout the volume of space represented by each release source. In the case of the overflow/screening plumes their releases consist of the volume of the density current ($V_{dredger}h_f l_f \Delta t$) and the area of the bed deposit ($V_{dredger} l_f \Delta t$). In the case of the sediment settling out of the plume this is a linear schematization of the dynamic plume path. The draghead plume is represented as a point source underneath the dredger and the surface plume is represented as a line source of length $V_{dredger}\Delta t$.

For simpler characterizations of the dredge plume the dynamic process can be switched off so that all the sediment sources outlined above are distributed evenly throughout the water column. This can be useful as an initial test to enable plume understanding or, in situations where vessel motion or propeller thrust are considered to re-suspend any material impacting onto the bed back into the water column.

4.7 Definition of the Dredging Path

There are two choices for defining the dredge path depending of the level of detail required. For most studies a linear representation of the dredge path is sufficient to give an adequate representation of the impact of dredging operations. The dredge path in these circumstances is defined by the ends of the dredge run x1,y1 and x2,y2 and the speed of the dredger. However, some dredging operations will not be adequately described in this way and, therefore, a facility is provided for the user to define the dredging path in terms of a series of x,y positions and a dredging speed.

5.0 DYNAMIC PLUME MODEL

5.1 Descent of Dynamic Plume

5.1.1 Introduction

The descent of the dynamic plume is reproduced using a lagrangian technique whereby a thin disc (which can be thought of as a section of a bent cone) of the released dynamic plume is tracked as it moves downward under the forces of momentum and negative buoyancy. The technique is common to both dredger plume and outfall plume modeling (e.g. Lee and Cheung, 1990, Brandsma and Divoky, 1976, Koh and Chang, 1973). During the descent ambient water is entrained into the turbulent plume, the path of the plume bends in the direction of the ambient current, and the vertical speed of the plume reduces. The entrainment of ambient fluid is reproduced using the method proposed by Lee and Cheung (1990). When the plume nears a level of neutral buoyancy or impacts on the bed the sequence terminates and the termination conditions are used as initial conditions for simulations of dynamic or bed collapse (see Section 5.2 and 5.3).

Some consideration must be given to the different frames of reference used in the modeling. The descent of the dynamic plume is undertaken in a lagrangian frame of reference, i.e. with respect to a plume element. Once the plume hits the bed or achieves neutral buoyancy the subsequent collapse is modeled in a frame with respect to the bed. The final state of collapse is passed through to the passive plume model with respect to the dredger position so that the results of the dynamic plume modeling can be used to represent sediment release over many time steps.

One of the possible problems with this type of approach is that the dynamic plume model effectively runs in a different time frame from the passive plume model. Unless the length of time represented by the dynamic plume is small compared to the passive plume time step, the dredger could move a significant distance while the dynamic plume descends. The method used solves this problem by introducing sediment at distances from the dredger calculated by the dynamic plume routine but this sediment is not released until a certain time has elapsed (equal to the duration of the dynamic plume phase). This method means that the dynamic plume phase does not have to be short compared to the time step of the model. However, the dynamic plume routine uses the hydrodynamic output from the time when the routine is called throughout the duration of the dynamic plume and thus the longer the duration of the dynamic plume simulation, the less accurate the simulation becomes. The length of the period of time for which tidal currents remain approximately constant is site-dependent but for most purposes can be taken to be about 30 minutes.

5.1.2 Model Implementation

The model examines the changes in the thin disc of the plume, or plume element, at discrete time steps. A constant time step of 0.01 seconds has been employed on the basis of allowing reasonable accuracy at the same time as keeping run times sufficiently small. Here the method of solution is eulerian integration (in time) which is different to that employed by Lee and Cheung who adopted an iterative, time-step varying approach.

The model implementation is as follows:

Consider the Cartesian coordinate system $\underline{X} = (x, y, z)$, where x and y are relative to some fixed position and z is relative to the sea bed. The dredger is moving with velocity $\underline{U}_{dredge} = (u_{dredge}, v_{dredge})$ in this coordinate system and the ambient currents are moving with velocity $\underline{U}_{amb} = (u_{amb}, v_{amb})$. Consider now the alternative coordinate system, $\underline{X}'$ given by,

$\underline{X}' = \underline{X} - \underline{U}_{dredge}.t$, where t represents time. (5.1)

This describes the coordinate system moving with the dredger. The lagrangian descent of the thin disc representing the release of the plume in a single timestep is modeled in the $\underline{X}'$ coordinate system, so that the initial velocity of the release is vertically downward, and the ambient current speed in this frame, $\underline{U}'_{amb}$, becomes $\underline{U}'_{amb} = (u'_{amb}, v'_{amb}) = \underline{U}_{amb} - \underline{U}_{dredge}$. The movement of the plume through space with reference to a fixed position is then derived using Equation 5.1.

Consider the dynamic plume after k time steps, (of length Δt). At this point the plume has velocity components (in the moving reference frame) of u'_k , v'_k and w_k , density ρ_k , radius b_k ,thickness h_k and mass M_k . The difference in density between the plume and the ambient fluid is $\Delta\rho_k = \rho_k - \rho_a$. The model calculates the mass entrainment, ΔM_k (See section 5.1.2). The new variables for the next step are given by:

Concentration: $$C_{k+1} = \frac{C_k M_k}{M_k + \Delta M_k} \quad (5.2)$$

Horizontal Momentum: $$u'_{k+1} = \frac{u'_k M_k + u'_{k+1} \Delta M_k}{M_k + \Delta M_k} \quad (5.3)$$

$$v'_{k+1} = \frac{v'_k M_k + v'_{k+1} \Delta M_k}{M_k + \Delta M_k} \quad (5.4)$$

Vertical Momentum: $$w_{k+1} = \frac{w_k M_k}{M_k + \partial M_k} + \left(\frac{\Delta\rho}{\rho}\right) g.\Delta t \quad (5.5)$$

where g is the acceleration due to gravity (= 9.81m/s^2).

Plume speed: $$V'_{k+1} = (u'^2_{k+1} + v'^2_{k+1} + w'^2_{k+1})^{1/2} \quad (5.6)$$

Thickness: $$h_{k+1} = \frac{V'_{k+1}}{V'_k} h_k \quad (5.7)$$

Plume radius: $$b_{k+1} = \left(\frac{M_k + \Delta M_k}{\rho_{k+1} \pi h_{k+1}} \right)^{1/2} \quad (5.8)$$

Position of the plume centroid: $$x_{k+1} = x_k + (u'_{k+1} + u_{dredge})\Delta t \quad (5.9)$$

$$y_{k+1} = y_k + (v'_{k+1} + v_{dredge})\Delta t$$

$$z_{k+1} = z_k + w_{k+1}\Delta t$$

5.1.3 Entrainment

The mass of the plume element is increased due to turbulent entrainment of the ambient fluid, which when drawn into the plume is mixed throughout. There are two mechanisms for this entrainment:

- Shear entrainment which occurs close to the release point or in conditions of very weak ambient current flow where the dynamic plume is more jet-like;
- Forced entrainment, which in general dominates except under the conditions stated above, and occurs due to the flow of ambient water into the plume.

Shear Entrainment

The increase in mass due to shear entrainment is given by:

$$\Delta M_s = \rho_a . 2\pi b_k h_k E \left| V_k - u'_{amb} \cos\phi_k \cos\theta_k \right| . \Delta t \quad (5.10)$$

where ρ_{amb} and u'_{amb} are the density and current speed (in the moving coordinate system) of the ambient fluid, respectively. Note that $u'_{amb} = u_{amb} - u_{dredge}$ where u_{amb} is the ambient current speed in the fixed coordinate system; ϕ_k is the angle of the plume path with the horizontal plane; θ_k is the angle of the plume path with the ambient current plane projected onto the horizontal; and E is an entrainment coefficient.

Lee and Cheung give a formula for E, which is dependent on the local densimetric Froude number, and the orientation of the plume path and is based on a hypothesis by Schatzmann (1979, 1981). The formula has been adapted by Lee and Cheung to suit a wide range of flows and to give the correct buoyancy for a pure jet (no buoyancy just momentum) and a pure plume (no initial momentum, just a density difference).

$$E = \sqrt{2}\frac{\left(0.057 + \frac{0.554\sin\phi_k}{F^2}\right)}{\left(1 + 5\frac{u'_{amb}\cos\phi_k\cos\theta_k}{\left|V_k - u'_{amb}\cos\phi_k\cos\phi_k\right|}\right)} \qquad (5.11)$$

where F, the local densimetric Froude number, is given by,

$$F = \frac{\left|V_k - u'_{amb}\cos\phi_k\cos\theta_k\right|}{\left(g\frac{\Delta\rho}{\rho}b_k\right)^{1/2}} \qquad (5.12)$$

Forced Entrainment

Lee and Cheung (1990) derived an equation for forced entrainment arising in a three dimensional trajectory. The resulting entrainment is as follows:

$$\Delta M_k = \rho_{amb}u'_{amb}h_k b_k\left[2\sqrt{\sin^2\phi_k + \sin^2\theta_k - (\sin\phi_k\sin\theta_k)^2} + \pi\frac{\Delta b_k}{\Delta s_k}\cos\phi_k\cos\theta_k\right.$$
$$\left. + \frac{\pi}{2}b_k\frac{(\cos\phi_k\cos\theta_k - \cos\phi_{k-1}\cos_{k-1})}{\Delta s_k}\right]\Delta t \qquad (5.13)$$

Note that if this equation is reduced to two dimensions by setting θ=0 then it takes the form:

$$\Delta M_k = \rho_{amb}u'_{amb}h_k b_k\left[2\sin\phi_k + \pi\frac{\Delta b_k}{\Delta s_k}\cos\phi_k + \frac{\pi}{2}b_k\sin\phi_k\frac{\Delta\phi_k)}{\Delta s_k}\right] \qquad (5.14)$$

which agrees with the derivation of forced entrainment in two dimensions given by Frick (1984).

In the three dimensional form there are three different contributions to forced entrainment which are all significant at different times suggesting that none of these terms can be neglected. The first term represents the forced entrainment due to the projected area of the crossflow while the second and third terms represent corrections due to the growth of the plume radius and the curvature of the trajectory (Frick 1984, Lee and Cheung 1990).

Combining Shear and Forced Entrainment

There are two possible options for combining shear and forced entrainment. Option 1 assumes they are independent can simply be added together. Option 2 assumes there is some inter-dependency and takes whichever is the greater entrainment of the two mechanisms. Either approach will ensure a smooth transition between the shear entrainment occurring initially and

the forced entrainment occurring later in the plume development. Here Option 2 is preferred as it has been used successfully by Lee and Cheung (1990).

More recently Lee and Cheung (1990) have developed a more sophisticated approach which seeks to model the transition between shear and forced entrainment more accurately. However, the increased sophistication merited by this approach is considered to be beyond the scope of the present study, in the absence of other uncertainties and the lack of quality field data for calibration of the model.

5.1.4 Settling from the Plume

In the case where the vertical descent of the plume becomes less than the settling velocity of one or more fractions of the sediment contained within the plume then this sediment is allowed to settle out of the plume at a rate $C.w_s$ where C is the concentration of the sediment fraction and w_s is the corresponding settling velocity.

The settling rate is calculated using Soulsby's (1997) formula for particles greater than 62 microns in size (fine sand and bigger),

$$w_s = \frac{\upsilon}{d}\left[\left\{10.36^2 + 1.049D_*^3\right\}^{1/2} - 10.36\right] \qquad (5.15)$$

where w_s is the settling velocity of the particle;

ν is the viscosity of water;

d is the diameter of the particle;

D_* is the dimensionless grain size of the particle given by $D_* = \left[\frac{g(s-1)}{\upsilon^2}\right]^{1/3} d$

This formula allows for both the settling of coarse particles (which obey a quadratic bluff-body drag law) and finer particles (which obey Stokes law of viscous drag).

For particles less than 62 microns in size (silt sized and smaller) a power law relationship is used,

$$w_s = a.C^b \qquad (5.16)$$

where a and b are (user-defined) empirical coefficients and C is the suspended sediment concentration. Recent advances in measurement of settling velocity using in situ video-imaging have led to re-assessment of settling velocities for cohesive sediment (e.g. Eisma et al, 1996, Dyer et al, 2000). Studies have found that the previous method of estimating sediment velocity of sampling from a settling column (containing in situ silty water) over time underestimated the settling velocity through the development of water circulations in the settling column

(Dearnaley, 1996). In this light many well-used empirical relationships between settling velocity and concentration are no longer reliable. The model allows the user to define his/her own relationship of the power law form but uses values of a=0.005 and b=1.0 (with a minimum value of w_s=0.00025mm/s) as the default option, based on various recorded recent measurements using in situ video-imaging. Note that this relationship is for flocculated sediment such as occurs in estuaries of appreciable tidal range or coastal situations. For riverine situations where salinity is below a few parts per thousand settling velocity for the silt/clay fractions will approach that given by Equation 5.15 above.

A simple methodology (originally proposed by Koh and Chang 1973, and adopted by Brandsma and Divoky, 1976) is adopted whereby the flux of each sediment fraction settling out of the plume is zero if the downward descent of the plume is faster than the settling speed of that fraction and is otherwise equal to the product of the settling speed, the concentration and the projected settling area of the plume.

The sediment falling out of the dynamic plume is passed back to the passive plume model. This process is often termed "stripping" but here we refer to it as settling to make a distinction with stripping through detrainment from the plume, which is dealt with below.

5.1.5 Stripping from the Plume

Field measurements of concentration increases resulting from bottom dumping in deep holes have found that a few percent of the total volume of material is released into the water column (Land and Bray, 1998) leading to the idea that sediment is "stripped" from the plume as it descends in the dynamic phase. If the distribution of sediment and momentum across a plume slice is gaussian, then it can be argued that near its edges, the plume is at near ambient conditions and thus can be transported passively.

However, the gaussian-like aspects of the distribution of momentum and sediment only exist in a time-averaged sense. At any given instant the separation between plume and ambient is actually very distinct. Moreover, the phenomenon of stripping is contradicted by the one-way movement of ambient water into the more turbulent plume, where it is trapped by the more dominant large eddy structures with the plume. It is suggested therefore that the phenomenon referred to as stripping is not caused by detrainment from the plume but rather but by other mixing mechanisms, which have been hitherto ignored. For instance the loss of sediment into the water column from bottom disposal can be explained by the slower release of fine particles that occurs in the top of the descending cloud as a result of release of fine sediment near the near the end of the bottom dumping process (Johnson et al, 1993). In the case of dredging, release mechanisms such as air entrainment and propeller mixing can cause mixing of the dynamic plume with the ambient water as well as settling of particles out of the plume (See Section 5.2.5).

5.1.6 Termination

The descent of the dynamic plume is terminated either when the plume (element centroid) touches the bed or when the vertical (downward) speed becomes less than zero. In the former case the end state of the descending plume is used as the initial conditions for a simulation of collapse of the plume onto the bed (see Section 5.2) and in the latter case the end state is used to provide initial conditions for dynamic collapse – i.e. when the plume collapses to form a thin layer of sediment at the position of neutral buoyancy.

5.2 Collapse on Bed

5.2.1 Introduction

Collapse onto the bed is reproduced using a basic equation attributed to Von Karman who found that for dense layers which are thin in comparison with the depth of fluid above, the speed of propagation of the front of the resulting density current along the bed, u_f, is related to the thickness of the density current, h_f, and the gravitational acceleration modified for buoyancy, $g' = g.^{\Delta\rho}/_{\rho}$ as follows:

$$u_f = F\left(g' h_f\right)^{1/2} \qquad (5.17)$$

where F is the Froude number of the flow.

If the density current is non-particulate, and if there is no entrainment and viscous and drag forces are small, then the motion of the front can be described by the similarity solution (Rottman and Simpson, 1983, Hallworth et al, 1998),

$$x_f = \left[\frac{27F^2}{12-2F^2}\right]^{1/3} \{g'A\}^{1/3} t^{2/3} \qquad (5.18)$$

where x_f is the distance traveled by the front of the plume;

A is the (non-varying) two-dimensional area of the plume;

t is the time from the initial release of the density current.

For the present case, the density current contains sediment particles of different fractions and, therefore, its motion is not well described by the similarity solution given above. Where the sediment particles belong to a single fraction, with a similar diameter, they have a similar settling velocity.

In the model the propagation of the current is achieved by repeated application of Equation 5.17 (but modified to allow for the effect of friction, see Section 5.2.3) keeping track of the concentrations of each sediment fraction in the plume and allowing the sediment particles to

settle out continuously. As the density current lengthens, continuity of mass implies that the thickness of the density current reduces correspondingly. All of the fractions are considered to be uniformly mixed throughout the density current and to deposit all along the length of the current. The settling rate is calculated using Soulsby's (1997) formula for particles greater than 62 microns (fine sand and bigger) in size, while for particles less than 62 microns in size (silt sized and smaller) a power law relationship is used, (see Section 4.2.4).

A "box-model" approach has been used in describing the shape of the density current – i.e. the density current height is assumed constant over the length of the density current. Box model approaches have been shown to give a good approximation to the collapse of the density current (Hallworth et al, 1998).

5.2.2 Entrainment

Entrainment does not seem to be a critical contribution to the behavior of the density current and numerical models assuming an absence of mixing have performed well against observations and measurements of entrainment which have shown it to be small or negligible (e.g. Rottman and Simpson, 1983, Hogg and Woods, 2001, Hallworth at al, 1998, Maxworth et al, 2002, Alavian, 1986).

For simplicity therefore we ignore any entrainment of ambient fluid.

Note however that these experiments tend to be carried out with small (or stationary) ambient flows and that strong ambient flows may enhance entrainment of the density current into the water column significantly, reducing the duration and propagation of the bed collapse process.

5.2.3 Friction

The effect of friction can be found by balancing the inertia and buoyancy forces with those of friction in the depth-averaged momentum equation.

$$\frac{\partial(uh)}{\partial t}+\frac{\partial\left(u^2h\right)}{\partial x}+\frac{\partial\left(\frac{1}{2}g'h^2\right)}{\partial x}=-C_Du^2 \qquad (5.19)$$

where u and h are the depth-averaged speed and depth of the density current at time t and position x;

C_D is the friction coefficient.

It can be shown that, to first order in $\left(\frac{C_Dx_f}{h_f}\right)$,

$$u_f \approx F\left(\frac{g'h}{1+\frac{2C_Dx_f}{3h_f}}\right)^{0.5} \qquad (5.20)$$

where x_f is the half-length of the density current (from its centroid to the front of the current).

Friction is therefore influential if $C_D \sim O(^h/_x)$ and therefore the onset of drag is very dependent on the shape (ratio of depth to length) of the density current.

Hogg and Woods (1998) show that for particulate density currents, when $C_D(Ag')^{1/3}/w_s << 1$ the density current is dominated by sedimentation rather than drag. For the density currents likely to occur in this study a range of fractions may be present and most of these fractions would produce density currents that fall into the sedimentation-dominant category. However density currents composed mainly of silt particles or smaller (falling at speeds of the order of 10^{-3} m/s or less) may fall into the category affected by drag rather than sedimentation.

5.2.4 Effect of Bed Slope

The effect of bed slope is to cause acceleration in the speed of the plume in the direction of the incline of the order of $g'\sin\varphi$, where φ is the angle of the slope, up to the point where drag forces become sufficient to oppose the effect of gravity. The model does not take this effect into account and assumes a flat or near flat bed level in the vicinity of the density current. Care should therefore be taken in interpreting the results in circumstances with steep slopes (such as sideslopes of navigation channels).

5.2.5 Model Implementation

A constant time step of 0.01 seconds has been employed on the basis of allowing reasonable accuracy at the same time as keeping run times sufficiently small. The initial conditions for the collapse are derived from the state of the dynamic plume as it hits the bed, in particular the plume radius and the vertical speed of the plume. The plume element is assumed to strike the bed near vertically but the motion of the dredger from which the plume is released together with the ambient currents means that the plume is "smeared" over the sea bed as it impacts.

The distance from the dredger release to the bed is almost always greater than the length-scale associated with the initial momentum of the release and therefore buoyancy forces dominate the motion of the plume when it impinges on the bed. Any initial radial momentum resulting from the impact is small compared with the motion induced by buoyancy forces and is therefore ignored.

The model implementation is as follows:

Consider the density current after k time steps. At this point, the plume has thickness $h_{f,k}$, and half-length, l_f . Then the new variables for the next step are given by:

Concentration of the i^{th} fraction:
$$C_{i,k+1} = \frac{l_{f,k} h_{f,k} C_{i,k} - l_{f,k} w_{s,i} C_{i,k}}{l_{f,k} h_{f,k}} \quad (5.21)$$

Front speed: $$u_{f,k+1} = F\left(\frac{g' h_{f,k}}{1+\frac{2C_D x_{f,k}}{3h_{f,k}}}\right)^{1/2} \quad (5.22)$$

Density current length: $$l_{f,k+1} = l_{f,k} + u_{k+1}\Delta t \quad (5.23)$$

Density current height: $$h_{f,k+1} = h_{f,k}\frac{l_{f,k}}{l_{f,k+1}} \quad (5.24)$$

Loss of mass due to settling: $$M_{k+1} = M_k - \sum_i C_{i,k} w_i \quad (5.25)$$

Advection of the density current centroid: $$x = x + u_a \Delta t \quad (5.26)$$

$$y = y + u_a \Delta t$$

5.2.6 Deposition onto the Bed from Particulate Density Currents

Deposition onto the bed is calculated by keeping a running total of the deposition flux for each fraction from the density current and by distributing this sediment over the bed according to the formula derived by Bonnecaze et al. (1996). This formula is derived from the numerical solution of equations for conservation of mass, momentum and particle volume and has been verified with success through laboratory experiments, although it is accepted that very close to the point of initial collapse the formula is less satisfactory.

The formula below relates to a two-dimensional density current (i.e. not axisymmetric). The total density of deposit (in terms of kg/m^2) resulting from the deposition of all fractions is,

$$m_{bed}(x) = \rho_{part} A^{1/2} \sum_i \varphi_{i0} \beta_i^{2/5} W(\beta_i^{2/5} x / A^{1/2}) \quad (5.27)$$

where x is the distance from the point of impact;

W is given by W(x)=0.820/(1+0.683x^2+0.017x^8) ;

A is the initial cross-sectional area of the plume (equal to $l_0 h_0$) ;

ρ_{part} is the density of the particulate plume;

φ_{i0} is the initial volume of the ith sediment fraction expressed as a proportion of A.

β_i is given by $ws_i / \left(g_0'^{1/2} A^{1/4}\right)$ and ws_i is the settling velocity for particles of the *ith* sediment fraction.

In using this formula, the prediction of the area of the footprint resulting from impact of the desired fraction is reduced but the depth of deposit is much greater. This is because in reality the deposit will be smeared along the path of the advecting density current.

The calculation of the deposition footprint represents the distribution of sediment settling to the bed from the density current. The model allows for the subsequent re-suspension of this sediment as suspended sediment. However, the formation and subsequent flow of fluid mud and/or dispersion of deposited sediment as sand transport bedload are beyond the scope of the model.

5.2.7 Termination of Bed Collapse

Termination of the bed collapse phase is achieved when the turbulence within the density current has reduced sufficiently to allow entrainment of the density current into the ambient waters – essentially when the density current can be regarded as a passive plume. Akar and Jirka (1994) cite experiments by Monin and Yaglom (1971) and Turner (1973) which suggest that this occurs when the Richardson Number corresponding to the density current is between 0.1 and 0.2. Akar and Jirka note further corroborating experiments by Pych (1970), and Schiller and Sayre (1973) and on this basis chose the critical Richardson number to be 0.15. Akar and Jirka further show that for a density current impinging on the bed the flux Richardson Number, R_f, can be approximated as,

$$R_f = \frac{g\sigma_s \dfrac{\partial \rho}{\partial z}}{\rho\left(\dfrac{\partial u}{\partial z}\right)^2} \approx \kappa^2 \frac{g'h}{u_*^2} \qquad (5.28)$$

where z is the height above the bed;
ρ is the fluid density;
u is the current speed;
σ_s is the Schmidt number which is approximately 1;
κ is the Von Karman constant, 0.4;
$g' = g.^{\Delta\rho}/_{\rho}$ where $\Delta\rho$ is the difference in density between the density current and the ambient fluid;

u_* is approximated by $u_* = \dfrac{\kappa u}{\ln\{h_b / z_0\}}$ (5.29)

and h_b is the density current thickness and z_0 is the physical roughness length.

5.2.8 Buoyant Collapse on the Bed

It is possible in certain stratified conditions that the dynamic plume could "graze" the bed yet be buoyant, the plume containing a significant proportion of the less dense ambient fluid found nearer the surface. Experiments producing this effect invariably showed the plume was only just buoyant, the difference in densities between the plume and the ambient water being small. This also means that the Richardson number becomes small and mixing can occur. In this situation therefore, the descent phase terminates on the plume meeting the bed and the remaining material in the plume is directly passed to the passive plume model.

5.3 Dynamic Collapse

5.3.1 Introduction

Dynamic collapse occurs in stratified situations where the dynamic plume does not impact on the bed but becomes positively buoyant as its initial momentum takes it past the level of neutral buoyancy. The plume centroid will then rise towards the level of neutral buoyancy and converge upon it after some transient oscillation. At the point of neutral buoyancy the situation is analogous to that of bed collapse – there is a density discontinuity between the edge of the plume and the ambient seawater and this density difference will cause density currents to flow or "pancake" outward from the centroid both above and below the neutral buoyancy level. The difference between the bed collapse and dynamic collapse scenarios lies mainly in the fact that there is a density gradient from the neutral buoyancy position throughout the thickness of the plume so that at the vertical extremities of the plume the density difference can be marked. The effect of stratification hinders the entrainment of ambient fluid. Axial forces influence and finally destroy the boundary layer evolution (Jirka, 1999).

The focus of the MMS project is towards aggregate dredging in offshore locations and beach dredging, which are therefore unlikely to experience significant stratification. Nonetheless, the model has been written to allow for dynamic collapse to make it more inclusive. Because of the focus on offshore locations, the rarity of experiments involving dynamic collapse and the similarities between the processes of dynamic and bed collapse, no section is included below on the validation and sensitivity testing of the dynamic collapse simulation.

Previous attempts at describing this process have used formulations analogous to that of collapse on the bed (e.g. Koh and Chang 1973, Brandsma and Divoky 1976, Akar and Jirka, 1994). Indeed for the idealized situation of dynamic collapse (i.e. no entrainment, no settling and the plume centroid fixed at the point of neutral buoyancy) it is possible to use a formulation for dynamic collapse that is very similar to that of bed collapse by using the average density difference over the height of the plume.

In the model, the propagation of the current is achieved by repeated application of Equation (5.16) but modified to allow for the effect of a stratified water column (Equation 5.32). As for collapse on the bed, all of the fractions are considered to be uniformly mixed throughout the density current and to deposit all along the length of the current. The settling rate is calculated using Soulsby's (1997) formula for particles greater than 62 microns (fine sand and bigger) in

size, while for particles less than 62 microns in size (silt sized and smaller) a power law relationship is used, (see Section 5.1.4).

As for bed collapse a "box-model" approach has been used in describing the shape of the density current – i.e. the density current height is assumed constant over the length of the density current. It has been assumed that entrainment is not significant and moreover there is no friction from the bed or effect of bed slope. However, there is an effect from pressure drag, which is discussed in Section 5.3.2.

5.3.2 Drag

The effect of drag becomes important with regard to the vertical motion of the plume. The effect of drag causes the damping of the oscillation about the level of neutral buoyancy. The drag force in the z direction is given by,

$$F_{drag} = 0.5 C_{Drag} l_{f,k} U_a^2 \rho_k \cos\phi \cos\theta \left(1 - \cos\phi \cos\theta\right)^{1/2} \qquad (5.30)$$

C_{drag} in this case is the coefficient for drag for an elliptical cylinder, given by (Hoerner, 1965),

$$C_{drag} = 0.005\left\{4 + 2\left(h_d / x_d\right) + 120\left(x_d / h_d\right)^2\right\} \qquad (5.31)$$

The effect of the collapse causes the value of the drag coefficient to increase rapidly which in turn dampens the vertical motion of the plume.

5.3.3 Model Implementation

The dynamic plume routine is called as soon as the vertical speed of the descending plume becomes less than zero (i.e. upward motion). The model implementation is as follows.

Consider the density current after k time steps. At this point the plume has a half-thickness $h_{f,k}$ and half-length $l_{f,k}$. Then the new variables for the next step are given by:

Front speed: $u_f = F\left(g' h_{f,k}\right)^{1/2} \approx F\left(0.5 \varepsilon h_{f,k}^2\right)^{1/2}$ where $\varepsilon = -\frac{g}{\rho}\frac{\partial \rho}{\partial z}$ (5.32) Density current length: $l_{f,k+1} = l_{f,k} + u_{k+1}\Delta t$ (5.33)

Density current height: $h_{f,k+1} = h_{f,k}\frac{l_{f,k}}{l_{f,k+1}}$ (5.34)

Loss of mass due to settling: $\partial m_k = \sum_i C_{i,k} w_i$ (5.35)

Advection of the density current centroid: $x = x + U_a \partial t$ (5.36)

$$y = y + U_a \partial t$$

5.3.4 Termination of Dynamic Collapse

The criterion for the onset of mixing with the ambient fluid (see Section 5.3.8) becomes in this case (Akar and Jirka, 1994),

$$R_f = \frac{g\sigma_s \dfrac{\partial \rho}{\partial z}}{\rho\left(\dfrac{\partial u}{\partial z}\right)^2} \approx \kappa^2 \frac{\varepsilon h}{u_*^2} < 0.15 \qquad (5.37)$$

where $g' = g.^{\Delta\rho}/_{\rho}$ where $\Delta\rho$ is the difference in density between the density current and the ambient fluid;

$$\varepsilon = -\frac{g}{\rho}\frac{\partial \rho}{\partial z}$$

u_* is approximated by $u_* = \dfrac{\kappa u}{\ln\{h_b / z_0\}}$ (5.38)

and h_b is the density current thickness and z_0 is the bed roughness length.

5.4 Validation and Sensitivity Testing of Dynamic Plume Model

5.4.1 Dynamic Descent of Plume

5.4.1.1 Validation

The investigators for this project are not aware of any published field measurements of the mixing and growth of dynamic plumes in the water column of a sufficient standard for validation of a dynamic plume model. For this reason, it has been necessary to resort to data from laboratory testing. It is further noted that the vast majority of investigations into such matters have been conducted using dissolved tracers rather than sediment. Two experiments were chosen for the calibration of the dynamic descent – Chu and Goldberg (1974) and Chu (1975), these were chosen because of the quality of the field experiments but also because they model the downward descent of negatively buoyant plumes.

In the case of the Chu and Goldberg experiments, the plume was simulated by injecting dyed saline solution vertically downward into uniform open channel flow (in a flume 9 m long by 45 cm deep by 30 cm wide) through a hyperdermic needle of 0.18 cm diameter at 2.5 cm below the free surface. Crossflow velocities varied over the range 0-24 cm/s and efflux velocities over the range 0-460 cm/s. These conditions corresponded to Reynolds numbers of 2,500-11,000. We consider the results for tests 2001, 2003 and 3006 and the conditions for these tests are given in Table 1.

TABLE 1. Model Comparisons to Chu and Goldberg (1974) Results

Test	Ambient current (cm/s)	Initial discharge velocity (cm/s)	Density difference (kg/m^3)
2001	0.04	0.3	115
2003	0.09	1.15	115
3006	0.2	1.7	191

Figure 3 shows the results for the Chu and Goldberg experiments. For the sake of continuity with the original data source - the Chu and Goldberg paper, the observations and model predictions are scaled with respect to the buoyancy length scale, l_b , given by,

$$l_b = \frac{4F_0}{\pi \rho_{amb} u_{amb}^3}$$

where F_0 is the buoyancy flux (which remains roughly constant along the plume for small variations in density) and is given by $F_0 = {}^1/_4 \, \pi D^2 g(\rho - \rho_{amb}).u_{amb}$ and D is the initial diameter of the release.

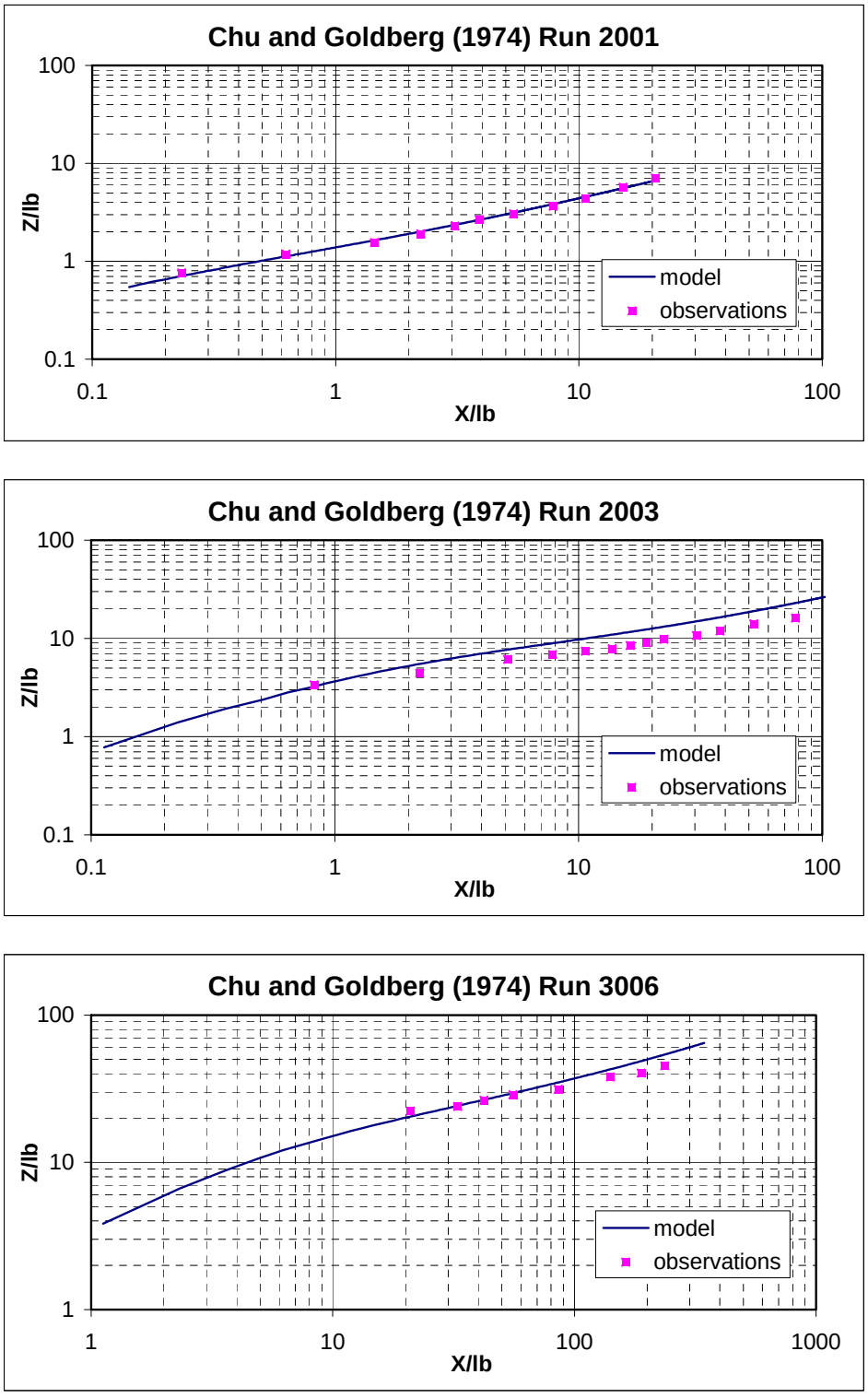

FIGURE 3. Comparisons to Chu and Goldberg (1974) Experiments

The figures show that the observations for Runs 2001, 2003 and 3006 are well reproduced by the model described in Section 5.1.

In the case of the Chu experiments, plumes were simulated by injecting dyed saline solution vertically upward into uniform open channel flow (in a flume 9m long by 45cm deep by 30cm wide) through an injection pipe of 1.0cm diameter at 5cm above the channel bottom. The concentration of injected solution was 3% for all tests. Simulations were undertaken for ambient flows of 5.77cm/s and 8.36cm/s with initial velocities of the injected fluid varying over the ranges 23-69cm/s and 33-100cm/s respectively. These conditions corresponded to Reynolds numbers of 2,500-11,000. We consider the results for tests 4003, 4005, 5002 and 5004 and the conditions for these tests are given in Table 2.

TABLE 2. Model Comparisons to Chu (1975) Results

Test	Ambient current (cm/s)	Initial discharge velocity (cm/s)
4003	5.77	0.46
4005	5.77	0.69
5002	8.36	0.50
5004	8.36	1.00

Figure 4 shows the results for the Chu experiments. Here we present the data (and model predictions) scaled by the diameter of the release (D = 1.0cm) as given in Lee and Cheung (1990). Presentation of the data in this way allows the reader to compare the performance of the model used here with the results of a model more widely validated and more targeted to the accurate derivation of the dynamic phase of the plume. The figures show that the results are reasonably well reproduced by the model described in Section 5.1, but that the results for the lowest ambient current speed overestimates the entrainment of ambient fluid during the ascent of the plume. The errors in the prediction of the maximum height of rise, the dilution at this point and the maximum distance traveled by the plume vary up to 5% for Run 2001, 30% for Run 2003 and up to 20% for Run 3006.

These tests are not exhaustive but serve to indicate the dynamic plume is robust and producing the correct behavior.

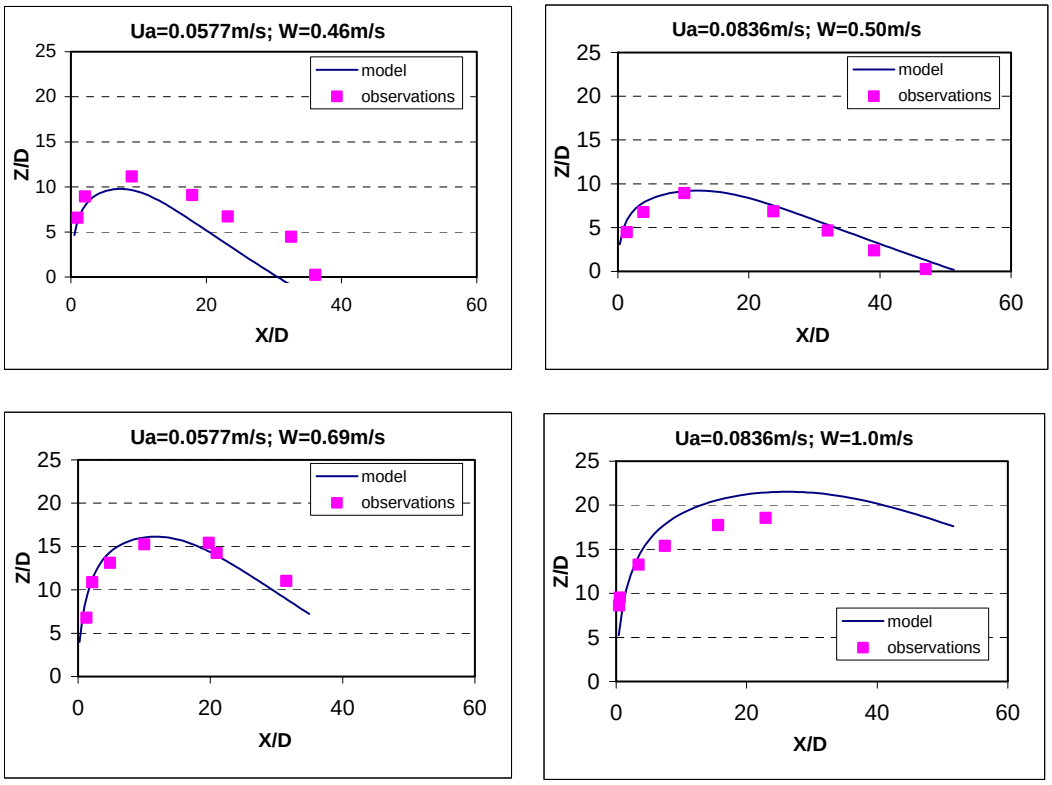

FIGURE 4. Comparisons to the Chu (1975) Experiments

5.4.1.2 Sensitivity Testing

This section presents a sensitivity analysis of the effects of changes in different parameters on the descent of the dynamic plume. The scenarios illustrated in the figures are based on the following parameters, (except where specified otherwise):

- Water depth, 25 m
- Area of release, 6 m^2
- Discharge, 5 m^3/s
- Density of discharge, 84 kg/m^3
- This 84 kg/m^3 is composed of sediment particles of which 10% is less than 63µm in diameter, 25% is 80µm in diameter, 40% is 120µm in diameter, and 20% is 170µm is diameter.
- Ambient current, 0.5 m/s in the opposite direction to the dredger motion
- Dredger motion, 0.5 m/s in the opposite direction to the ambient current

The figures presented in the following section show the path of the plume centroid together with the extremities of the plume. The descent of the plume is given in fixed reference frame relative to the sea bed.

Effect of Hull Release

Figure 5 shows the effect of release at 25 m above the bed with a 6 m^2 release area (top graph) and at 18 m from bed above the bed but with a smaller release area of 1 m^2 more typical of a central hull spillway (bottom graph). The figure shows the effect of hull release in reducing the extent of dilution and the horizontal distance traveled before impact on the bed.

Effect of Current Strength

The effect of current strength is illustrated in Figure 6, which shows the plume descent for 0 m/s, 0.5 m/s and 1.0 m/s ambient current speeds, (the current speed increasing from top to bottom). The effect of current strength is mainly in the degree of entrainment (dilution) during descent although it must be recognized that the current strength also governs the extent of the advection during the descent and (after impact on the bed) collapse of the dynamic plume. The plume descent for still water (0.0 m/s) is straight down (with some initial effect resulting from the dredger motion) while the plume descent for 1.0 m/s shows the plume traveling up to 50 m from the point of release before forming a density current.

Effect of Dredger Pump Rate

The dredger pump rate effectively controls the rate of discharge and therefore the initial momentum of the dynamic plume (although this will be modified by the screening process if used). The effect of a change in dredger pump or discharge rate is shown in Figure 7. The figure shows the descent of plumes for discharges of 1 m/s, 5 m/s and 10 m/s and it can be seen that as the discharge increases the distance traveled by the plume before contact with the bed reduces and the size of the plume also reduces slightly.

Effect of Sediment Concentration

The effect of changes in sediment concentration is illustrated by Figure 8. The higher the concentration, the greater the negative buoyancy and the more quickly the plume descends to the bed. The figures show the descent of the plume for initial concentrations of sediment of 42 kg/m^3, 84 kg/m^3 and 168 kg/m^3. It can be seen that the distance traveled by the plume before impinging on the bed varies roughly linearly with the initial density. The extent of dilution is reduced with increasing density.

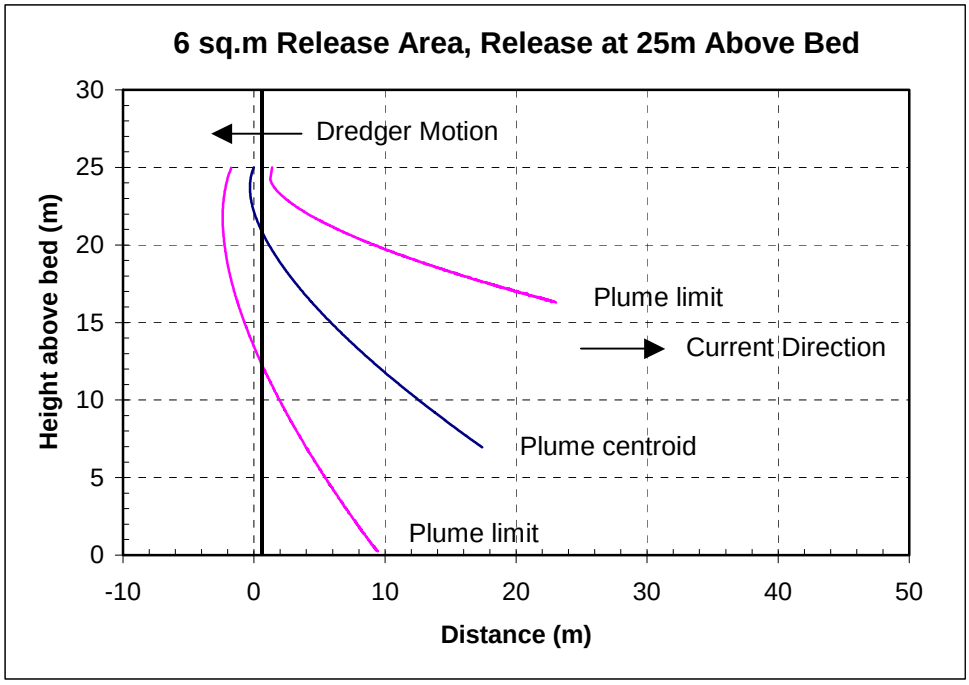

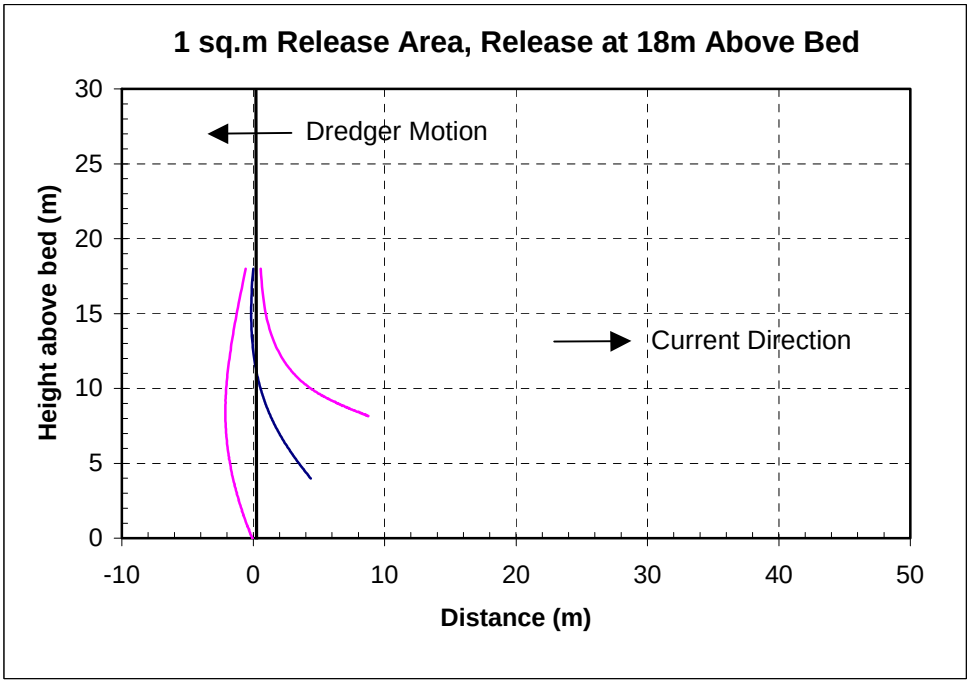

FIGURE 5. The Effect of Hull Release

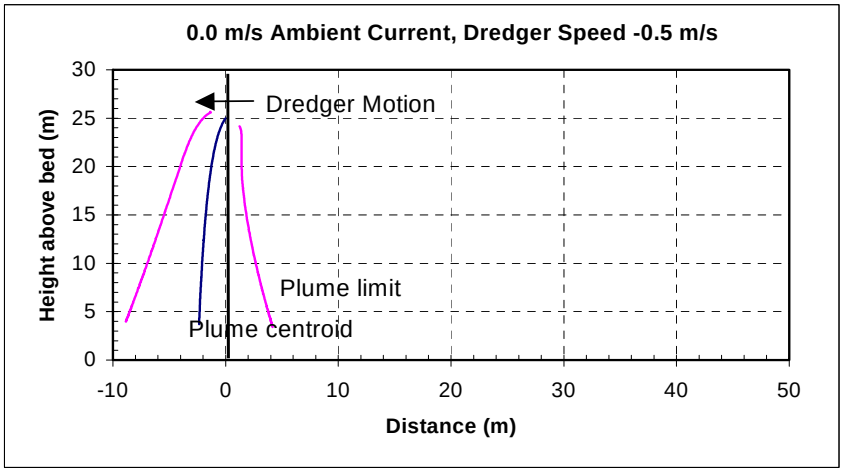

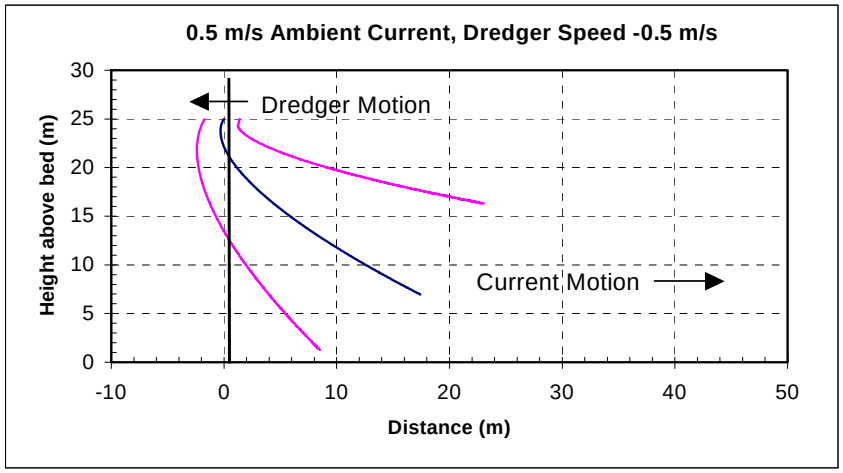

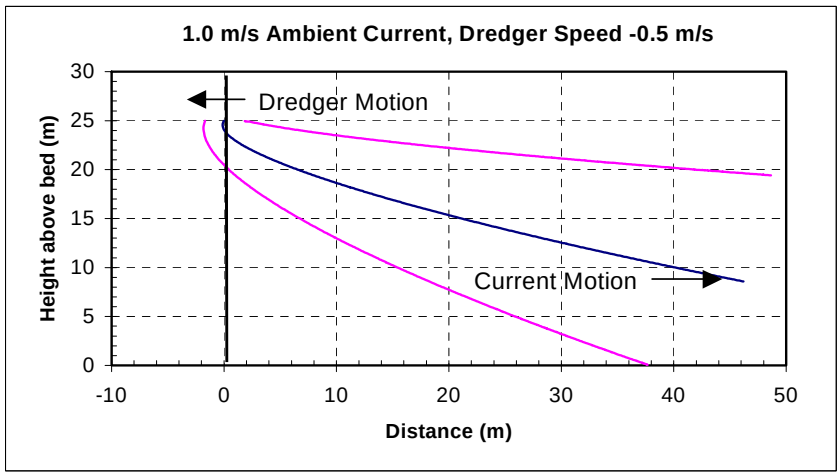

FIGURE 6. The Effect of Current Speed

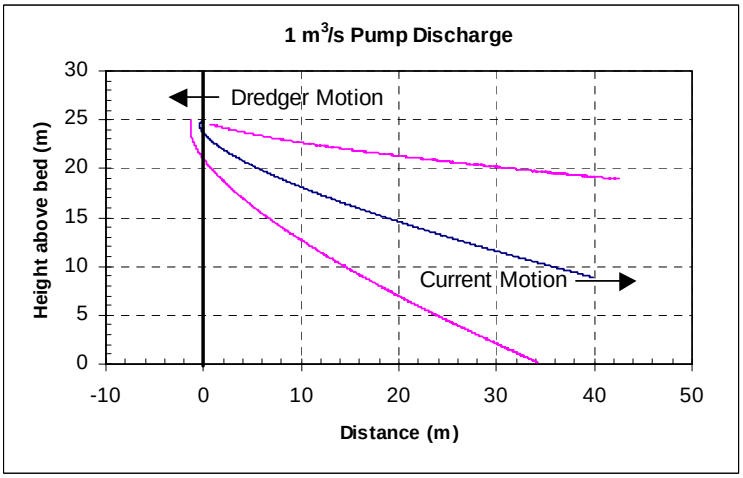

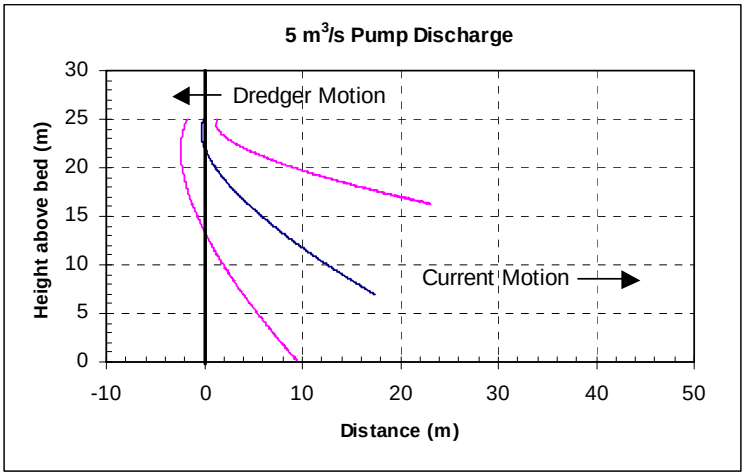

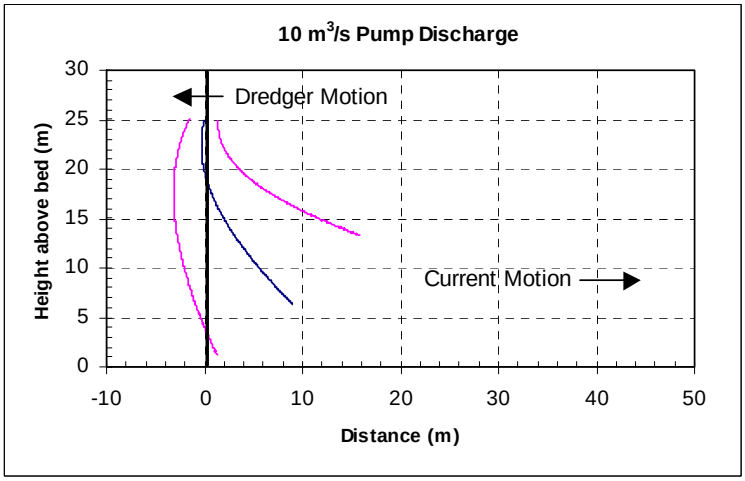

FIGURE 7. Effect of Dredger Pumping Rate

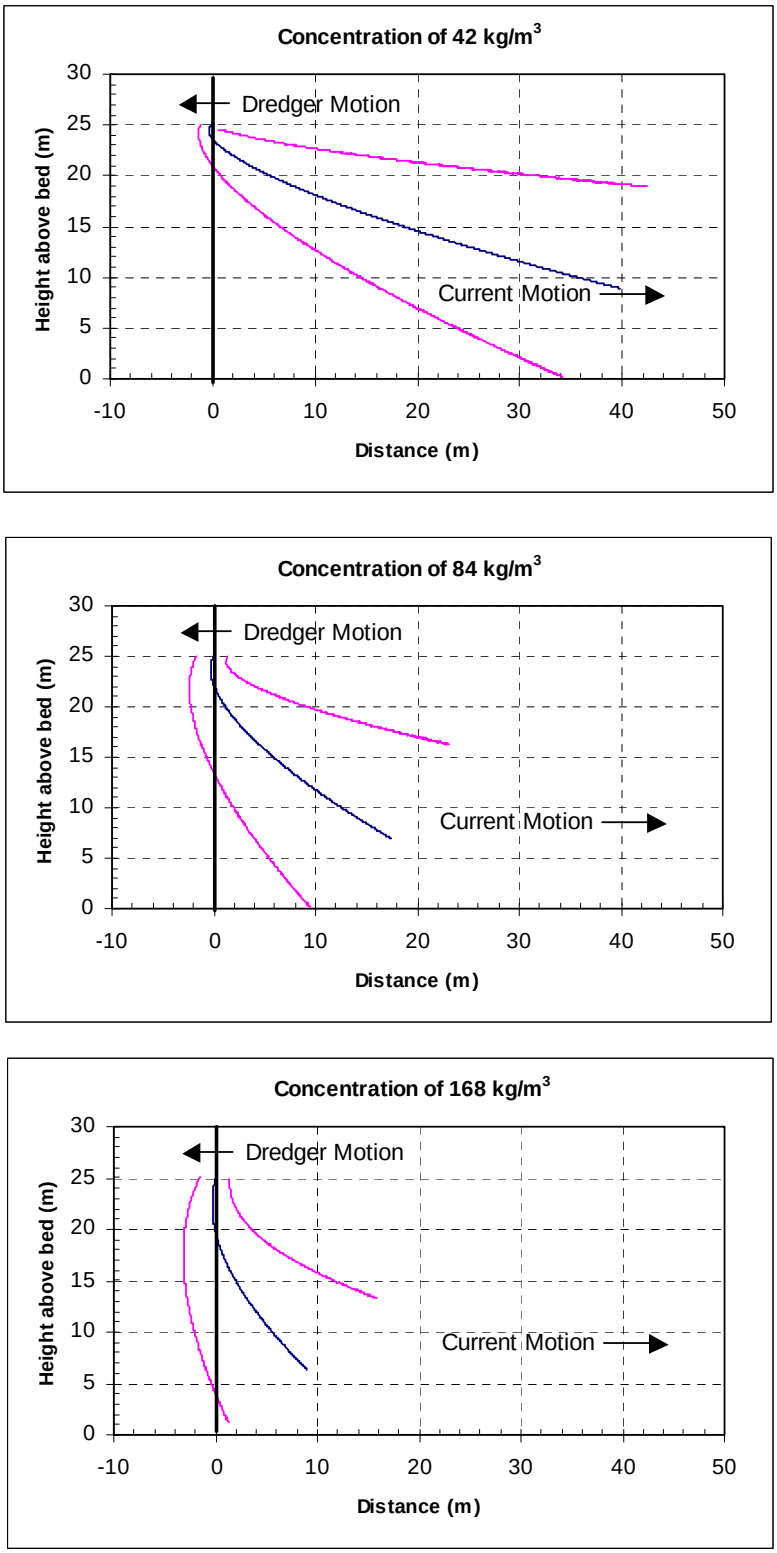

FIGURE 8. Effect of Sediment Concentration

Effect of Stratification

In stratified waters the density of ambient water increases with depth. Therefore as the dynamic plume is released near the surface (in the case of hull release the release is still "nearer" the surface) the entrained ambient water is of a reduced density compared to the density of water near the bed. Since the density differences resulting from salinity differences can be several kilograms per cubic meter it is therefore possible, assuming there is sufficient depth for some initial mixing, for the dynamic plume to reach a level of neutral buoyancy. In practice, the plume will "overshoot" this level due to its inherent momentum but will converge towards this level.

The effect of salinity is illustrated in Figure 9. The descent of a plume in 40 m of stratified water (with the other parameter values listed at the head of Section 5.4.1.2) is illustrated together with the corresponding descent of a plume in unstratified waters. The salinity profile corresponding to the stratified simulation is a linear variation with a bottom density of 1025 kg/m^3 and a surface density of 1020 kg/m^3. The figure shows the path of the plume until its vertical downward speed slows to zero (i.e. including the "overshoot" but not the oscillation and convergence towards the level of neutral buoyancy). It can be seen that the paths of the unstratified and stratified plumes are approximately the same until the terminal depth of descent is approached. This behavior matches the findings of Wright (1984) with buoyant plumes.

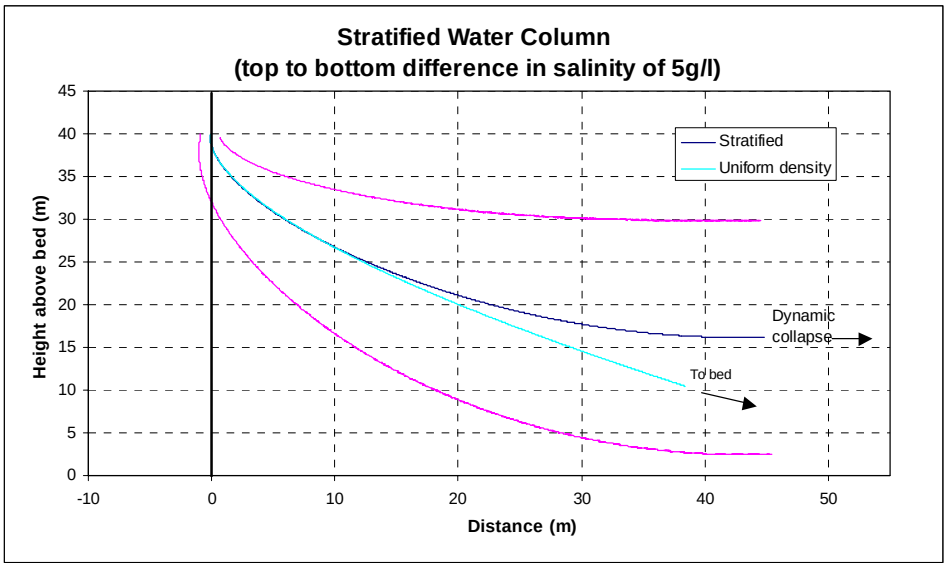

FIGURE 9. The Effect of Salinity on the Dynamic Plume

5.4.2 Collapse of Density Current on Bed

5.4.2.1 Validation

The investigators for this project are not aware of any published in situ field measurements of the validation of the collapse of dynamic plumes resulting from impact on the bed. For this reason it has been necessary to resort to data from laboratory testing. The experiments chosen for the validation of the collapse of two-dimensional dynamic plumes resulting from impact on the bed are those undertaken by Hallworth et al (1998) which include the intrusion of compositional currents (i.e. formed by dissolving salt into water), particle currents (i.e. those formed by suspended sediment) and both types of currents under the influence of ambient current flow.

The experiments were undertaken in a 9.4 m long flume of width 0.26 m and with a depth of water of 0.287 m. A fixed volume of dense fluid, initially held in a reservoir above the mid-point of the channel, was allowed to drain rapidly (in less than a second) into the flow stream through a 3 cm diameter tube positioned just below the free surface. The emerging jet of dense fluid inevitably entrained a significant volume of ambient fluid during its descent and subsequent lateral deflection upon impinging on the solid channel floor.

Compositional (i.e. dissolved) currents were generated by releasing 2 liters of water containing 50 g, 200 g and 400 g of dissolved salt into the ambient flow, to give *initial* (i.e. at the start of the plume descent) excess densities of 25 kg/m^3, 100 kg/m^3 and 200 kg/m^3 respectively. Note that for compositional currents it is the product of the initial cross-sectional area, (which varies linearly with dilution), and g', (a parameter which varies inversely with dilution), which governs the speed of the front. Dilution therefore has no effect for this type of density current.

Particle (i.e. suspended sediment) currents were generated by releasing 2 liters of water containing 50 g, 100 g, 200 g and 400 g of particles made of silicon-carbide, to give initial excess densities of 25 kg/m^3, 100 kg/m^3 and 200 kg/m^3 respectively. These particles were "fairly" (*sic*) monodisperse sizes, non-cohesive and had a (solids) density of 3217 kg/m^3. Three sets of particle sizes were tested - 23μm, 37μm and 53μm – with corresponding differences in settling velocity. For the purposes of this study the tests for the different particle sizes with initial excess density of 100 kg/m^3 were reproduced using the bed collapse model. For this type of density current, the speed of the front is affected by the initial dilution during downward descent. The density at the onset of collapse was calculated using the dynamic descent model (See Section 5.1) and was found to be approximately 12 kg/m^3.

In the paper by Hallworth et al. these experiments were carried out with no ambient current and were repeated with an ambient flow of 2.6 cm/s. For our purposes, we consider the effect of ambient currents on compositional density currents alone as this is sufficient to illustrate the validity of the bed collapse model.

The comparison of observed compositional density current collapse and that predicted by the bed collapse model is shown in Figure 10. The figures show that the model reproduces the

observations well. The corresponding results with ambient current flow are shown in Figure 11. The observed data is reproduced well although the rate of advection of the front for the density current of lowest initial excess density is slightly under-predicted.

The comparison of observed particulate density current collapse and that predicted by the bed collapse model is shown in Figure 12. The results show that the model reproduces the observations well.

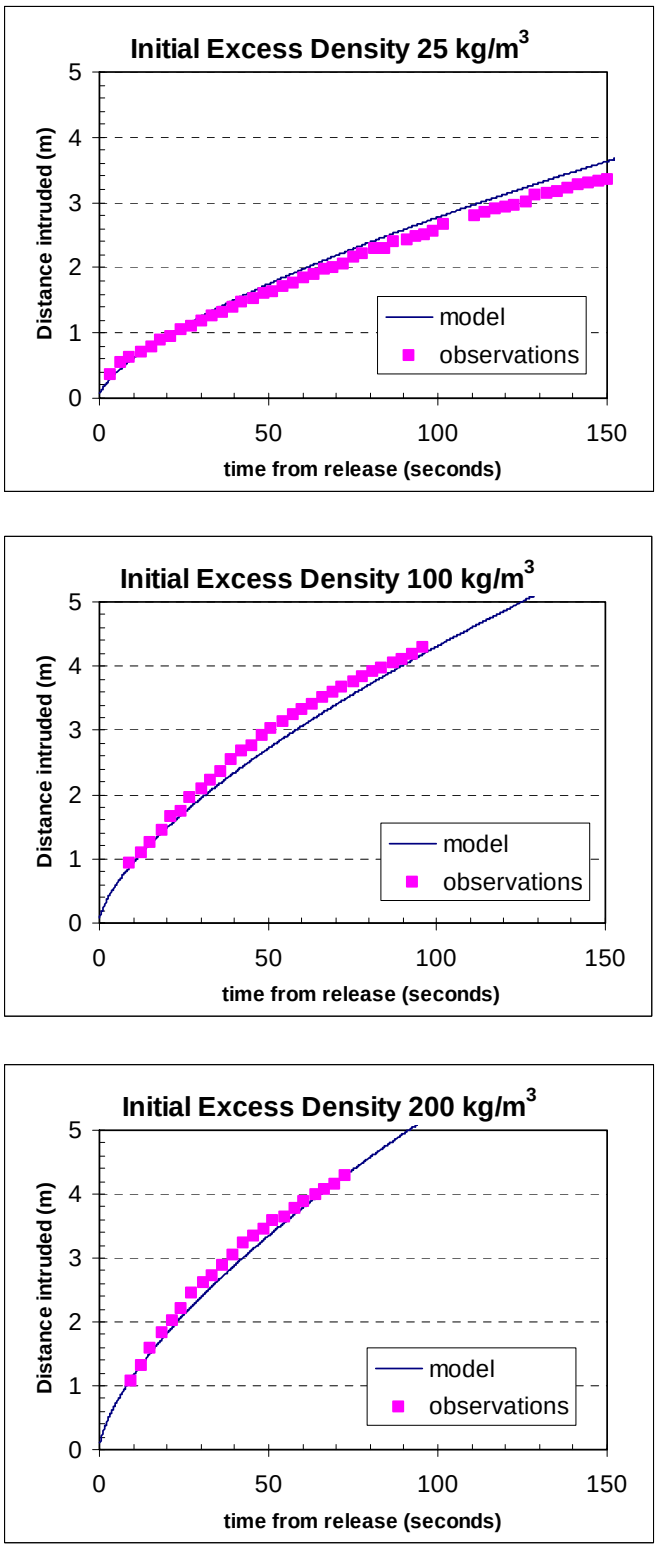

FIGURE 10. Compositional Density Current Collapse

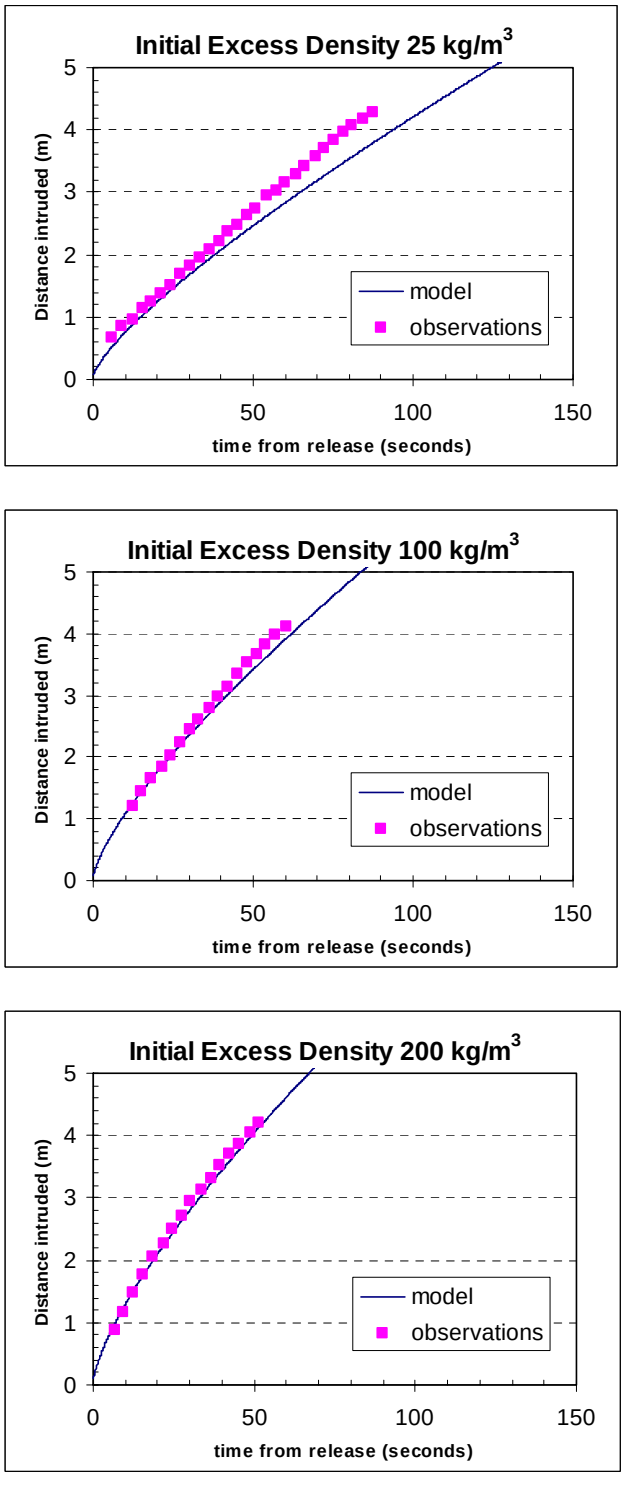

FIGURE 11. Compositional Density Plume Collapse with Ambient Current Flow

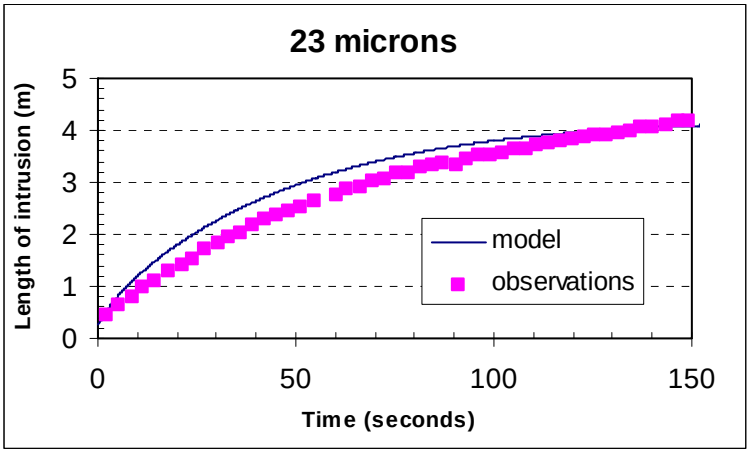

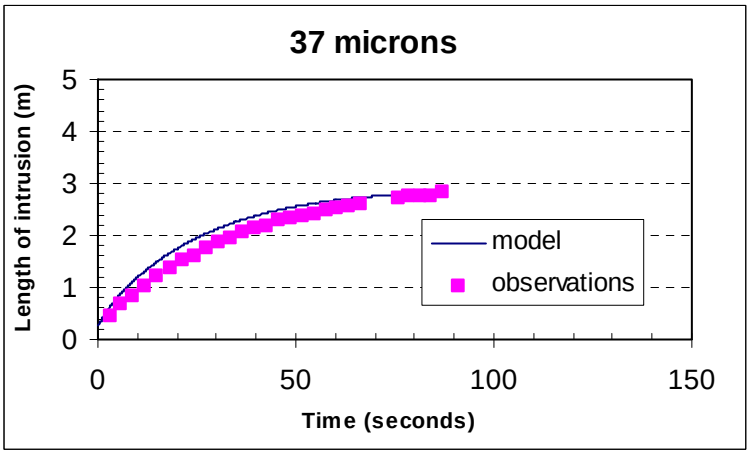

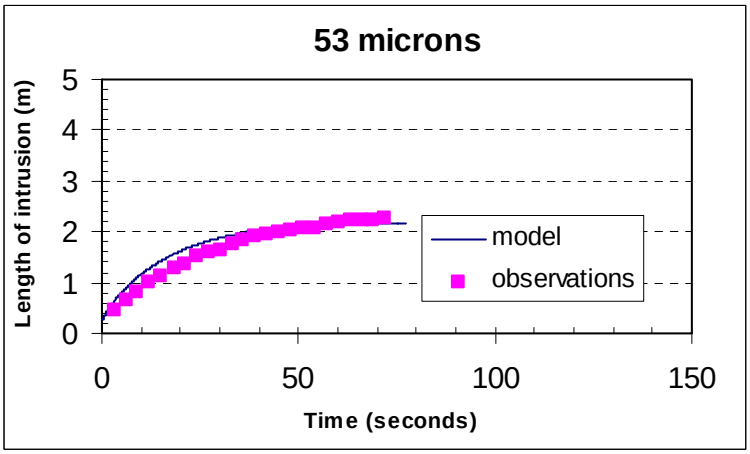

FIGURE 12. Particulate Density Plume Collapse

5.4.2.2 Sensitivity Tests

To illustrate the dependence of the nature of bed collapse on the values of the various governing parameters sensitivity tests were undertaken. The scenarios illustrated in the figures are reasonably representative of those that could be arise from dredging activity and are based on the following parameters (except where specified otherwise):

- Initial cross-sectional area of release (or volume per meter length of density current), 100 m^2
- Excess density of discharge, 1 kg/m^3 (with an ambient density of 1000 kg/m^3)
- Particle size, 150μm.

The figures presented in the following section show the advance of the front of the density current with respect to the original position of the density current centroid.

Effect of Mixture Density (excess above ambient) and Initial Volume

The effects of changes in excess density and changes in initial volume are very similar though the influence of initial volume becomes greater than the effect of mixture density for particulate intrusions. These parameters govern the rate and extent of intrusion of the density current – the greater the excess density and the greater the initial volume, the greater the rate and extent of the intrusion. The influence of these parameters is illustrated in Figure 13.

Effect of Dredger Speed

Dredger speed affects the smearing of the plume impinging on the bed and therefore the initial cross-sectional area ($A = l_0 h_0$) of the density current. A slower dredge speed will result in a greater initial cross-sectional area.

Effect of Particle Size

This parameter also affects the extent of intrusion of the density current in particulate plumes and the concentration of deposited sediment near the initial source. The particle size, the greater the settling velocity and the more quickly the intrusion comes to a halt. The smaller the particle size, the lower the settling velocity and the greater the extent of the intrusion and the more like a compositional current the particulate current becomes. The influence of these parameters is illustrated in Figure 14. The excess density was 1 kg/m^3 for all tests.

Effect of Friction

The effect of friction is smaller than the influences above although friction will become influential when $Cd \sim O(^{h}/_{x})$ providing the settling velocity of the particles is sufficiently small. Increased friction will reduce the rate and extent of intrusion. The influence of this parameter is also illustrated in Figure 15. It can be seen that where settling velocity is relatively high (such as the top graph) the density current comes to a halt well before the effect of friction becomes significant. Where settling velocity is low, however, and the density current is much more like a compositional rather than a particulate density current the effect of friction in the end becomes significant, in this case after about half an hour.

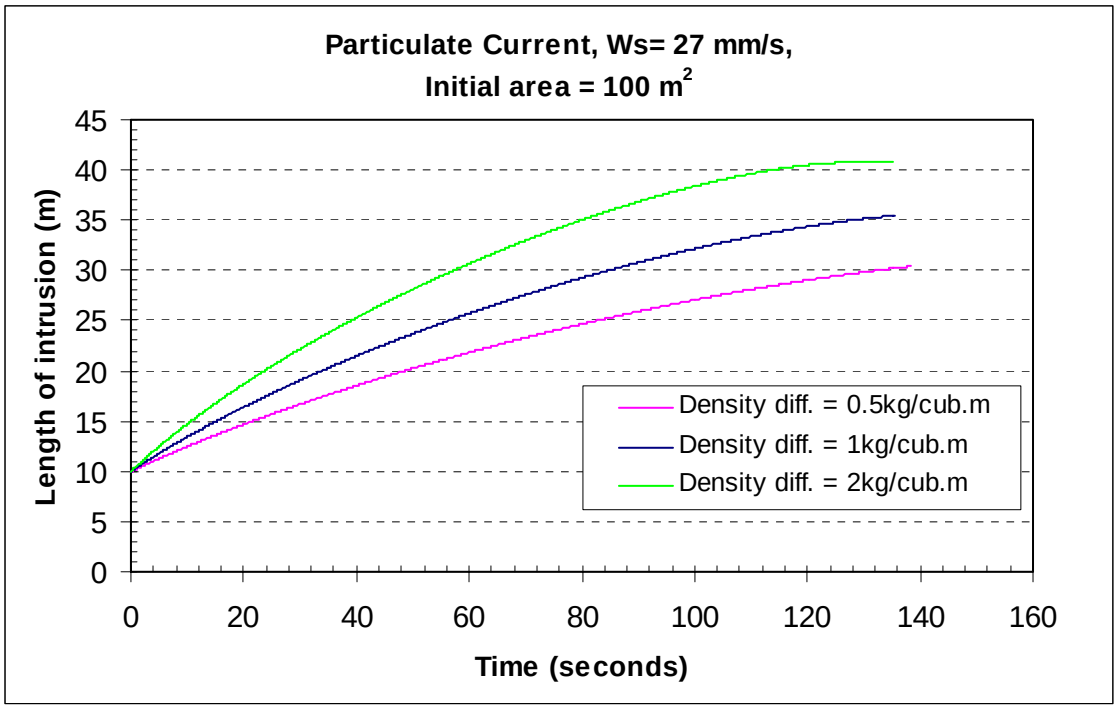

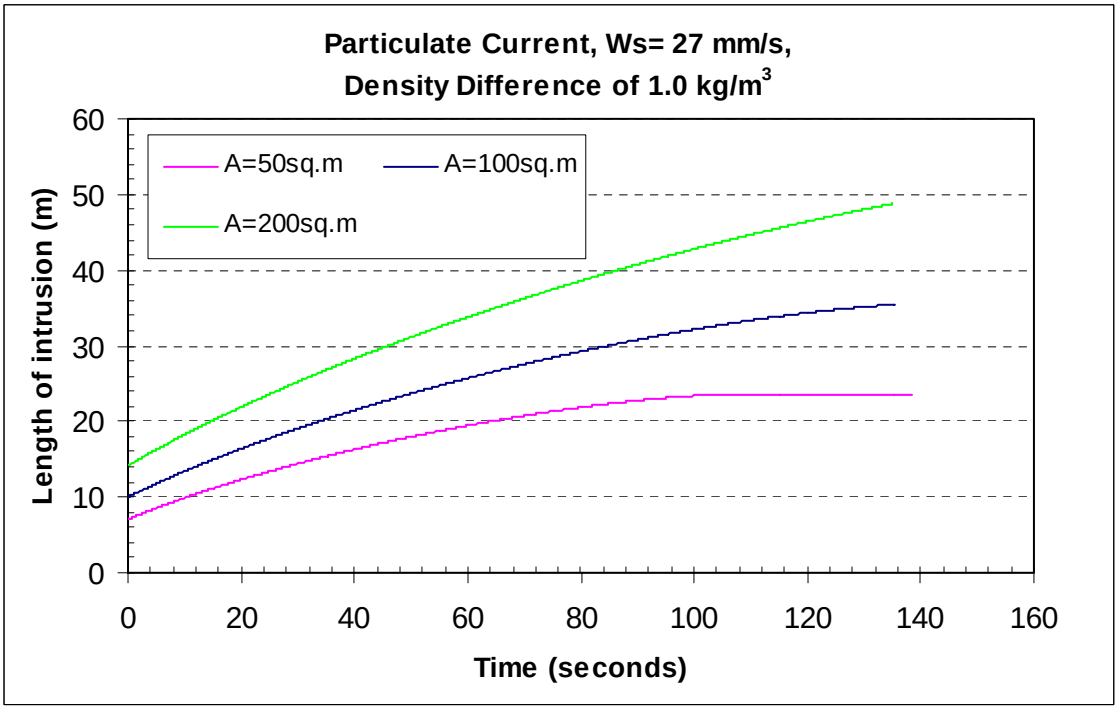

FIGURE 13. The Effect of Mixture Density (Top) and Initial Cross-Section area (Bottom) on Plume Collapse

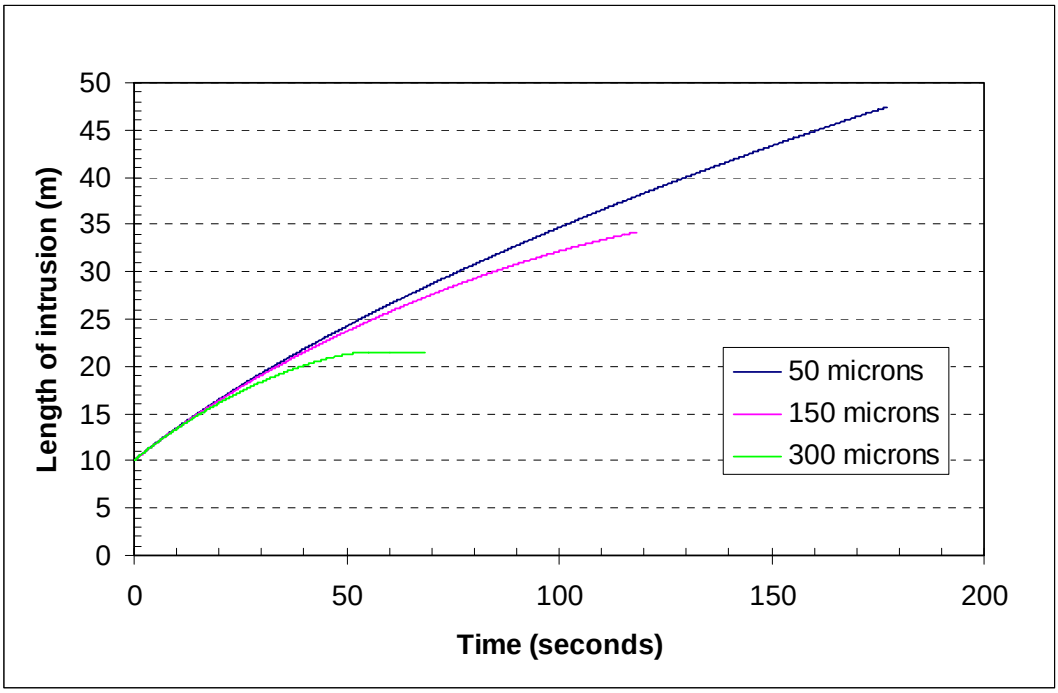

FIGURE 14. The Effect of Particle Size on Density Plume Collapse

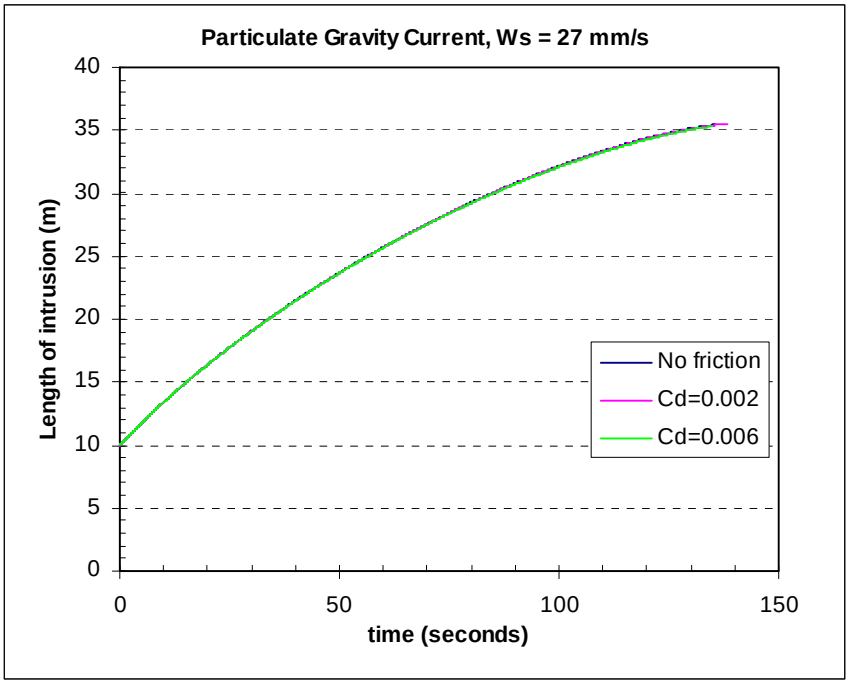

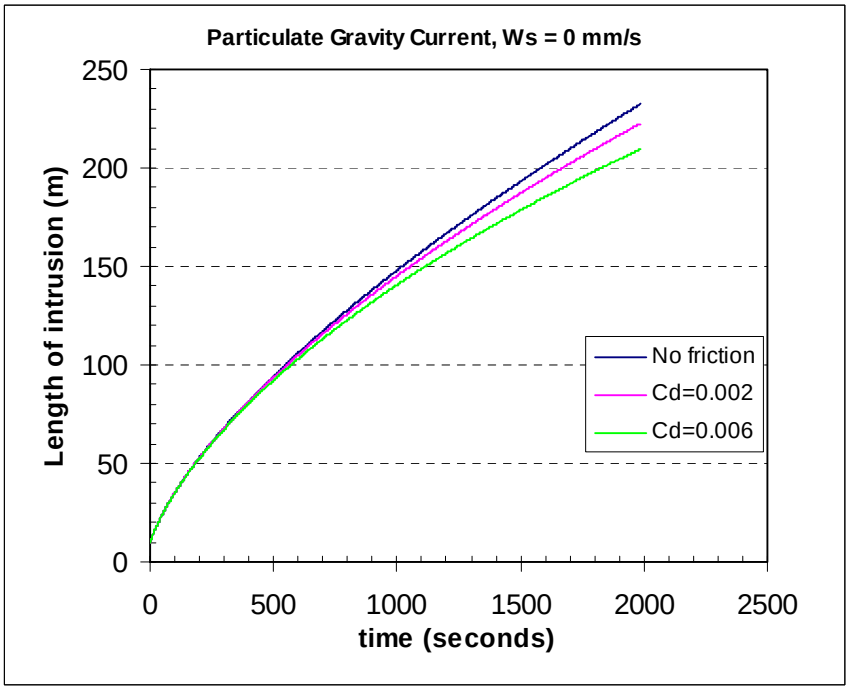

FIGURE 15. The Effect of Particle Size and Bottom Friction on Density Plume Collapse

6.0 THE PASSIVE PLUME MODEL

6.1 Introduction

Flow in a coastal region consists of large-scale tidal motion, wind-driven currents and small-scale turbulent eddies. In order to model the dispersal of suspended mud in such a region, the effects of these flows on suspended mud plumes must be simulated. The random walk dispersal model, the plume model, represents turbulent diffusion as random displacements from the purely advective motion described by the turbulent mean velocities computed by the free surface flow models ADCIRC and TELEMAC.

6.2 Representation of Mud Disturbance

In the plume model, the release of suspended mud in coastal waters is represented as a regular or intermittent discharge of discrete particles. Particles are released throughout a model run to simulate continuous mud disturbance or for part of the run to simulate mud disturbance over an interval during the tidal cycle, for instance to represent the re-suspension of fine sediment during dredging operations. At specified sites a number of particles are released in each model time-step and, in order to simulate the release of suspended mud, the total mud released at each site during a given time interval is divided equally between the released particles. Particles can be released either at the precise coordinates of the specified sites, or distributed randomly, centered on the specified release sites. The particles can be released at the surface or evenly distributed through the water column. This allows the representation of the initial spreading of plumes of material released by, for example, a dredger.

6.3 Large Scale Advection

ADCIRC and TELEMAC simulate tidal flows in coastal waters, including the effects of any thermal or saline stratification and any three-dimensional structure induced by bed friction or wind stress (in this case, estimated from 2D currents). Three components of current speed are calculated at a number of points through the depth and these values are interpolated to establish the precise current at the position of each plume model particle. Each particle is then advected by the local flow conditions. Because the three-dimensional structure of the flow field, effects such as shear dispersion of plumes are automatically represented.

6.4 Turbulent Diffusion

In order to simulate the effects of turbulent eddies on suspended mud plumes in coastal waters, particles in the plume model are subjected to random displacements in addition to the ordered movements which represent advection by mean currents. The motion of simulated plumes is, therefore, a random walk, being the resultant of ordered and random movements. Provided the lengths of the turbulent displacements are correctly chosen, the random step procedure is analogous to the use of turbulent diffusivity in depth-averaged mud transport models. This is discussed in more detail below.

6.4.1 Lateral Diffusion

The horizontal random movement of each particle during a time-step of the plume model consists of a displacement derived from the parameters of the simulation. The displacement of the particle in each of the orthogonal horizontal directions is calculated from a Gaussian distribution, with zero mean and a variance determined from the specified lateral diffusivity. The relationship between the standard deviation of the displacement, the time-step and the diffusivity is defined in Fischer et al. (1979) as:

$$\frac{\Delta^2}{\Delta t} = 2D \qquad (6.1)$$

where

Δ = standard deviation of the turbulent lateral displacement (m)

Δt = time-step (s)

D = lateral diffusivity (m^2s^{-1}).

In the plume model simulation, a lateral diffusivity is specified, which the model reduces to a turbulent displacement using Equation (6.1). No directional bias is required for the turbulent movements, as the effects of shear diffusion are effectively included through the calculated depth structure in the mean current profile.

6.4.2 Vertical Diffusion

Whilst lateral movements associated with turbulent eddies are satisfactorily represented by the specification of a constant diffusivity, vertical turbulent motions can vary significantly horizontally and over the water depth, so that vertical diffusivities must be computed from the characteristics of the mean flow field, rather than specified as constants. In neutral conditions, the vertical diffusivity, K_z, is given by:

$$K_z = 0.16\, h^2 \left(1 - \frac{h}{d}\right) \frac{\partial u}{\partial z} \qquad (6.2)$$

where

h is the height of particle above the bed;

d, the water depth;

0.16, the square of Von Karman constant;

u, the current speed; and

z, the vertical coordinate.

The value of the vertical diffusivity is calculated at each particle position then a vertical turbulent displacement is derived for each particle from its K_z value using an equation analogous to (6.1) for the lateral turbulent displacement.

If the water density varies in the vertical, then stable stratification can occur, whereby the turbulence is damped by buoyancy effects. In this case the mixing length is adapted by a function of the Richardson number, based on field measurements (Odd and Rodger, 1978).

6.4.3 Drift Velocities

A particle undergoes a random walk as follows:

$$x^n = x^{n-1} + A(x^{n-1}, t^{n-1})\Delta t + B(x^{n-1}, t^{n-1})\sqrt{\Delta t}\ \xi^n \qquad (6.3)$$

where x^n is the position of the particle at time t^n, A is the advection velocity at timestep $n-1$ and B is a matrix giving the diffusivity. ξ is a vector of three random numbers, each drawn from a normal distribution with unit variance and zero mean. In the case of the plume model, B is diagonal, with the first two entries equal to $2D$ (as introduced in the previous section) and the third diagonal entry being equal to the local value of $2K_z$.

The movement of a particle undergoing a random walk as described in Equation (6.3) can be described by the Fokker-Planck equation in the limit of a very large number of particles and a very short timestep, where we introduce subscripts i,j and k running over the three coordinate directions:

$$\frac{\partial f}{\partial t} + \frac{\partial}{\partial x_i}(A_i f) = \frac{\partial^2}{\partial x_i \partial x_j}\left(\frac{1}{2} B_{ik} B_{jk} f\right) \qquad (6.4)$$

The probability density function $f(x,t|x_0,t_0)$ is the probability of a particle which starts at position x_0 at time t_0 being at position x at time t.

Equation (6.4) can be compared with the advection-diffusion equation for the concentration of a pollutant, c:

$$\frac{\partial c}{\partial t} + \frac{\partial}{\partial x_i}(u_i c) = \frac{\partial}{\partial x_i}\left(K_{ik} \frac{\partial}{\partial x_k} c\right) \qquad (6.5)$$

where K_{ik} is the eddy diffusion matrix, diagonal in our case but not necessarily so. Thus identifying f with c, we can see that the two equations are equivalent provided that we take the advection velocity as:

$$A_i = u_i + \frac{\partial}{\partial x_k} K_{ik} \qquad (6.6)$$

In the case of the plume model, the diffusivity varies only in the vertical and is constant in the horizontal, so the horizontal advection velocity is simply the flow velocity (assuming that the relatively small effects of changing water depth can be neglected). However, when considering the movement of particles in the vertical it is important to include the gradient of the diffusivity (often referred to as a drift velocity) in the advection step. If this term is omitted then particles tend to accumulate in regions of low diffusivity, which in our case means at the surface and at the bed.

This subject is discussed in considerably more detail in Monin and Yaglom (1971), Tompson and Gelhar (1990), Dimou and Adams (1993), and Legg and Raupach (1982).

6.5 Sedimentation Processes

6.5.1 Settling

In the plume model, the settling velocity (w_s) of suspended mud is assumed to be related to the mud concentration (c) through an equation of the form:

$$w_s = \max(w_{\min}, Pc^Q) \qquad (6.7)$$

where w_{min}, P and Q are empirical constants. Having computed a suspended mud concentration field, as described subsequently in this section, a settling velocity can be computed in each output grid cell from Equation (6.7) and used to derive a downward displacement for each particle during each time-step of a model simulation. This displacement is added vectorially to the other computed ordered and random particle displacements. Note that there is a specified minimum value of w_s. This results in settling velocities being constant at low suspended mud concentrations.

6.5.2 Deposition

The plume model computes bed shear stresses from the input tidal flow fields using the rough turbulent, based on a bed roughness length input by the user. If the effects of storm waves on mud deposition and erosion at the sea bed are to be included in a model simulation, a bed shear stress associated with wave orbital motions, computed from the results of mathematical wave model simulations, is added to that resulting from the simulated tidal currents (HR Wallingford, 1991). Where the computed bed stress, τ_b, falls below a specified critical value, τ_d, and the water is sufficiently deep, then deposition is assumed to occur. Mud deposition is represented in the plume model by particles approaching the seabed becoming inactive when τ_b is below τ_d. Whilst active particles in the water column contribute to the computed suspended mud concentration field, as described subsequently in this appendix, inactive particles contribute to the mud deposit field.

In shallow areas, where tidal currents are sufficiently weak to allow mud accretion, normal wave action can prevent mud deposition. This effect is included empirically in the plume model, by specifying a minimum water depth below which deposition does not occur.

6.5.3 Erosion

The erosion of mud deposits from the sea bed is represented in the plume model by inactive particles returning to the water column (becoming active) when τ_b exceeds a specified erosional shear strength, τ_e. The number of particles, which become re-suspended in each cell of the output grid in each time-step of a simulation is determined by the equation:

$$\text{Erosion Rate} = M(\tau_b - \tau_e) \qquad (6.8)$$

where M is an empirical erosion constant.

6.6 Computation of Suspended Mud Concentrations

In the plume model, suspended mud concentrations are computed on a multi-layer square grid designed to resolve the essential features of relatively small-scale plumes. The layers of the output grid are separated by the element planes of the ADCIRC grid, so that if there are N planes in the ADCIRC/TELEMAC mesh, there are N-1 layers in the plume model output grid. In each the plume model grid cell a concentration is derived by dividing the total suspended mud represented by all the active particles in that cell by the volume of the cell.

6.7 Computation of Mud Deposit Distributions

The plume model computes mud deposit distributions by summing the mass of mud represented by the inactive particles in each cell of the output grid, and assuming that the resulting mass is evenly distributed over the cell area.

The model is usually used to simulate the dispersal of mud released by dredging-related activity in one of the following three ways:

(a) Dredging in shallow areas releases small quantities of mud into the water column close to the seabed.

(b) When dredging for marine fill, the coarse sediment content of dredged material may be increased by over-filling of the receiving barge; with coarse material settling rapidly in the barge and the fine mud component remaining in suspension and re-entering the water column.

The disposal of dredged spoil in deep water results in a dense column of sediment descending rapidly to the seabed. Entrainment of water into this column results in some of the fine mud component entering the water column.

The model is most suited to simulating detailed distributions of suspended mud and mud deposits near areas of dredging-related activity over a few tidal cycles. The far-field effects of dredging-related activity can be simulated using other models in use at HR Wallingford.

7.0 THE HYDRODYNAMIC MODEL

7.1 Introduction

Accurately defining the hydrodynamic (water levels and currents) flow field is an important first step in the overall plume modeling process. The model used as the basis for development of the MMS Plume Model operates with the TELEMAC model developed in France. In this study, linkages have been developed to a second, widely used numerical model, ADCIRC-2D.

7.2 Description of ADCIRC

ADCIRC is a finite element-based, hydrodynamic model supported and used extensively by the U.S. Army Corps of Engineers for coastal and estuarine numerical simulations. The model has been undergoing development since about 1990, with J.J. Westerink, R.A. Luettich, and Norman Scheffner being the major contributors to the model. The model is available as either a two-dimensional depth integrated model or as a barotropic three-dimensional model, both of which use an unstructured triangular mesh to represent the bathymetry. ADCIRC is part of a new generation of finite element models that is replacing the older model technology that was developed in the 1970's. ADCIRC uses the Generalized Wave Continuity Equation (GWCE) formulation of the shallow water equations. Figure 16 shows a typical example of a finite element grid used as input to ADCIRC.

ADCIRC has been widely applied by both U.S. Government agencies and the private sector for tidal and storm surge predictions in regions including the western North Atlantic, the Gulf of Mexico, the Caribbean Sea, the eastern Pacific Ocean, the Mediterranean Sea as well as many other sites around the world. The model is capable of either Cartesian or spherical coordinates, and may optionally include tidal potential (gravitational forces) for large-scale simulations. Boundary conditions in the model may be either tidal constituents or time series. Flooding and drying is implemented in the model, as is atmospheric forcing such as wind and pressure fields.

Full details in use of the model may be found in either Leuttich and Westerink (2000) or an on-line users manual available at:

http://www.marine.unc.edu/C_CATS/adcirc/document/ADCIRC_main_frame.html

Leuttich and Westerink (2003) provides a complete description of the theory and equations behind the ADCIRC model.

Although many different hydrodynamic models could potentially be used as input to the Plume model, some of the advantages of the ADCIRC model with respect to the goals of MMS are:

- ADCIRC is widely supported and used. The model has a relatively low cost, and an excellent graphic interface for use of the model, the Surface Modeling System (SMS), has been developed by the Corps of Engineers.

- The model is available in both two-dimensional and three-dimensional versions. Although the present version of the Plume model only has an interface into ADCIRC-2D, linkages to the three-dimensional version could be easily developed.

- The use of the finite element approach is ideal for undertaking detailed hydrodynamic simulations of the offshore shoals. A high-resolution grid can be developed that properly resolves the shoal details, and transitions to a coarse grid spacing at model boundaries distant from the area of interest. The grid resolution can vary through several orders of magnitude in terms of spacing.

- A complete ADCIRC tidal constituent database has been developed for the western North Atlantic and the Gulf of Mexico. Users of the model can readily extract model boundary information from this database, bypassing the time consuming and difficult process of creating suitable model boundary conditions at each shoal site.

- The model is fast and efficient, important when using the model to explore various "what-if" scenarios.

The ADCIRC model may be purchased commercially through various sources.

In this project, the two-dimensional version of ADCIRC has been utilized; however, a three-dimensional flow field is created for input to the Plume Model using a logarithmic vertical profile based on the input ADCIRC bottom roughness value.

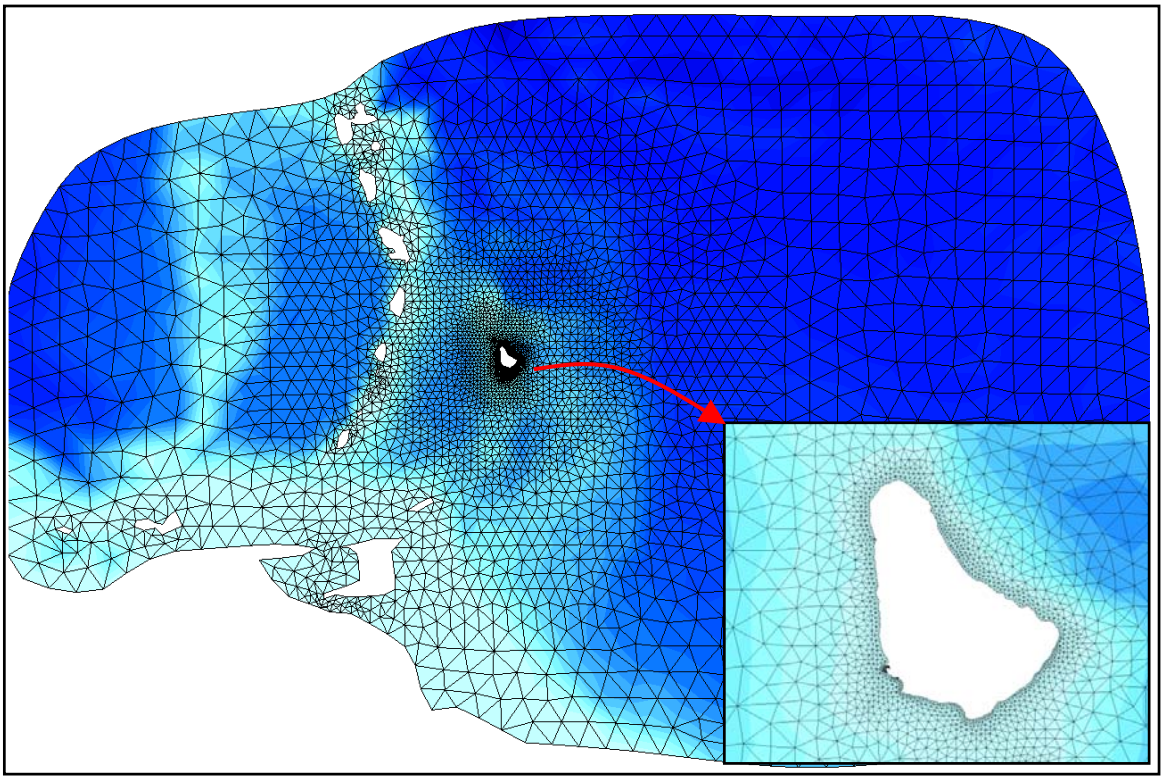

FIGURE 16. An ADCIRC Finite Element Grid Developed for the Island of Barbados

7.3 Description of TELEMAC-3D

TELEMAC is a finite element-based, hydrodynamic model developed by LNHE, Paris and supported by HR Wallingford (UK), SOGREAH (France). The model is available as either a two-dimensional depth integrated model or as a three-dimensional model which has both hydrostatic and non-hydrostatic options. Both versions of the model use an unstructured triangular mesh and solve the shallow water equations.

TELEMAC has been widely applied by consultants and Universities throughout Europe for tidal and storm surge predictions in all regions of the world. The model is capable of either Cartesian or spherical coordinates. The model is written to allow the user full flexibility in introducing initial and boundary conditions. Flooding and drying is implemented in the model, as is atmospheric forcing such as wind and pressure fields.

A description of the TELEMAC model may be found at www.telemacsystem.com

8.0 NUMERICAL MODEL INTEGRATION AND VISUALIZATON

The MMS Plume Model requires a wide range of information at input and generates an extensive amount of data at output. In order to aid in the use and interpretation of the model, various pre- and post-processing facilities were developed. Specifically, the following software components were created:

- A Graphical Users Interface for input.
- A three-dimensional visualization tool for examining the model output.

Various features of these tools are outlined in the following sub-sections. More detailed descriptions of the software are provided in both the Plume Model Users Guide (Baird, 2004a) as well as in the Plume Animator Users Guide (Baird, 2004b).

8.1 The Plume Model Graphical User Interface (GUI)

A key input to the Plume Model is a "steering file" that contains information on all of the variables and files utilized within the model. The GUI simply provides a straight-forward means to systematically generate this steering file. It is designed a stand-alone software tool that can be invoked separately from any visualization or use of the model itself, and carries out some basic error checking on the various model inputs. Default values are provided for many of the input fields.

There are two distinct portions to the GUI, triggered by a push-button, that address generation of steering files for both the Process Model as well as the actual Plume Model. Figures 17 and 18 show example screen snapshots from both model input configurations. The input data are grouped by function under a set of tabs along the top of the interface. Basic input to the model is performed by use of direct alphanumeric entry or checkbox, depending on the type of data considered.

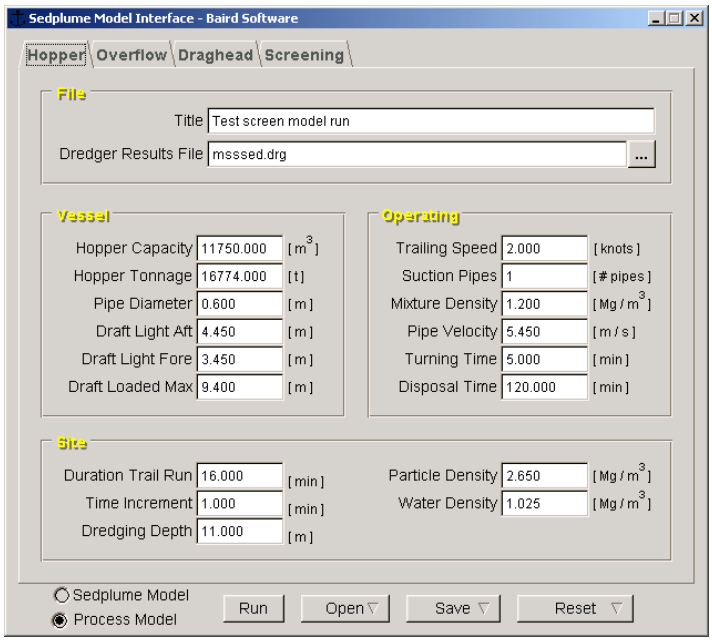

FIGURE 17. Snapshot of the GUI for the Process Model

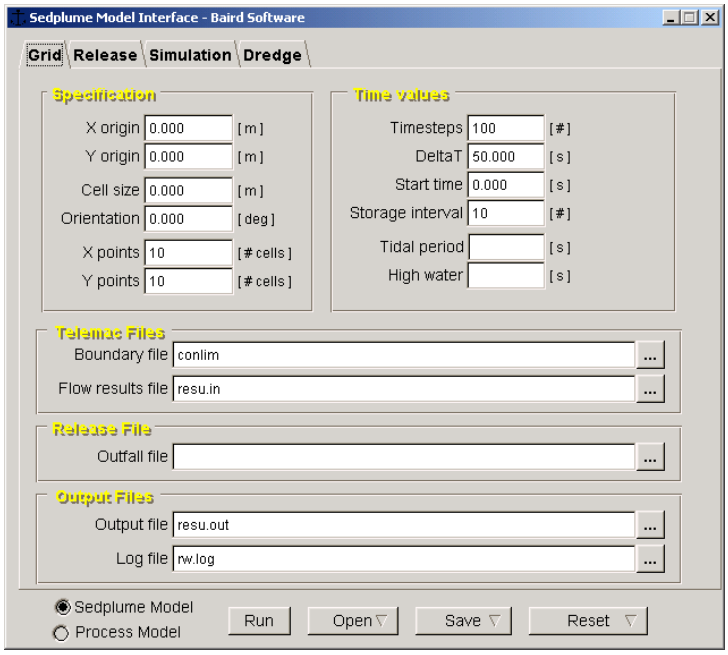

FIGURE 18. Snapshot of the GUI for the Plume Model

8.2 The Plume Animator

Built upon the framework of a very powerful Unix visualization tool developed by Baird Software, the Plume Animator provides a comprehensive three-dimensional visualization environment for exploring the Plume Model output. It contains a variety of features including:

- The ability to generate time-varying 3D views of the sediment plumes and seabed bathymetry.
- Show time-varying sediment accumulations by means of color-contoured maps draped over the existing seabed bathymetry.
- Vertical and horizontal slicing through the plume concentration data.
- Display of the ADCIRC hydrodynamic data (water levels, current vectors, etc.).
- Generate animated flights through the datasets.
- Fully interactive graphical exploration of the data by means of mouse control.
- View two or more datasets simultaneously in different viewports for model run comparisons.
- A wide range of contour coloring options and display types.

Figure 19 illustrates a small portion of the type of visualization that can be created with the Plume Animator.

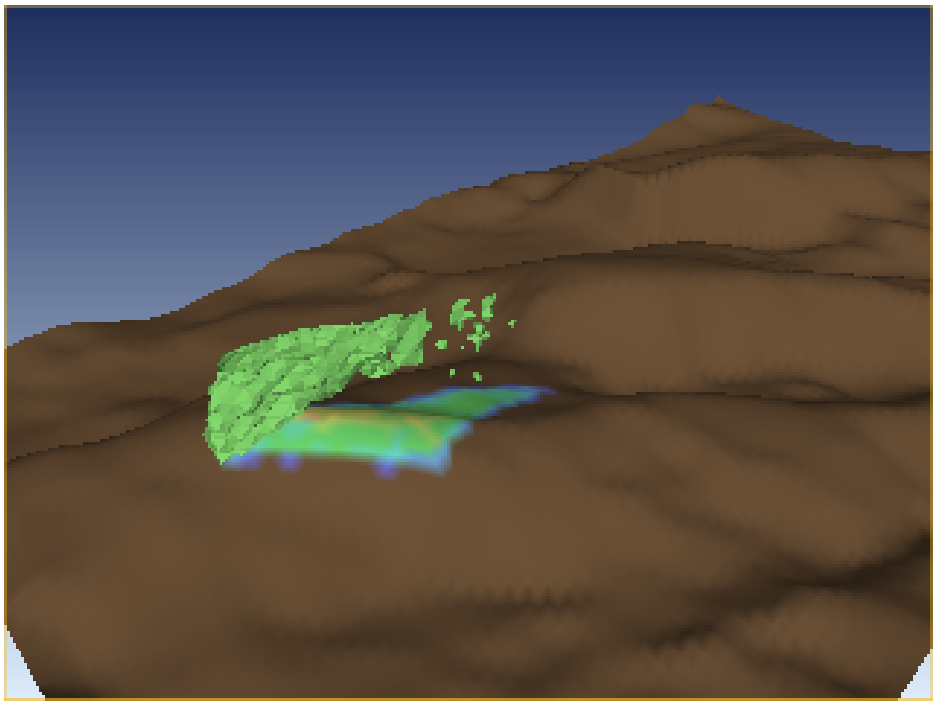

FIGURE 19. Example Output from the Plume Animator [plume isosurface is shown along with color contours of seabed sediment accumulation]

9.0 PLUME MODEL SENSITIVITY TESTING

9.1 Introduction

A sensitivity analysis was carried out separately for both the Process Model and the Plume Model. The following section summarizes the trends observed during the analyses. The sensitivity analysis that was carried out for the Plume model included the following two different sets of test cases.

1. Model Sensitivity to Physical Parameters (Passive Model Only): Assuming a stationary outfall and use of the Passive Plume model only (no Dynamic Plume), various physical parameters were examined.

2. Model Sensitivity to Physical Parameters (Dynamic Plume Model Included): Using the model in its most complete sense with the trailer process result file and the trailer path file, key parameters such as sediment size, mass rate and flow rate were examined.

The model results were compared and analyzed using two-dimensional horizontal and vertical (slice) plots from the Baird Plume Animator, which describe the plume dynamics in the test basin as well as bed accumulation. Samples of these plots are presented in Figure 20.

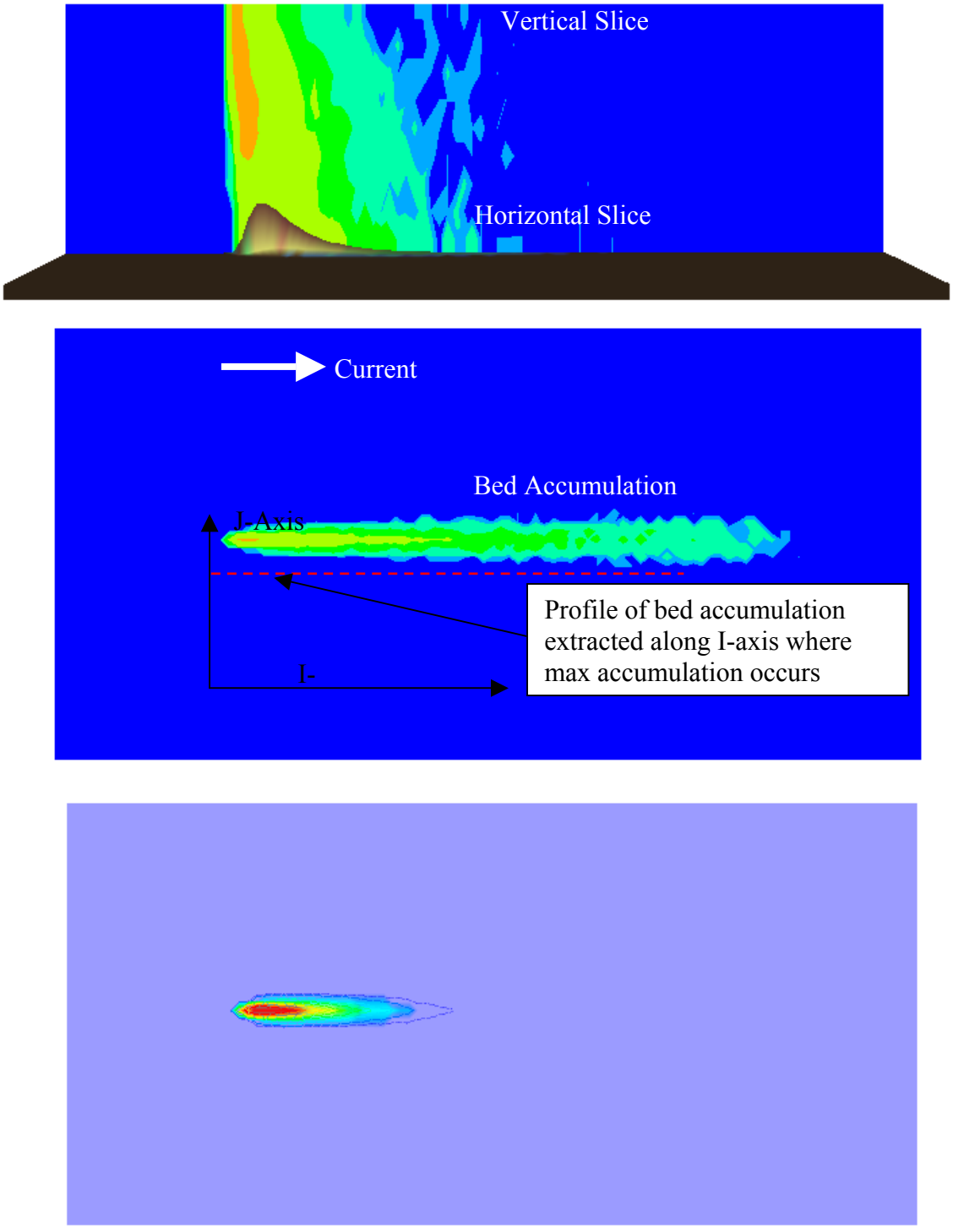

FIGURE 20. Sample 2D Plots Used to Aid in the Analysis of the Model Results.

Graphical methods were also used to compare various test cases. A utility program was developed that could extract a profile of bed accumulation in meters along the *I-axis* where the maximum bed accumulation occurred (see Figure 20). The program also calculated the footprint of bed accumulation on the test basin floor by determining the number of grid points in the model that exceed pre-defined depths of 0.001, 0.003, 0.005, 0.01, 0.025, 0.05, 0.1, 0.25, 0.5, 1.0, and 2.5 m. Examples of these two types of plots are presented in Figure 21.

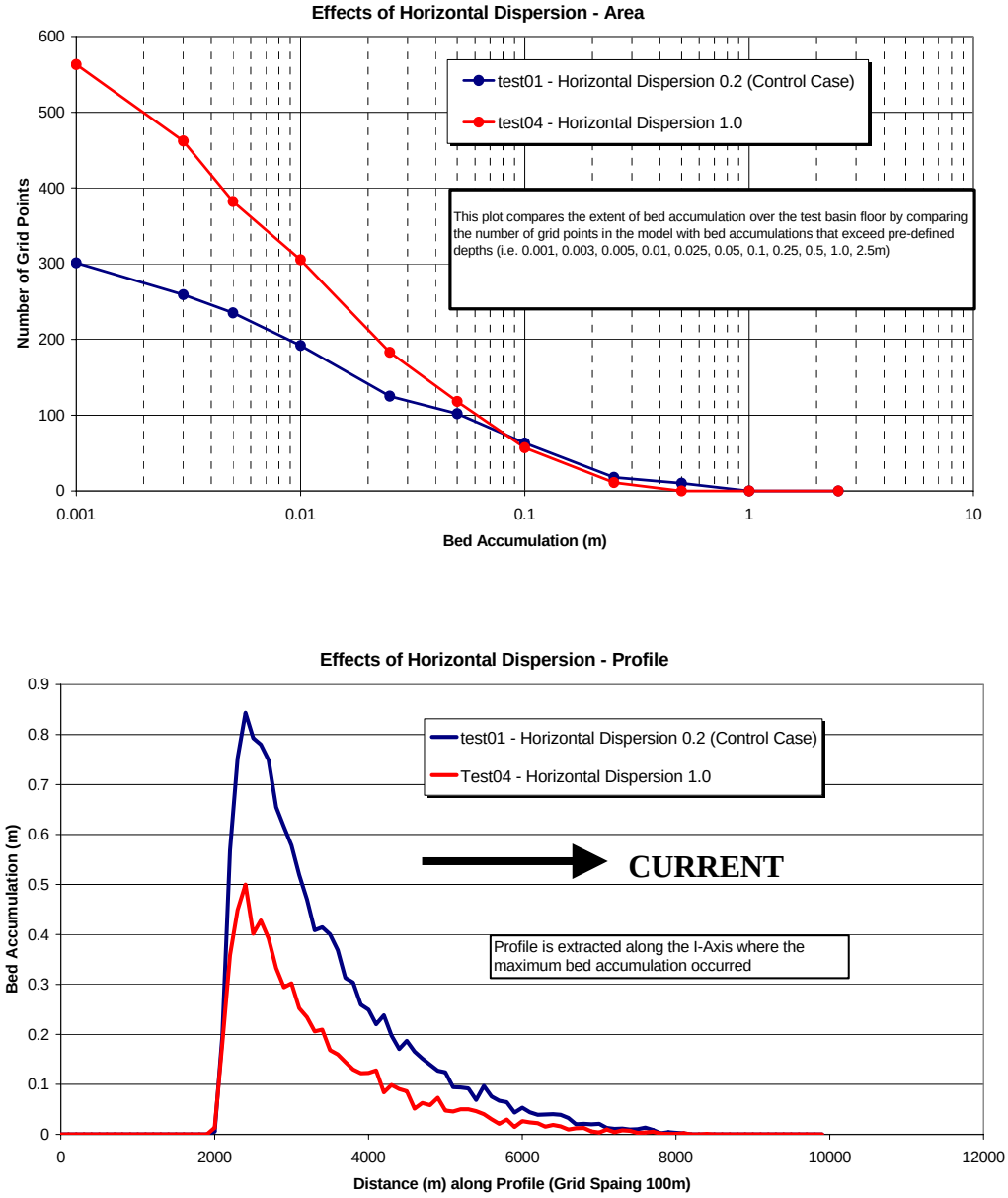

FIGURE 21. Graphical Plots used to Aid in the Analysis of the Model Results.

9.2 Physical Features of the Test Basin

9.2.1 Flow Model

The 2D finite element model ADCIRC was used to develop the flow fields in the test basin. These currents were then converted to a three-dimensional flow field by applying a logarithmic velocity profile that was determined based on a bed roughness coefficient. The dimensions of the grid are 40 km long x 10 km wide x 15 m deep. Unless otherwise stated, a flow field with 15 cm/s surface currents was used and is shown in Figure 22.

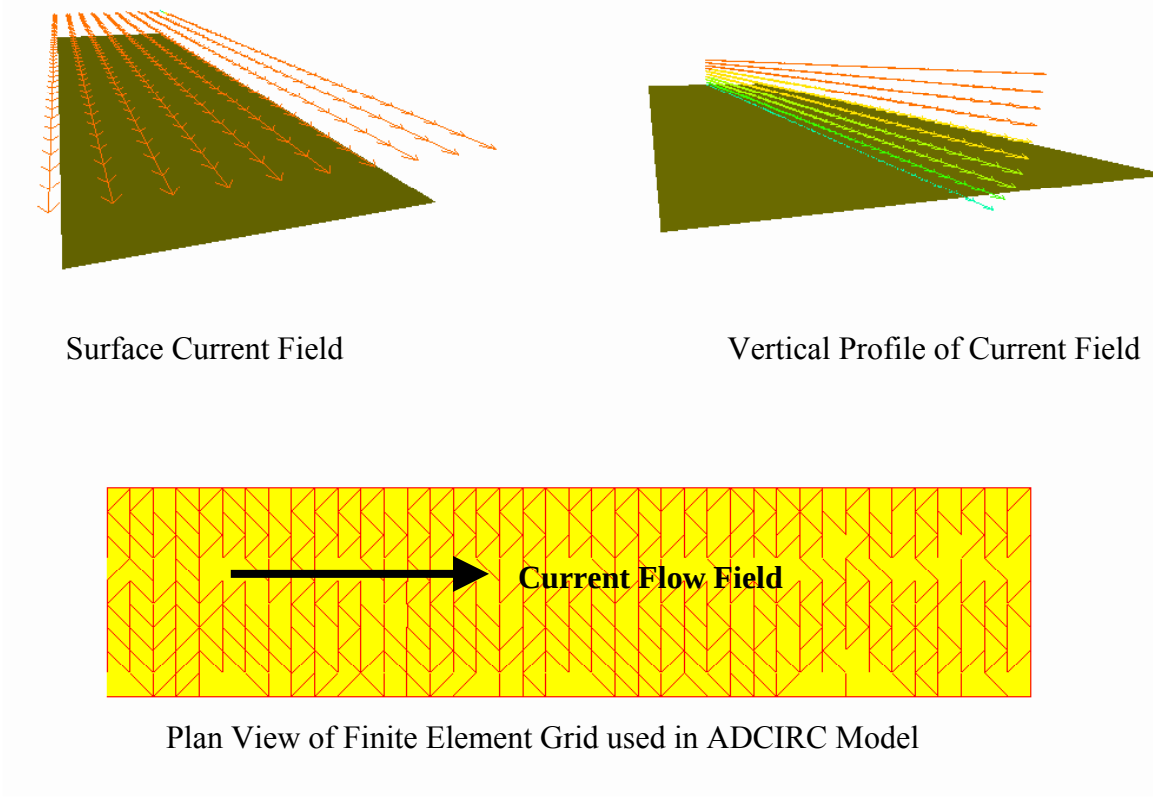

FIGURE 22. 3D Flow Fields Developed from the 2D ADCIRC Model Results

9.2.2 Plume Model Setup

Although the Plume model reproduces the 3D movement of sedimentation a finite element grid, the results are output onto a rectangular grid. The grid is shown in Figure 23 along with grid dimensions.

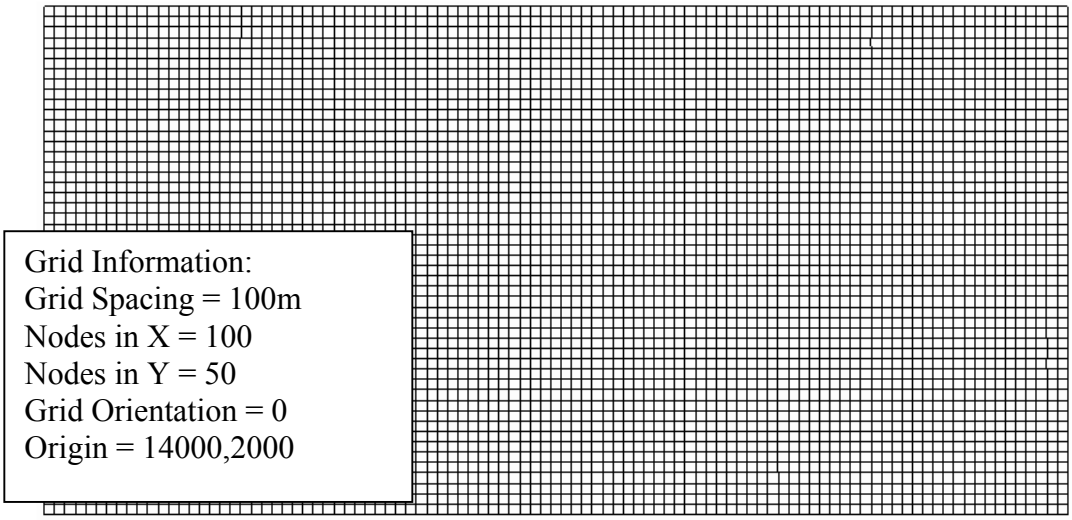

FIGURE 23. Shows the Grid Dimensions of the Plume Model Grid

As noted previously, the Plume model is capable of simulating three distinct phases of the dredging process using the following integrated models:

1. Process Model – Simulates the removal of in-situ sediment, the screening process including discharge of rejected material, settlement in the hopper and the loss of fine fractions to the water column as a plume.
2. Dynamic Plume Model – Reproduces the initial (dynamic) phase of dispersion. It reads in the output from the process model (i.e. sediment distribution of the overflow) and simulates the interaction of the sediment plume as it descends to the ocean floor.
3. Passive Plume Model – Reproduces the second (passive) phase of dispersion that is the plume dynamics that occur as a result of ambient current fields.

It is important to recognize that different time steps and frames of reference are used at various stages of the modeling process (i.e. Dynamic versus Passive). Descent of the dynamic plume is simulated using a Lagrangian technique (i.e. relative to the plume element), once the plume hits bottom or achieves neutral buoyancy the numerical modeling is referenced to the ocean bed. The results from the Dynamic Plume model are passed through to the passive model during the final state of collapse and it is here that the modeling is relative to the dredger position so that the results from the dynamic plume model can be used to represent sediment release over many time steps.

The following sections focus on the sensitivity analysis that was carried out on the Plume model. The discussions presented below describe the trends that were observed during the analysis.

9.3 Model Sensitivity to Physical Parameters (Dynamic Plume Not Included)

The first set of sensitivity cases involved a stationary outfall and did not include the dynamic plume model. Sediment was discharged into the ambient water body from a stationary source where the plume dynamics were described by the passive plume model. Key physical parameters such as vertical distribution of overflow discharge, horizontal dispersion, outfall flow rate, settling velocity and roughness, were considered.

9.3.1 Initial Vertical Distribution of Outfall Discharge

In the steering file the user can define the **release point depth range** thus giving the initial vertical distribution in the water column of the sediment plume discharged from the outfall. For this set of test cases the overflow from the outfall was distributed in the top 1 m, top 5 m and over then entire 15 m depth. Results from these three simulations are summarized in Figure 24.

The vertical distribution of the outfall discharge did not have a significant impact on the area (of the test basin floor) impacted by sedimentation. However there is a significant jump in the maximum bed accumulation when overflow from the outfall is distributed throughout the entire water column (test02), as more particles were able to settle out. Sediment discharged near the surface experienced more mixing and remained suspended longer therefore bed accumulations remained lower. The vertical slice showing particle concentrations through the water column confirms the initial jump in bed accumulation below the outfall with similar concentration levels observed as the distance from the outfall increases.

9.3.2 Horizontal Dispersion

Horizontal Dispersion (HD) controls the amount of horizontal spreading that occurs by the sediment plume. Higher HD values are expected to promote an increase in spreading whereas lower HD values should reduce the amount of spreading that occurs. As illustrated in Figure 25, an increase in the HD parameter generated an increase in the extent of the test basin floor impacted by sedimentation and a decrease in the depth of bed accumulation along the profile line where maximum bed accumulation occurred.

9.3.3 Mass Rate from Outfall

The following considers how discharge from the outfall can influence the sedimentation process. Under the Control Case condition (i.e. test01) the flow rate is defined as 10 kg/s. By reducing the flow rate, less sediment is being discharged to the water body therefore the amount of sediment that accumulates on the floor of the test basin as well as the overall depth of the settled particulates should be reduced. Figure 26 confirms the above statement. A reduction in the flow rate to 2 kg/s caused a decrease in the area of the test basin floor impacted by sedimentation and in the depth of the bed accumulation.

9.3.4 Effect of Settling Velocity Factor

The Settling Velocity Factor is a proportionality constant by which suspended sediment concentrations are multiplied to derive settling velocities (m/s). For this test case the Settling Velocity Factor was increased from 0.002 (test01 - Control Case) to 0.02 (test06) as is expected to promote settling. The results showed little to no change in the area (of the basin floor) impacted by sedimentation, however an increase in the maximum bed accumulation was observed as the Settling Velocity Factor increased (see Figure 27). It can be noted from the 2D vertical slice plots that the shape of the plume field under the outfall is denser and extends closer to the test basin floor under test06, therefore allowing more sediment to settle out thereby increasing the depth of accumulation.

9.3.5 Minimum Settling Velocity

Using the results from test06 in the previous section (i.e. Settling Velocity Factor = 0.02), the Minimum Settling Velocity was increased from 0.00025 m/s (in test06) to 0.0025 m/s (test07). A comparison of the results from test06 and test07 are shown in Figure 28. A decrease in the area impacted by sedimentation was observed for test07, which would be expected as the particles are settling out faster. The increase in the minimum settling velocity also generated a significant initial increase in bed accumulation. Further comparison of the 2D vertical slice and bed accumulation plots showed a decrease in the extent of the area impacted by the plume field confirming the trends discussed above. These observations suggest that the settling velocity is a key factor that can have a significant impact on the results

9.3.6 Roughness Length

The Roughness Length (RL) is a measure of roughness in a coastal environment. This study uses the Nikuradse form of the Roughness length, which in most coastal situations is roughly equivalent to $30*Z_0$, where Z_0 is the physical roughness length. Figure 29 compares the effect of the Roughness Length in the Plume model. A Nikuradse Roughness Length of 0.01 and 0.1 were defined for the Control Case condition (i.e.test01) and test08 respectively. The increase in Roughness Length by an order of magnitude had no impact on the results suggesting that this parameter will not have a significant influence over the results generated by the plume model.

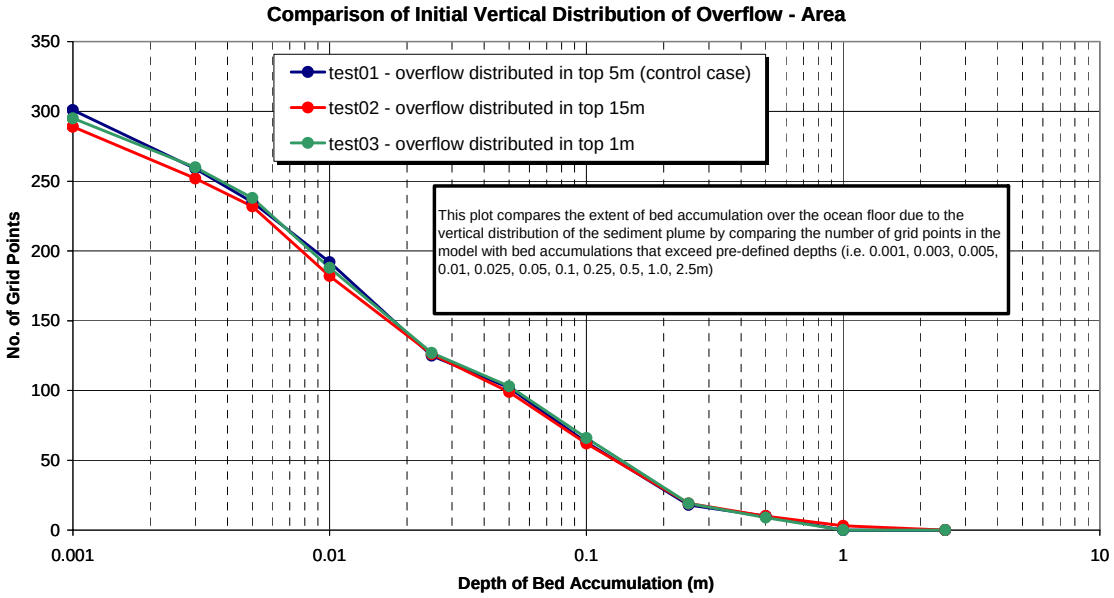

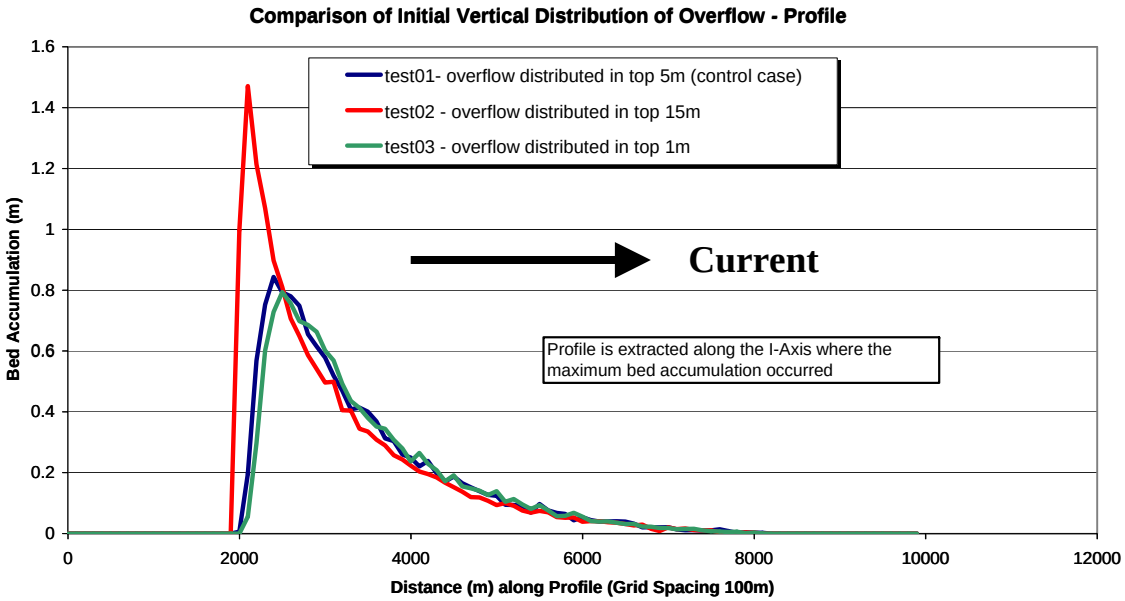

Figure 24. Impact of Vertical Distribution of Overflow on Plume Dynamics

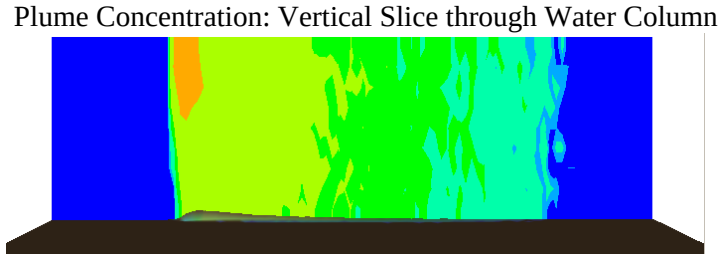

Overflow distributed in top 5m of water column

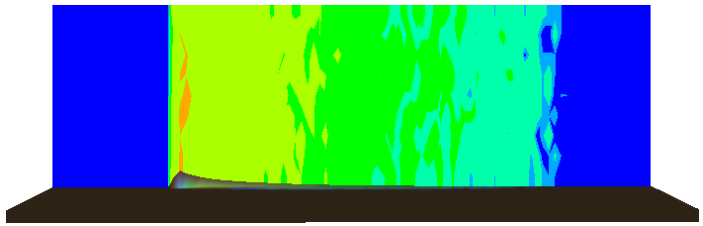

Overflow distributed over 15m depth

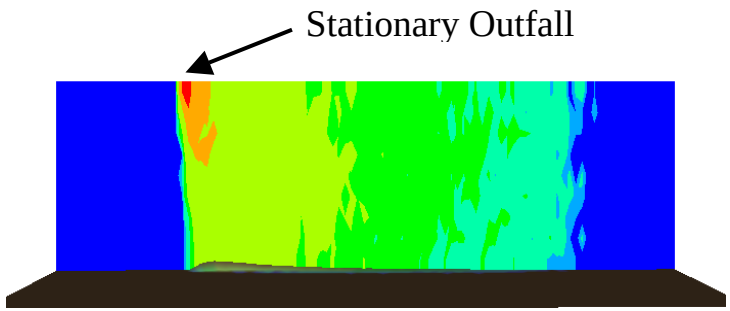

Overflow distributed in top 1m of water column

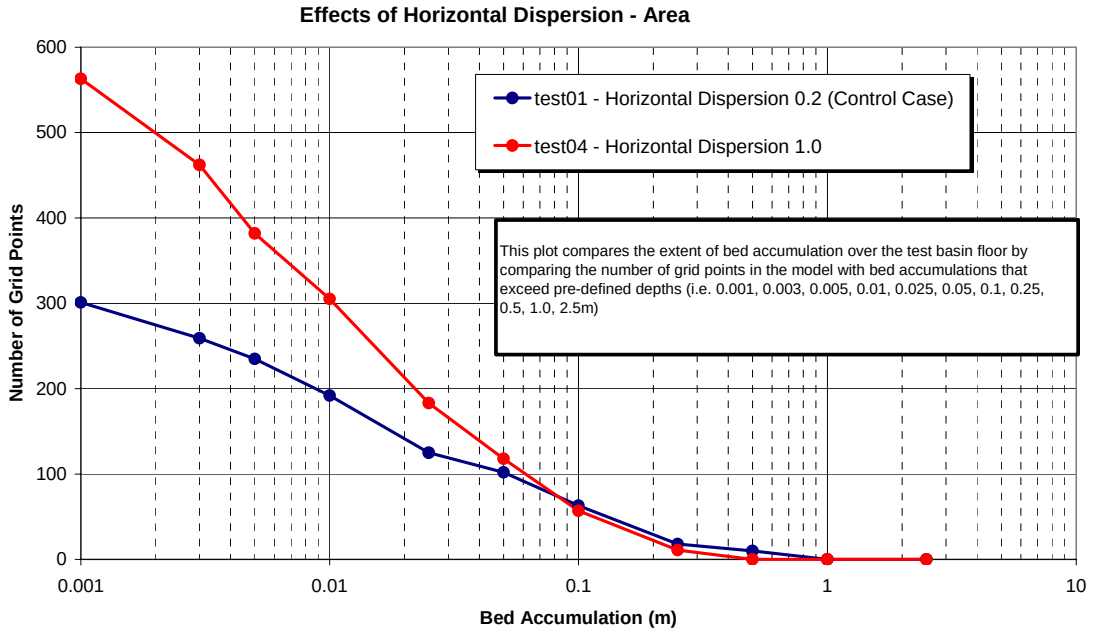

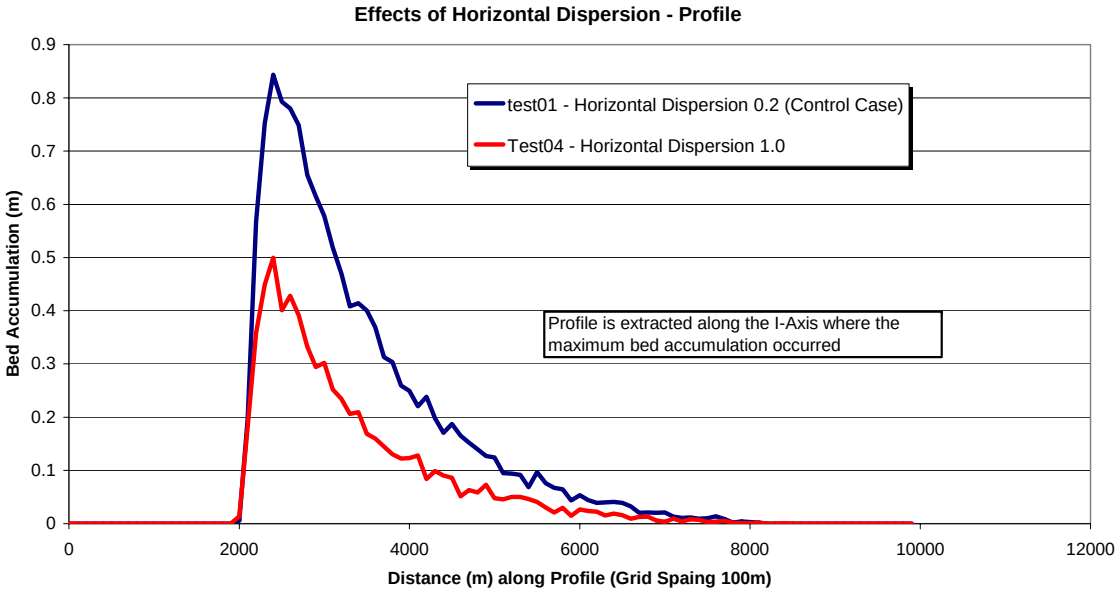

Figure 25. Impact of Horizontal Dispersion on Plume Dynamics

Plume Concentration: Plan View at Surface

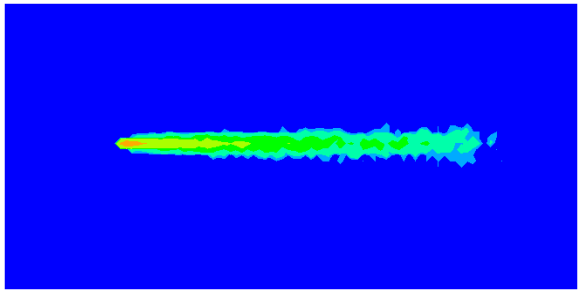

Test01 (Control Case): Horizontal Dispersion = 0.2

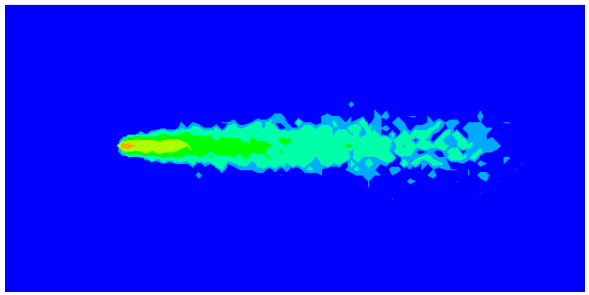

Test04: Horizontal Dispersion = 1.0

Plume Concentration: Vertical Slice through Water Column

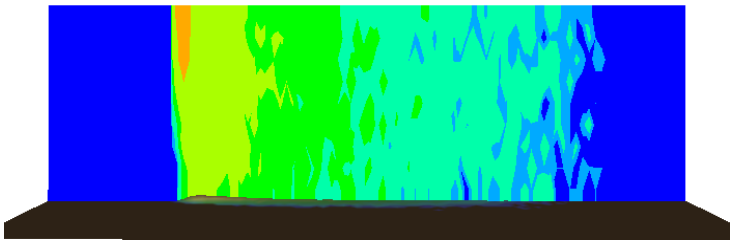

Test04: Horizontal Dispersion = 1.0)
(Compare with Test01 – Vertical Distribution)

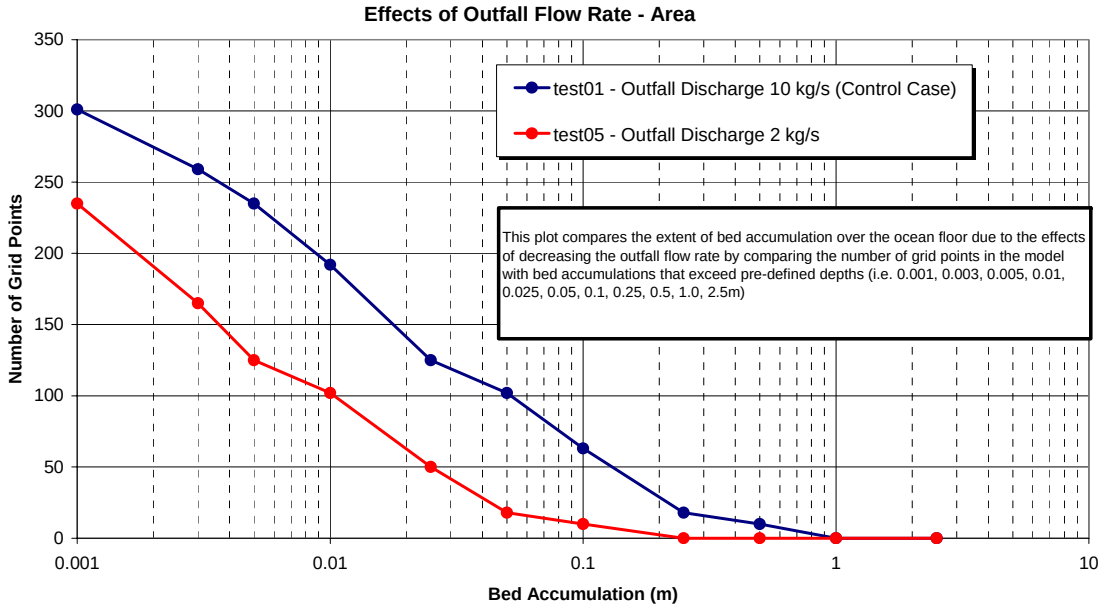

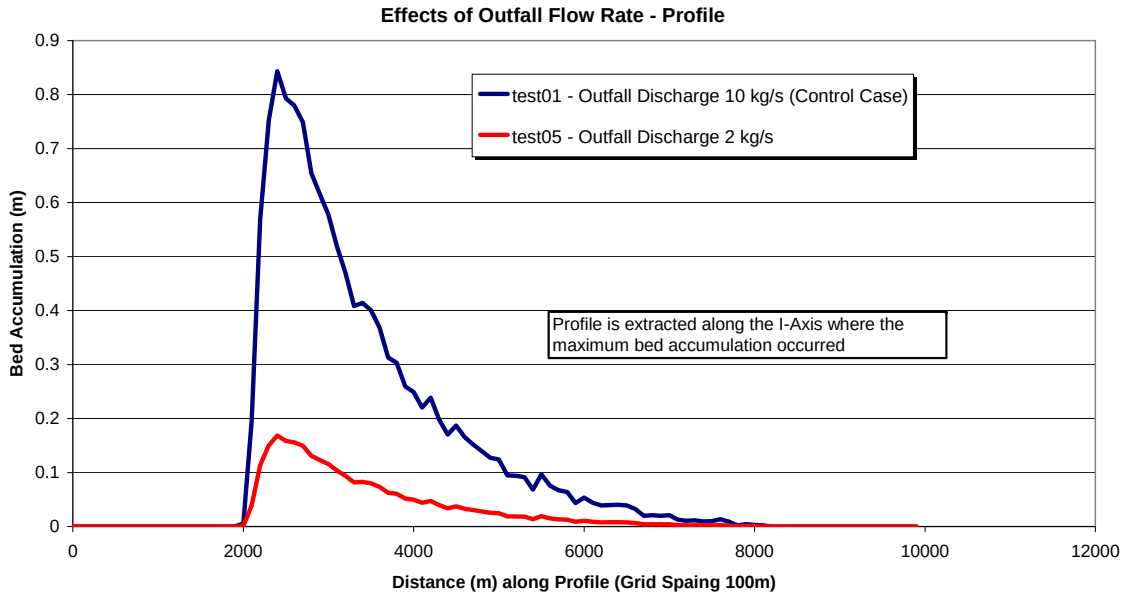

Figure 26. Impact of Mass Rate from Outfall on Plume Dynamics

Plume Concentration: Vertical Slice through Water Column

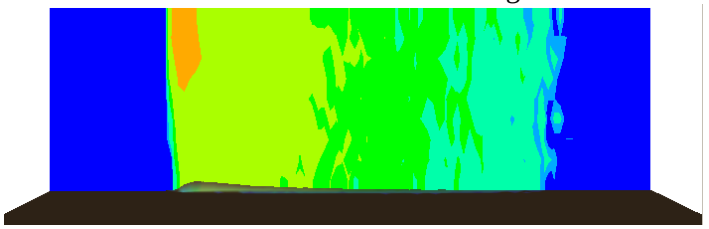

Test01 (Control Case): Outfall Discharge = 10kg/s

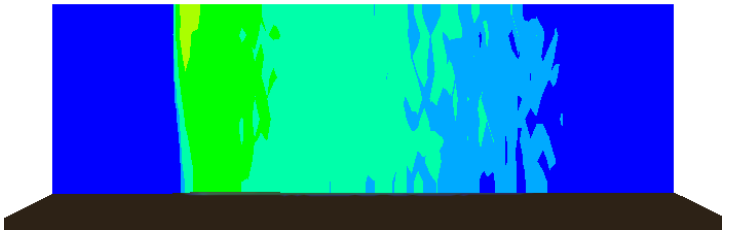

Test05: Outfall Discharge = 2kg/s

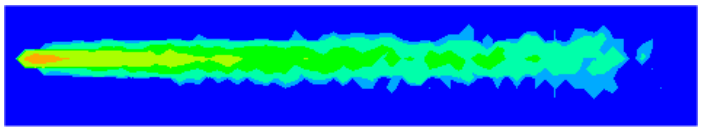

Test01: Plan View of Plume at Surface

Test05: Plan View of Plume at Surface

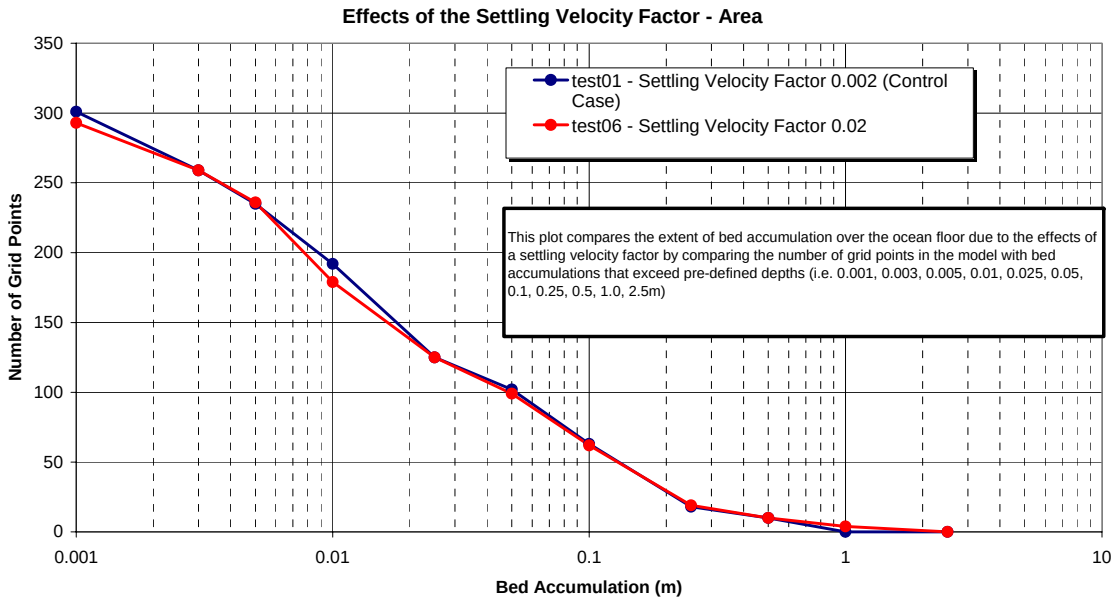

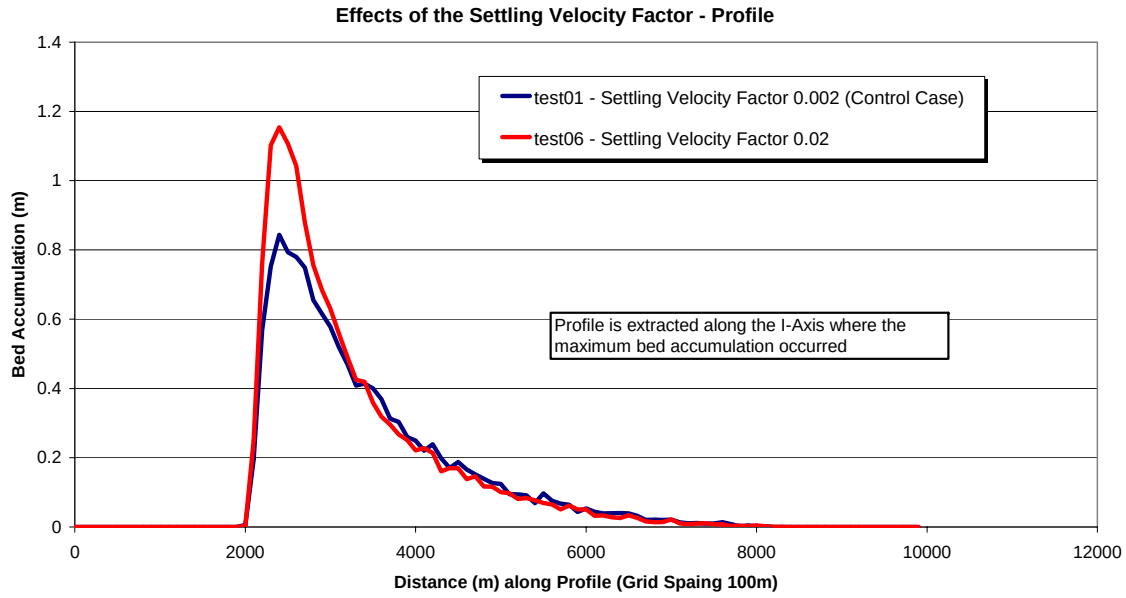

Figure 27. Impact of the Settling Velocity Factor on Plume Dynamics

Plume Concentration: Vertical Slice through Water Column

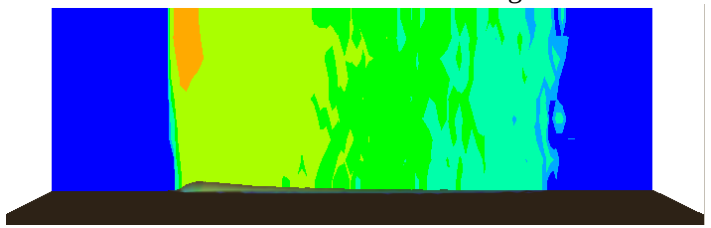

Test01: Settling Velocity Factor = 0.002

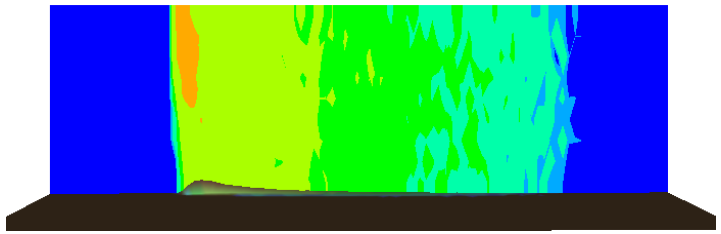

Test06: Settling Velocity Factor = 0.02

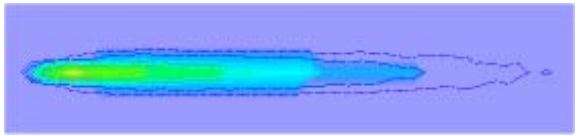

Test01: Plan View of Bed Accumulation

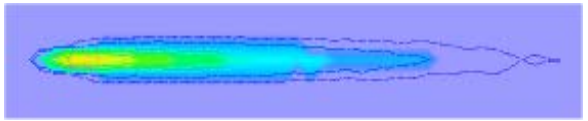

Test06: Plan View of Bed Accumulation

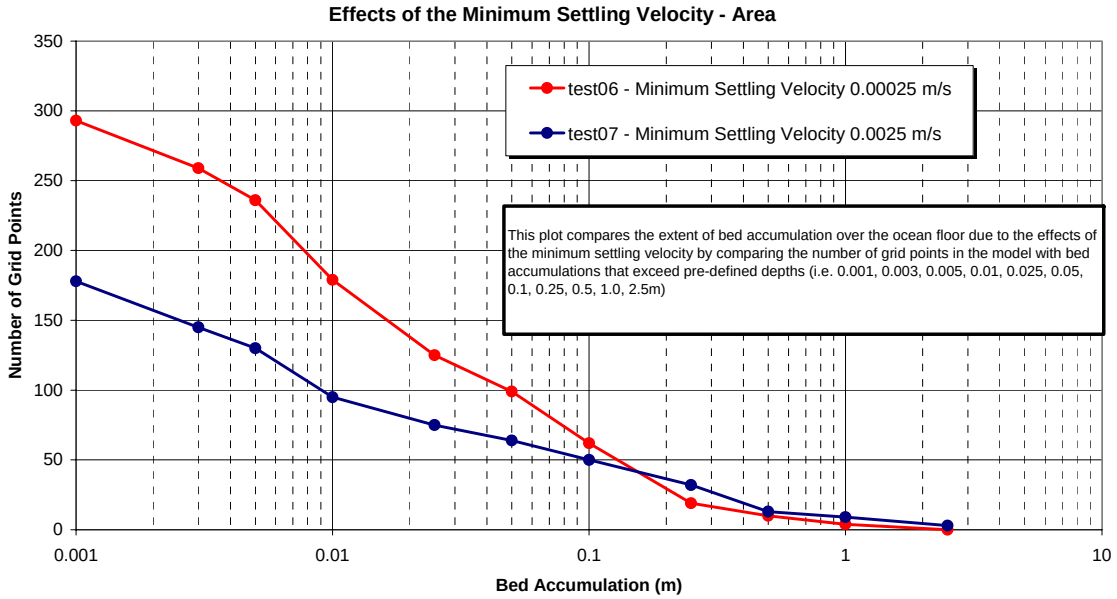

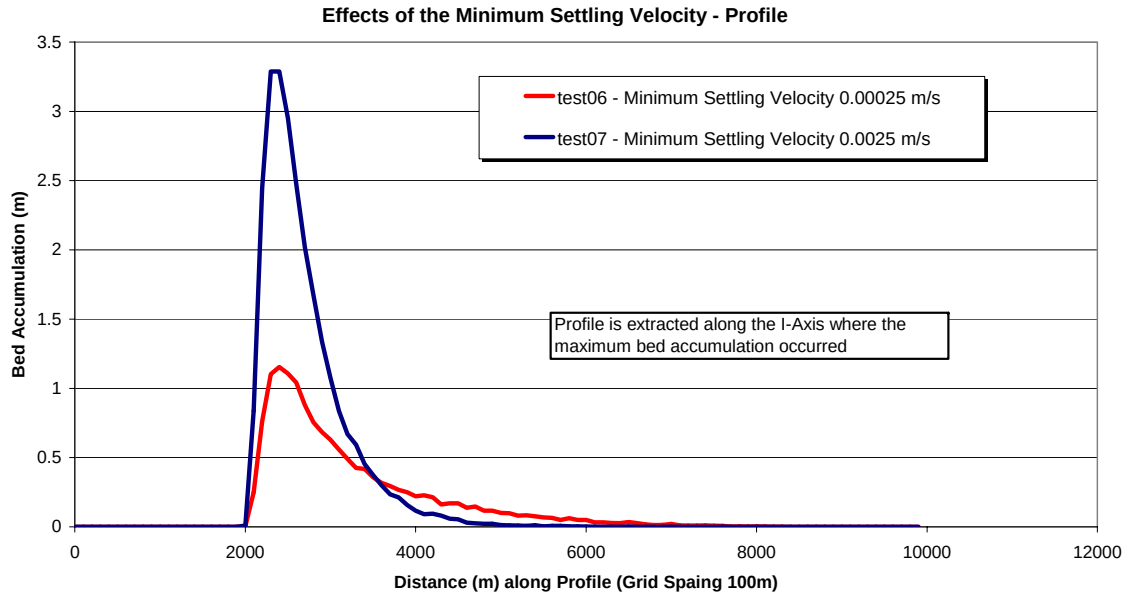

Figure 28. Impact of Minimum Settling Velocity on Plume Dynamics

Plume Concentration: Vertical Slice through Water Column

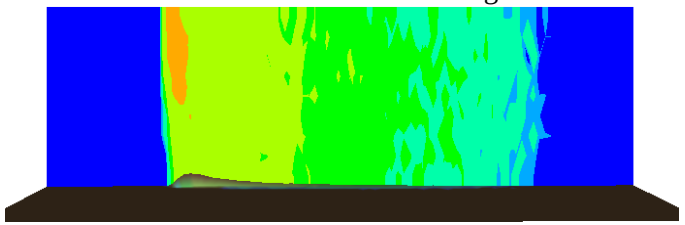

Test06: Minimum Settling Velocity = 0.00025m/s

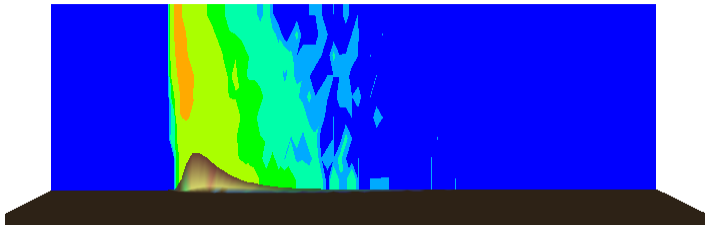

Test07: Minimum Settling Velocity = 0.0025m/s

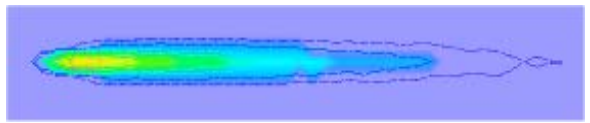

Test06: Plan View of Bed Accumulation

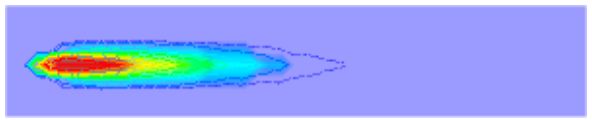

Test07: Plan View of Bed Accumulation

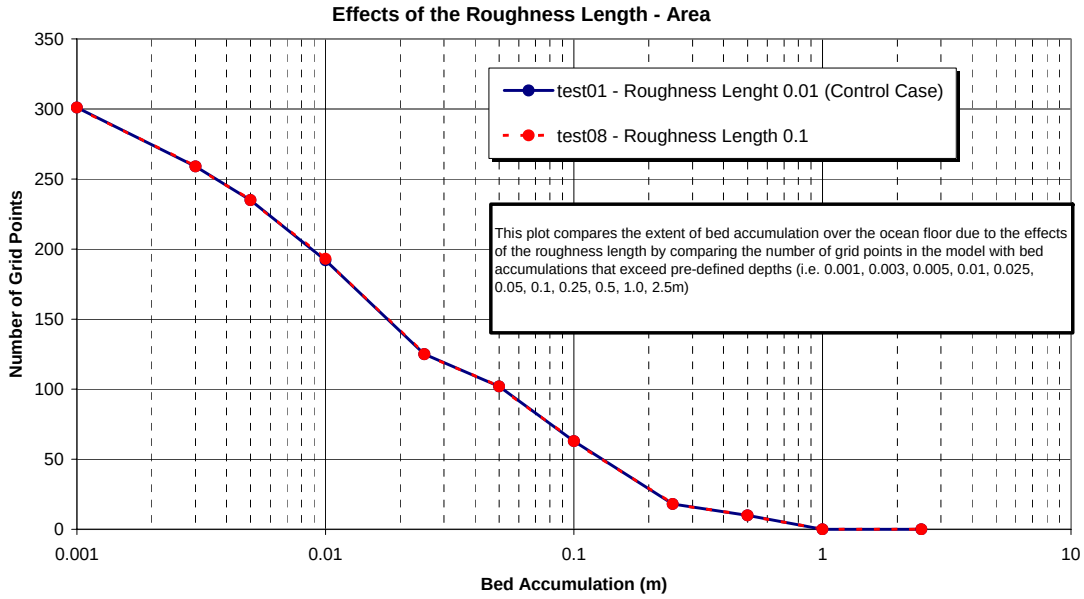

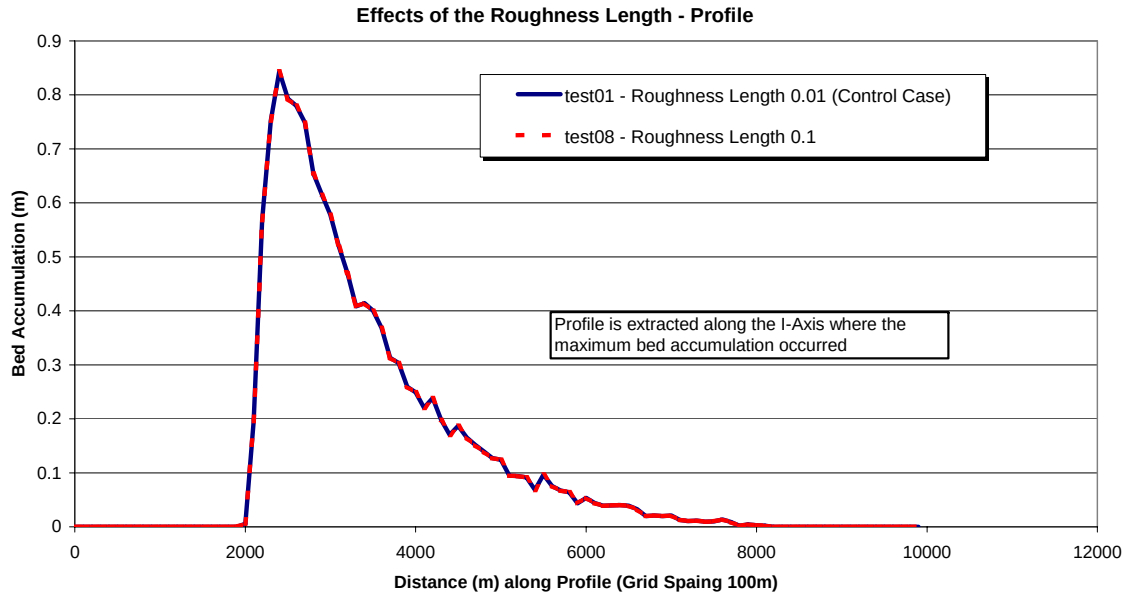

Figure 29. Impact of the Roughness Length on Plume Dynamics

Plume Concentration: Vertical Slice through Water Column

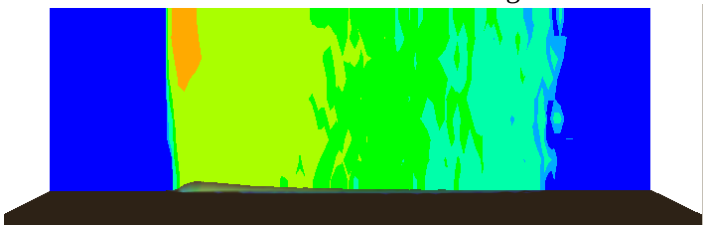

Test01: Roughness Length = 0.01

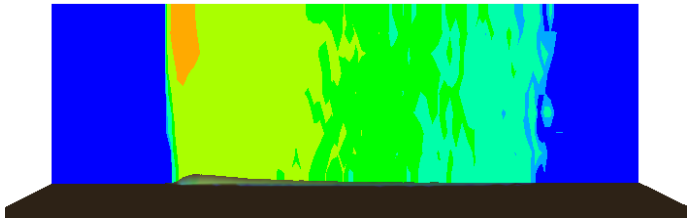

Test08: Roughness Length = 0.1

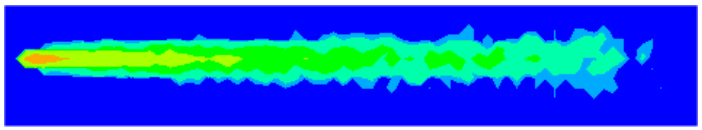

Test01: Plan View of Plume at Surface

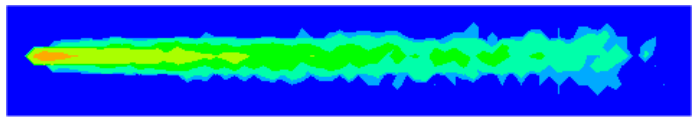

Test08: Plan View of Plume at Surface

9.3.7 Model Sensitivity – Vertical Distribution of the Profile

For all Plume model simulations to this point, the drag coefficient in the flow model was defined as 0.05. The flow model was re-run for drag coefficients of 1 x 10^{-20} and then 0.4. Figure 30 illustrates the change in the vertical velocity profile based on the bottom roughness coefficient. As the roughness coefficient decreases, a more vertical velocity profile is observed.

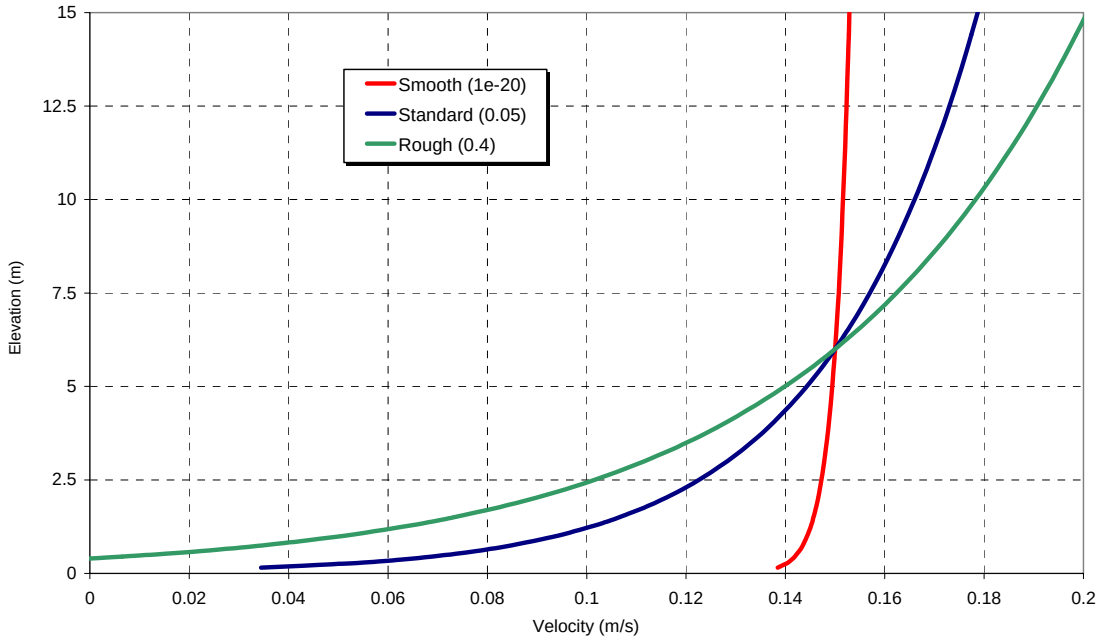

FIGURE 30. Impact of Bottom Roughness on the Velocity Profile

The results from the Plume model based on these two new flow files along with the control case (test01) are summarized in Figure 31. For a bottom roughness of 0.4, there was a decrease in the area impacted by sedimentation. Maximum bed accumulation occurred further from the outfall than the base case most likely due to the higher velocities present near the surface transporting the material further downstream. As the bottom roughness coefficient decreases (i.e. getting smoother) the depth of sedimentation along the maximum bed accumulation profile becomes more evenly distributed due to the vertical velocity profile.

9.4 Model Sensitivity to Physical Parameters (Dynamic Plume Model Included)

To this point only the passive plume model has been considered, that is the dispersion of the plume is a function of the ambient current conditions. The dynamic plume model simulates the initial phase of dispersion where the sediment plume is dominated by the nature and conditions of the release. The dynamic plume model reads the Trailer Process result file, which describes the sediment mixture (i.e. grain size, mass rate, flow rate) that is being released during the dredging process (i.e. output from the Process Model). As a result the Plume model becomes more complex with the inclusion of the dynamic plume model as the following two stages are now simulated

- Dynamic Plume Model – simulates the initial release and density plume of overflow from the dredging process back into the ambient water body
- Passive Plume Model – simulates the plume movement that occurs as a result of the hydrodynamic conditions of the ambient water body

Various simulations were performed to determine the model's response to key parameters in the trailer process file such as trailer fraction size, flow rate and mass rate. The tools (i.e. 2D plots and graphs) that have been used to aid in the sensitivity analysis to this point continue to be used. It is important to note that the results from the Plume model are determined from the final stage in the modeling process, that is the passive plume model. With the inclusion of the Dynamic Plume Model, the plume field appears as if it is being generated from the test basin floor. As the dynamic plume descends, released material hits the ocean floor as a density current. Entrainment with the flow fields re-suspends sediment into the passive plume model.

9.4.1 Effect of Mass Rate

In the trailer process file the mass rate (in kg/s) for each sediment size that is discharged back into the surrounding water body is defined at each timestep. Using Trailer Fraction 1, which is defined as a grain size of 10 microns or 0.01 mm, the Plume model was used to simulate the dynamic and passive phases of dispersion for mass rates of 0.319 kg/s, 5.319 kg/s and 25.319 kg/s. Table 3 summarizes the test cases below.

TABLE 3. Test Cases used to assess mass rate sensitivity

Test Cases	Mass Rate (kg/s)	Trailer Fraction	Grain Size (mm)
test30 (control case)	5.319	1	0.001
test31	25.319	1	0.001
test32	0.319	1	0.001

The results from each simulation are summarized in Figure 32. An increase in the mass rate (MR) means an increase in the amount of sediment discharged per second, therefore both the bed accumulation and the area/footprint of bed accumulation over the test basin floor would be expected to increase in both cases as shown in Figure 32. The 2D vertical slice plots show how the mass rate can impact the shape and extent of the plume field. As the mass rate increases the plume field becomes more pronounced because more sediment is being released and the density current is hitting the test basin floor with more energy allowing these particles to become re-suspended.

9.4.2 Effect of Sediment Size on Bed Accumulation

For this set of simulations we considered the impact of grain size (i.e. Trailer Fraction) on the plume dynamics. The mass rate remained constant at 5.319 kg/s and the minimum settling velocity for each grain size was calculated from the Soulsby formula.

$$w_s = \frac{\upsilon}{d}\left[\{10.36^2 + 1.049D^3\}^{1/2} - 10.36\right]$$

The test cases are summarized in Table 4.

TABLE 4. Test cases to assess impact of Sediment size

Test Cases	Mass Rate (kg/s)	Trailer Fraction	Grain Size (mm)	W_s (m/s)
test30 (control case)	5.319	1	0.001	0.00025
test33	5.319	4	0.09	0.0083
test35	5.319	9	0.5	0.5262

Figure 33 compares the results from each test case. Trailer Fraction 1 (test30) has the most significant impact with respect to the area (of test basin floor) covered by sedimentation, however the depth of bed accumulation is much less than the other two test cases. Trailer Fraction 4 and 9 show very similar trends with respect to area and depth of bed accumulation suggesting that for a particular mass rate there is a point where particle size no longer plays a significant role.

9.4.3 Effect of Overflow Rate

Using Trailer Fraction 1 various overflow rates (m^3/s) were tested while keeping the mass rate constant (i.e. the overflow density varied) . The results, which are summarized in Figure 34, show that the overflow rate does not have a significant impact on the depth of bed accumulation or the area influenced by sedimentation.

9.4.4 Effect of Trailer Speed

The effect of trailer speed on plume dynamics were compared and the results are presented in Figure 35. Three trailer speeds were modeled (i.e. 1,2 and 3 knots), the results from these simulations offer the following observations

- The distance covered during the dredging process increases with trailer speed
- At slower trailer speeds there is an increase in the depth of bed accumulation however this occurs over a smaller distance
- The overall area of the test basin floor impacted by sedimentation does not change significantly.

9.4.5 Effect of Water Depth

Overflow from the dredging process was discharged into various depths of water in order to examine how water depth impacts plume dynamics. For all cases the velocity profile used to develop the current fields (surface current speed equal to 15 cm/s) remained constant. Water depths from 10 m to 50 m at 10 m increments were considered and the results are shown in Figure 36.

At shallow depths a decrease in the overall area impacted by sedimentation was observed however the depth of accumulation increased. As water depths increased there was more opportunity for the ambient current field to interact and transport the sediment greater distances (as shown by the 2D vertical slice plots) thus increasing the area impacted by sedimentation but decreasing the depth of bed accumulation.

9.4.6 Effects of Current Speed

Current speed can have a significant effect on sediment plume dynamics. At higher current speeds more mixing of the dredger overflow with the ambient water body would be expected, this would increase the suspension time of particles creating a large plume field and amplifying the area impacted by sedimentation.

For this set of sensitivity runs, the water depth in the test basin remained constant at 15m deep. Current speeds were increased from 0 cm/s to 30 cm/s at 10 cm/s increments. The results of the simulations were compared using graphs and 2D plots and are summarized in Figure 37. Trends similar to those stated above were observed. An increase in current speed generated larger plume fields, increased suspension time and subsequently increased the area of the test basin floor impacted by sedimentation. For test48, which involved no current field, the sediment basically settled out creating a very evenly distributed bed accumulation.

9.4.7 Trends Observed Due to Trailer Path

The purpose of this test case is to simulate a wiggly trailer path and to evaluate the plume dynamics through graphs and 2D plots in order to determine if the trends look reasonable. The results from the simulation were compared with the control case (test30), which simulated a straight trailer path, and are summarized in Figure 38.

It is unlikely in the field that a dredger path would be parallel to the current. In this particular case the dredger moves at an approximate angle of 45 degrees to the current as it zigzags back and forth pushing upstream. As the dredger moves across and against the current the plume field is expected to increase and the area of the test basin floor impacted by sedimentation should also increase. These observations are confirmed in Figure 38, which shows that the area impacted by sedimentation is much larger under the wiggly dredger path than the straight path. It is difficult to draw any inferences from the bed accumulation profile as the utility program extracts sediment accumulations along the *I-axis* at the location where maximum accumulation occurs, however it can be noted that the maximum bed accumulation occurs at the point of the dredger and that depths are less than the control case.

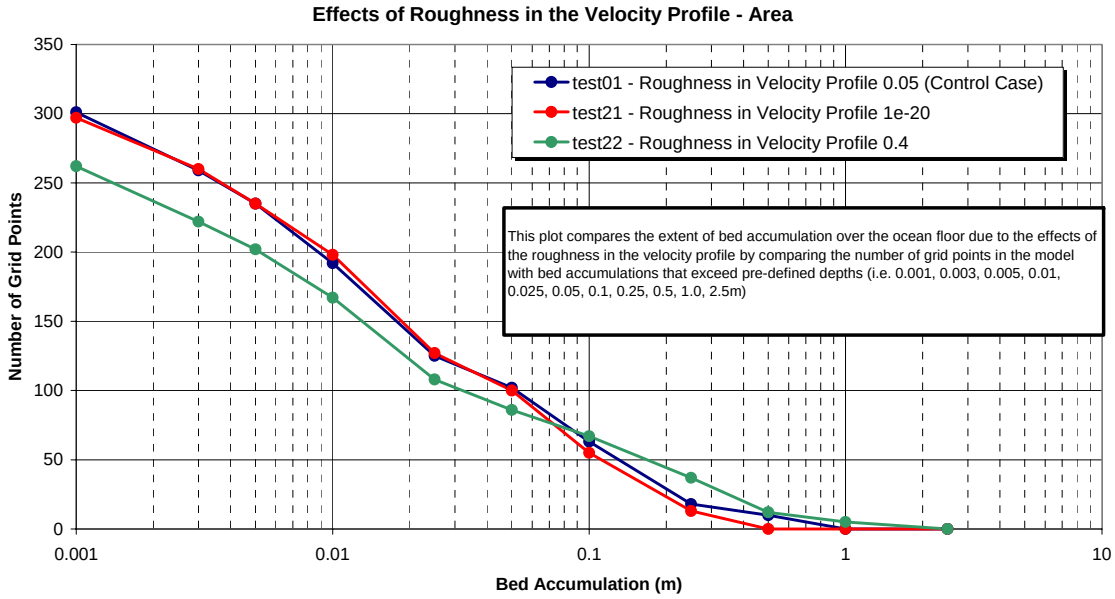

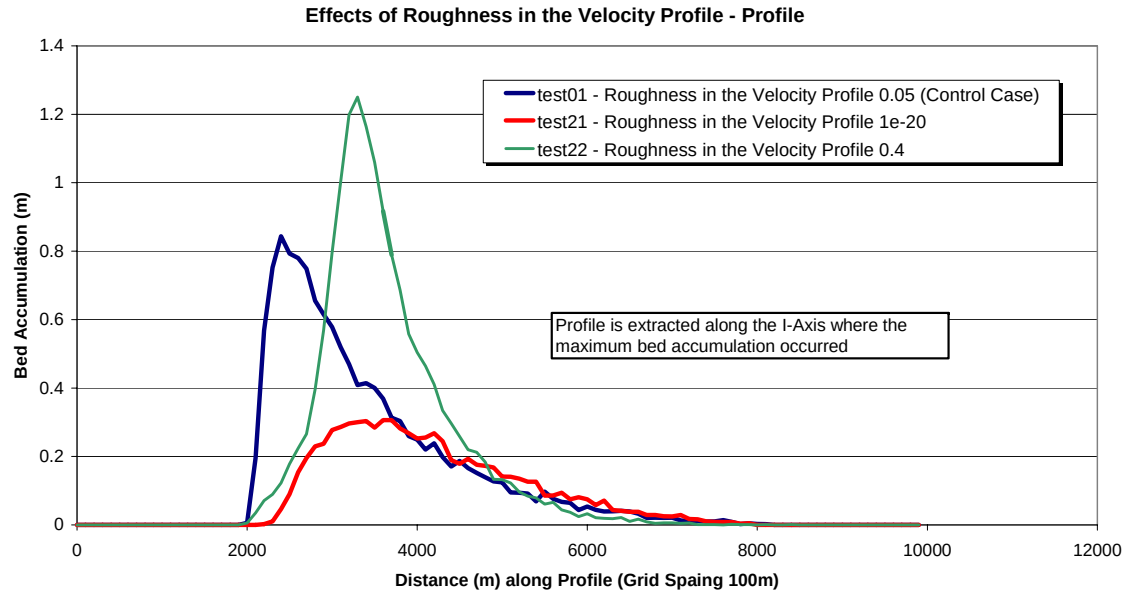

Figure 31. Impact of Velocity Profile (Basedd on Roughness) on Plume Dynamics

Plume Concentration: Vertical Slice through Water Column

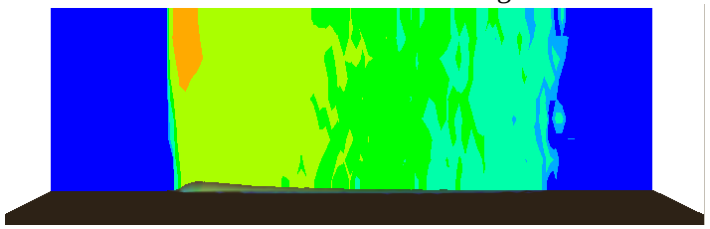

Test01: Roughness in Velocity Profile = 0.05

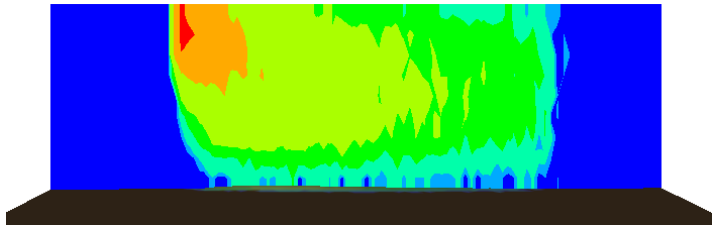

Test21: Roughness in Velocity Profile = 1e-20

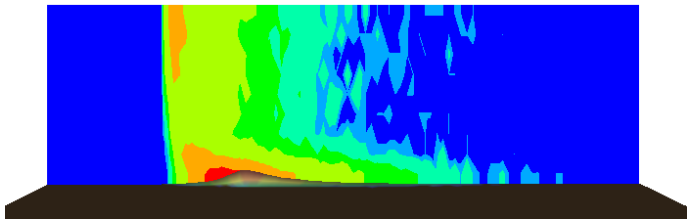

Test22: Roughness in Velocity Profile = 0.4

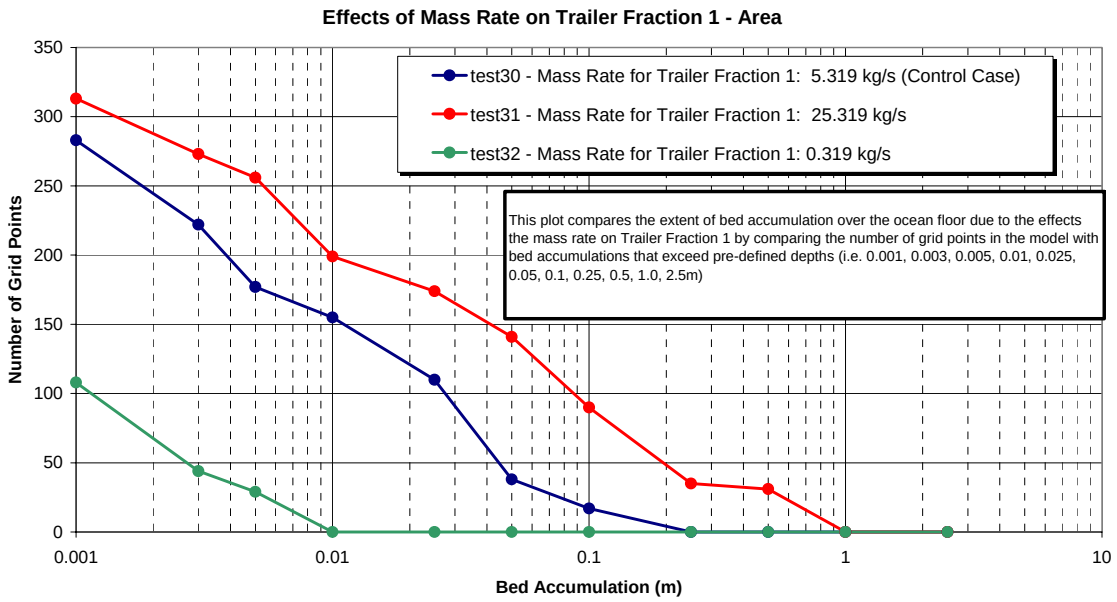

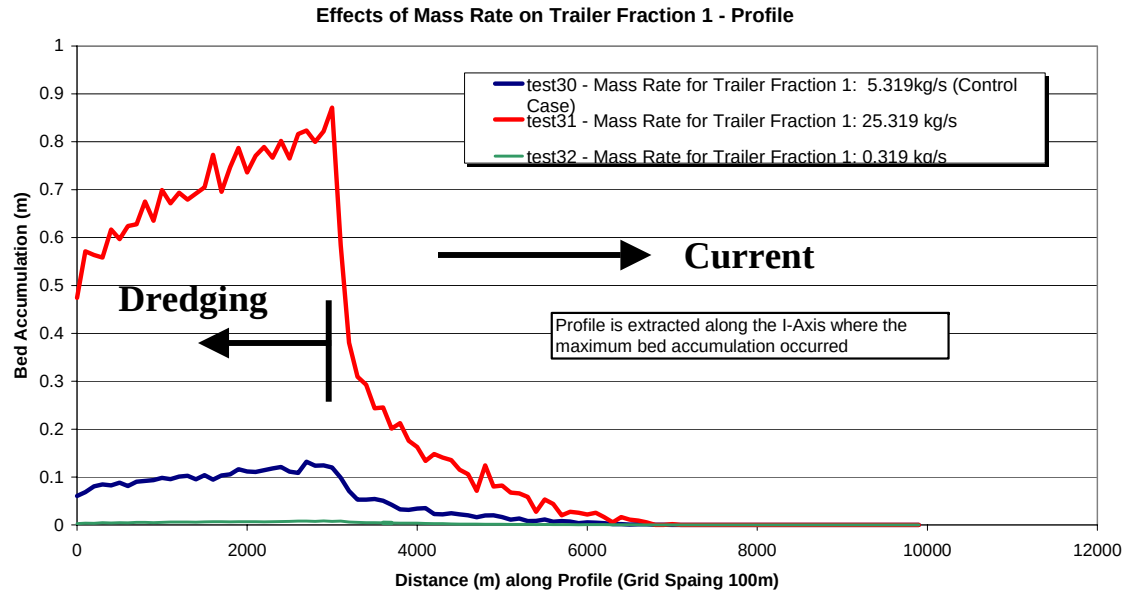

Figure 32. Impact of Mass Rate on Plume Dynamics

Plume Concentration: Vertical Slice through Water Column

Test30 (Control Case): Mass Rate for Fraction 1= 5.319kg/s

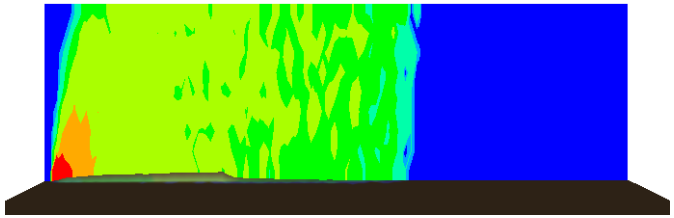

Test31: Mass Rate for Fraction 1 = 25.319kg/s

Test32: Mass Rate for Fraction 1 = 0.319kg/s

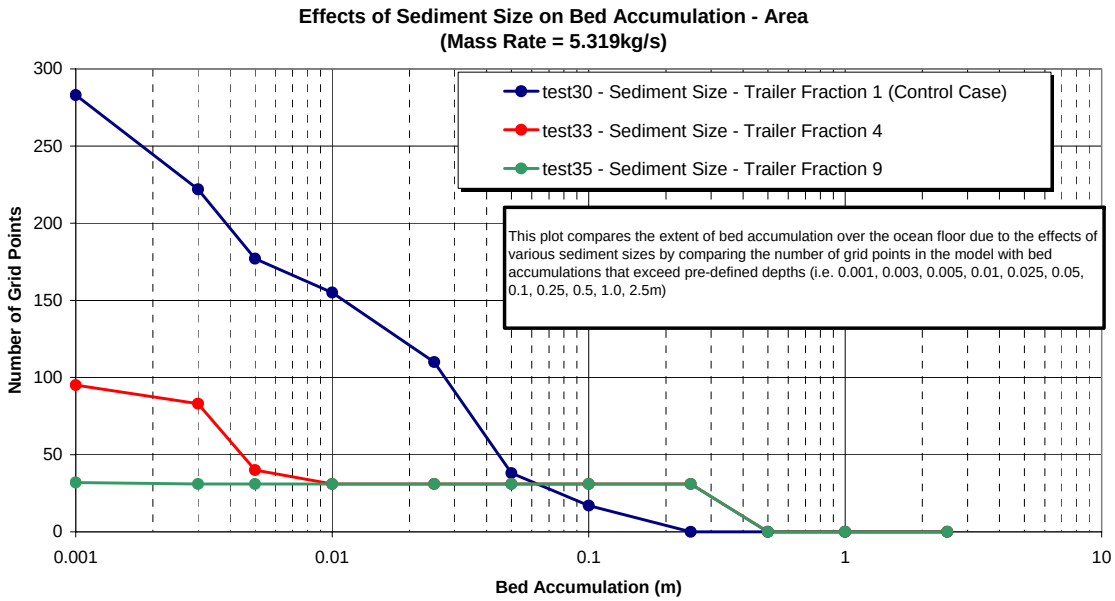

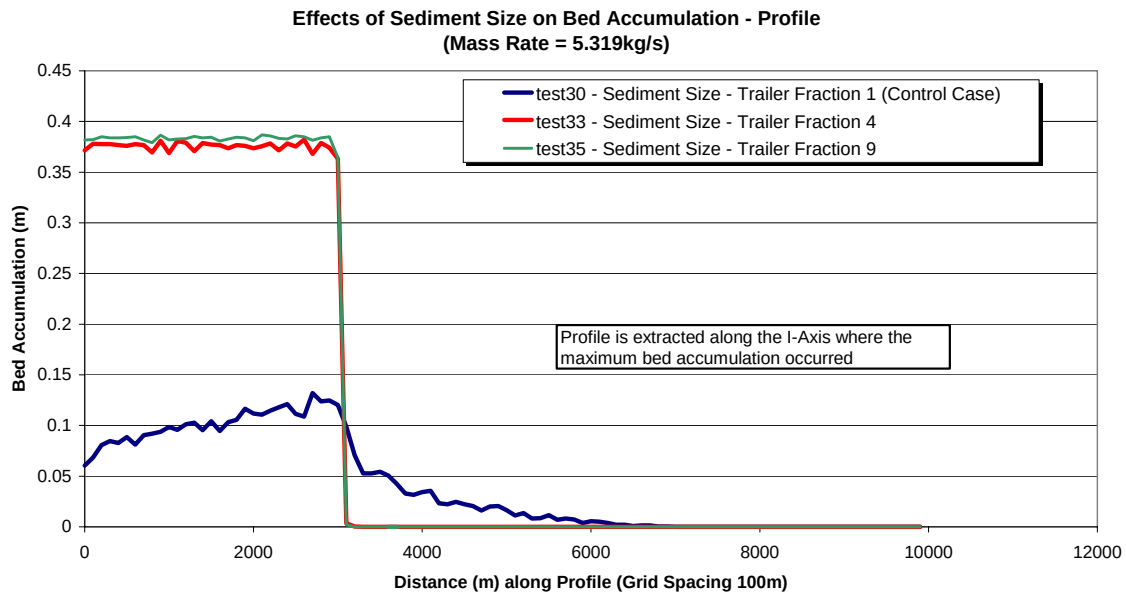

Figure 33. Impact of Trailer Fraction Size on Plume Dynamics

Plume Concentration: Vertical Slice through Water Column

Test30 (Control Case): Fraction 1= 5.319kg/s

Test33: Fraction 4 = 5.319kg/s

Test35: Fraction 9 = 5.319kg/s

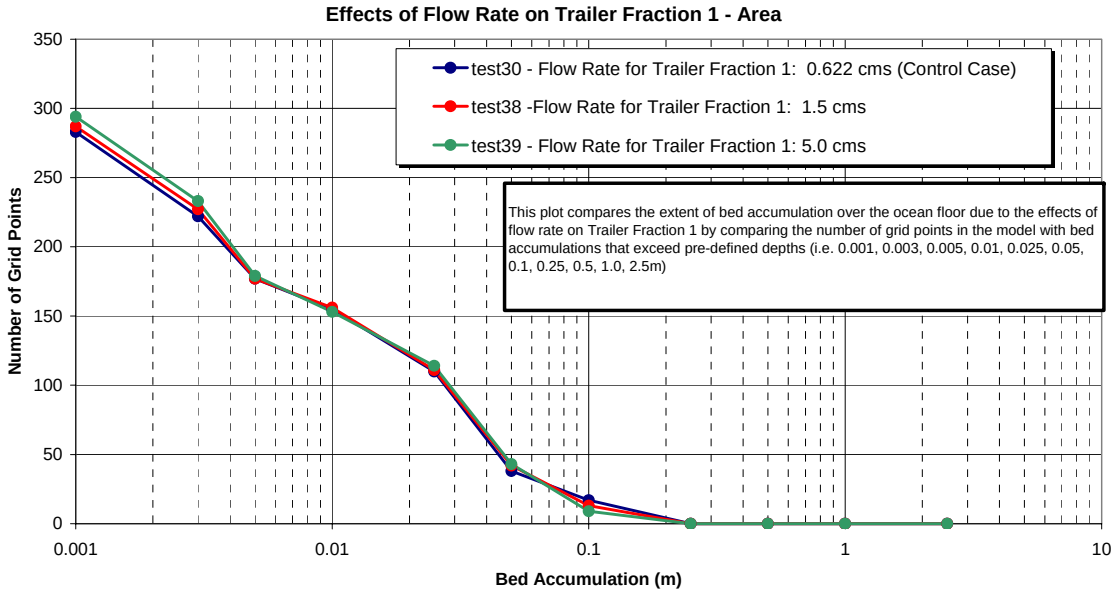

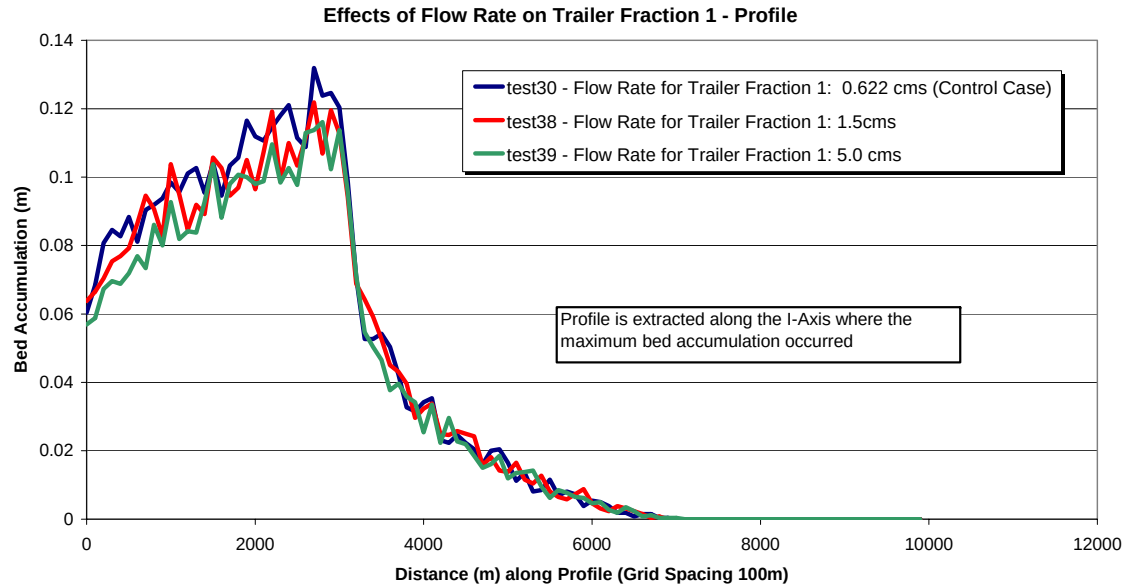

Figure 34. Impact of Overflow Rate on Plume Dynamics

Plume Concentration: Vertical Slice through Water Column

Test30 (control case): Flow Rate = 0.622cms

Test38: Flow Rate from Trailer Result File = 1.5cms

Test39: Flow Rate from Trailer Result File = 5.0cms

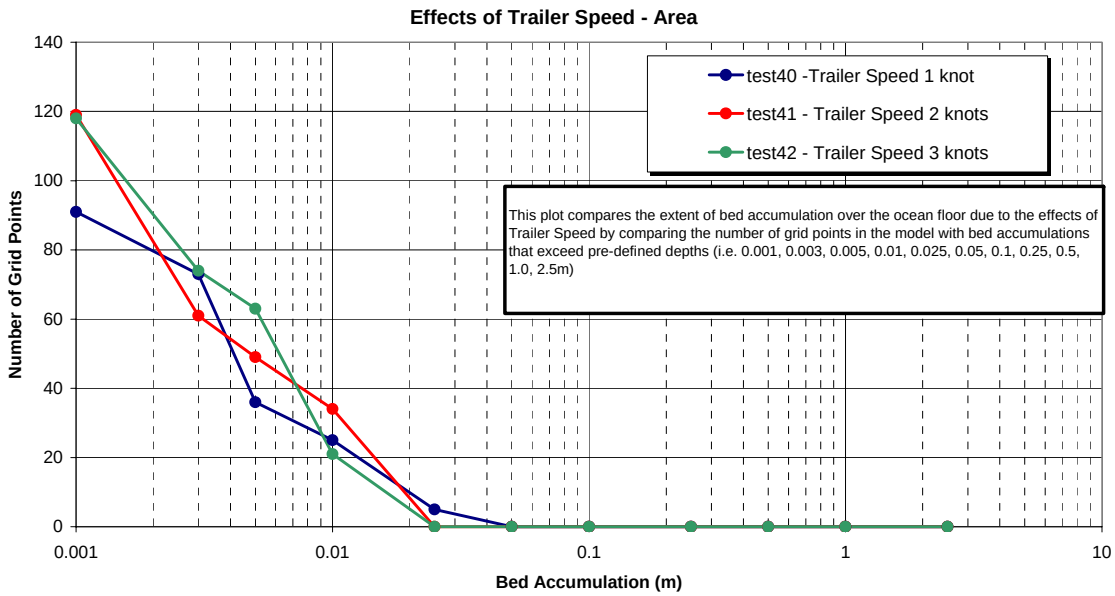

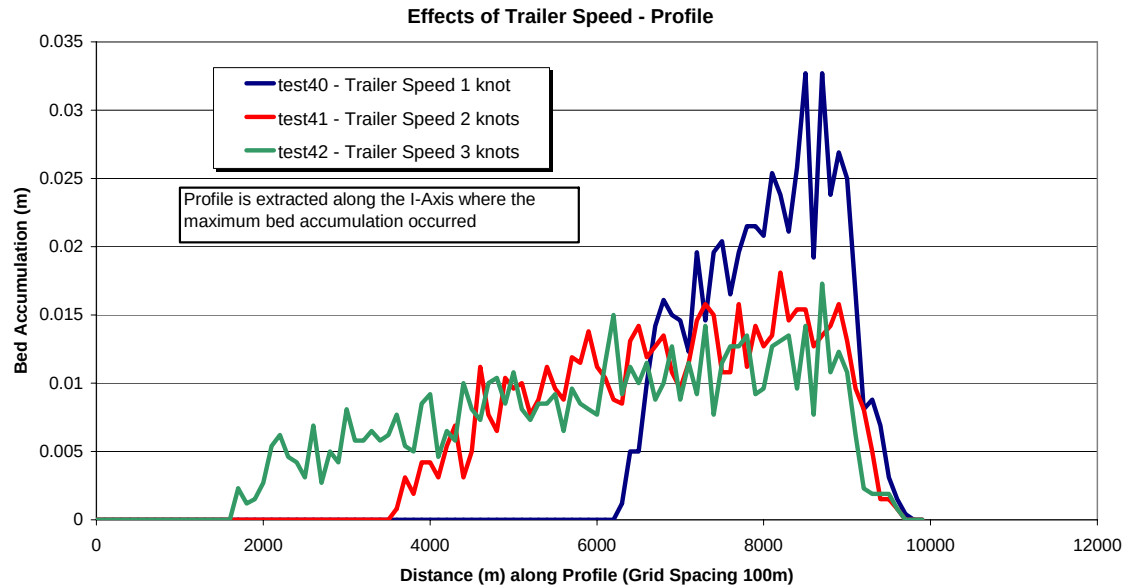

Figure 35. Impact of Trailer Speed on Plume Dynamics

Plume Concentration: Vertical Slice through Water Column

Test40: Trailer Speed 1 knot

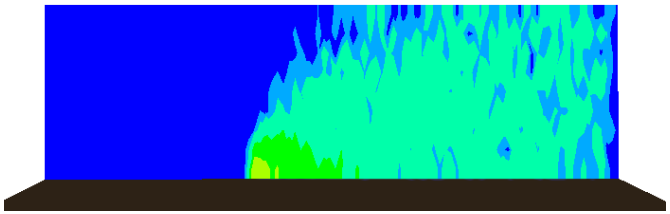

Test41: Trailer Speed 2 knots

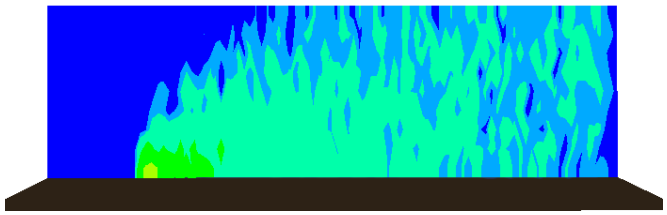

Test42: Trailer Speed 3 knots

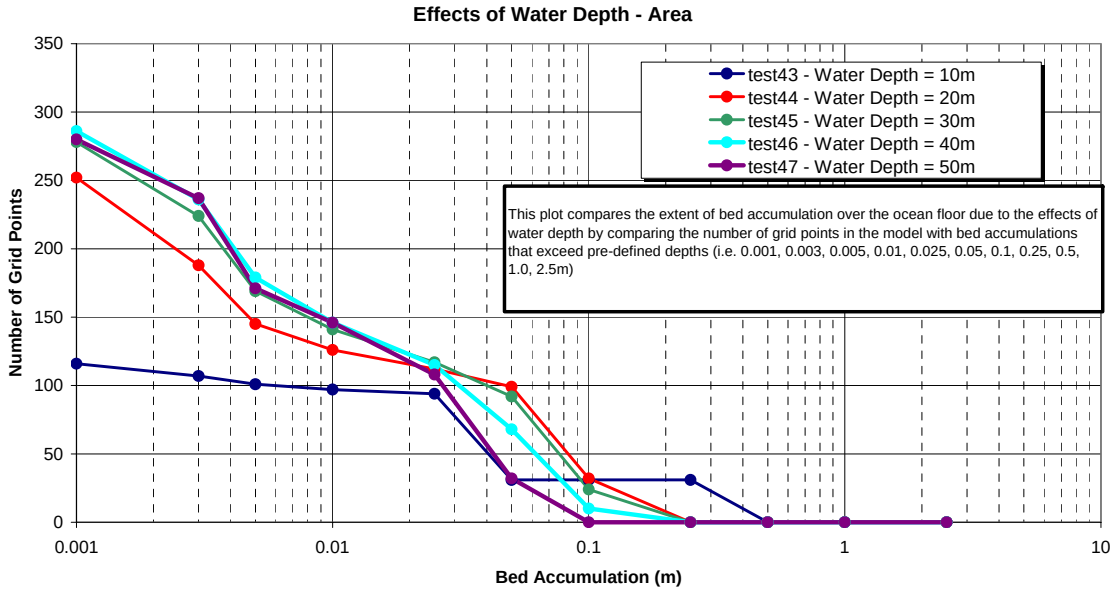

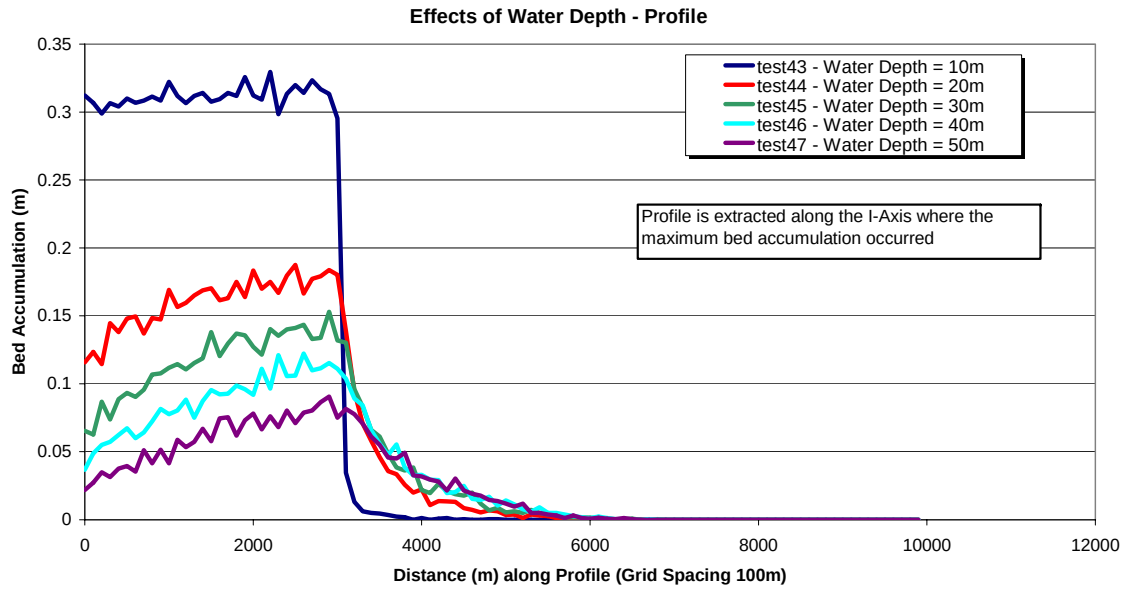

Figure 36. Impact of Water Depth on Plume Dynamics

Plume Concentration: Vertical Slice through Water Column

Test43: Water Depth = 10m

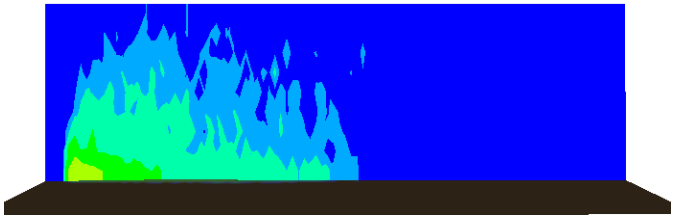

Test45: Water Depth = 30m

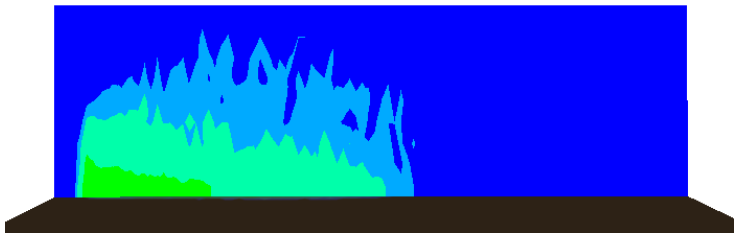

Test47: Water Depth = 50m

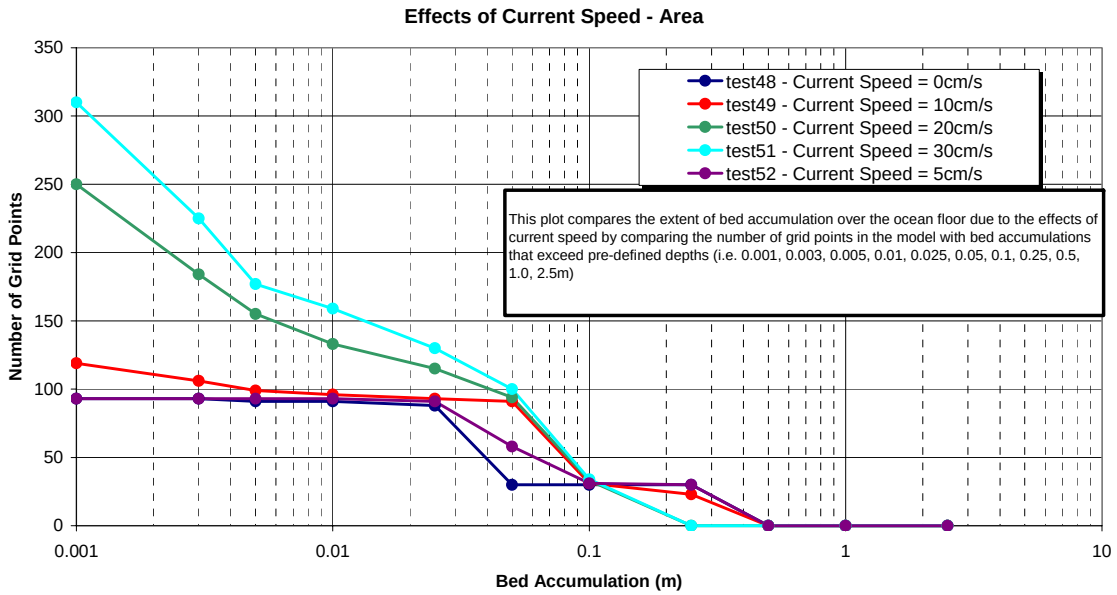

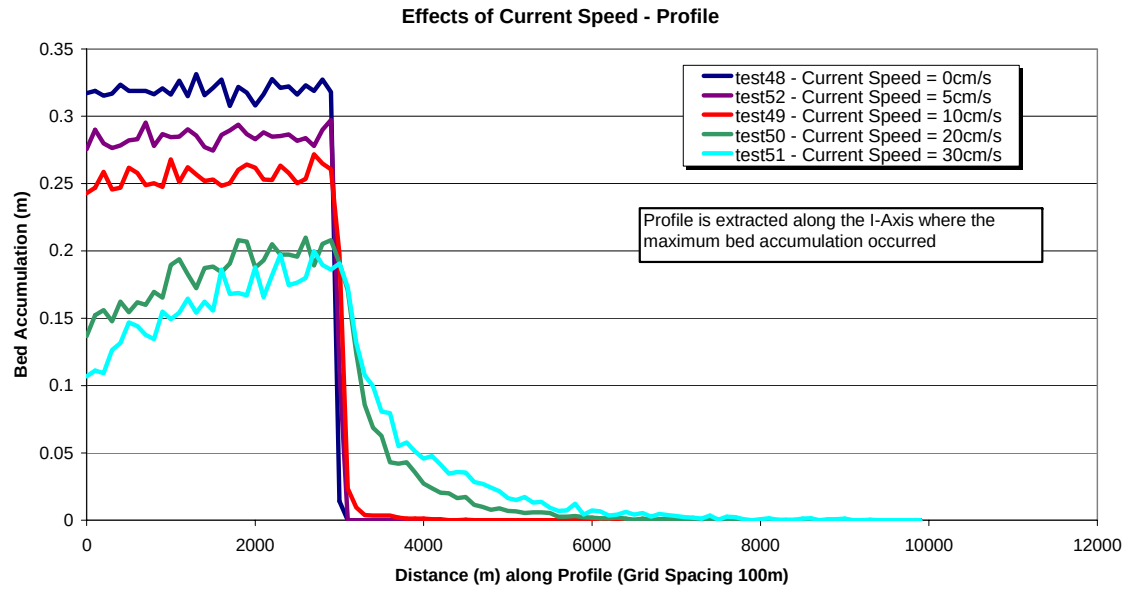

Figure 37. Impact of Current Speed on Plume Dynamics

Plume Concentration: Vertical Slice through Water Column

Test48: Current Speed = 0 cm/s

Test49: Current Speed = 10 cm/s

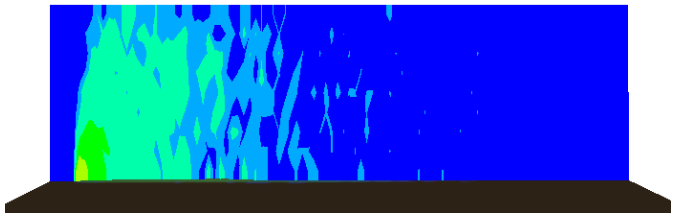

Test51: Current Speed = 30 cm/s

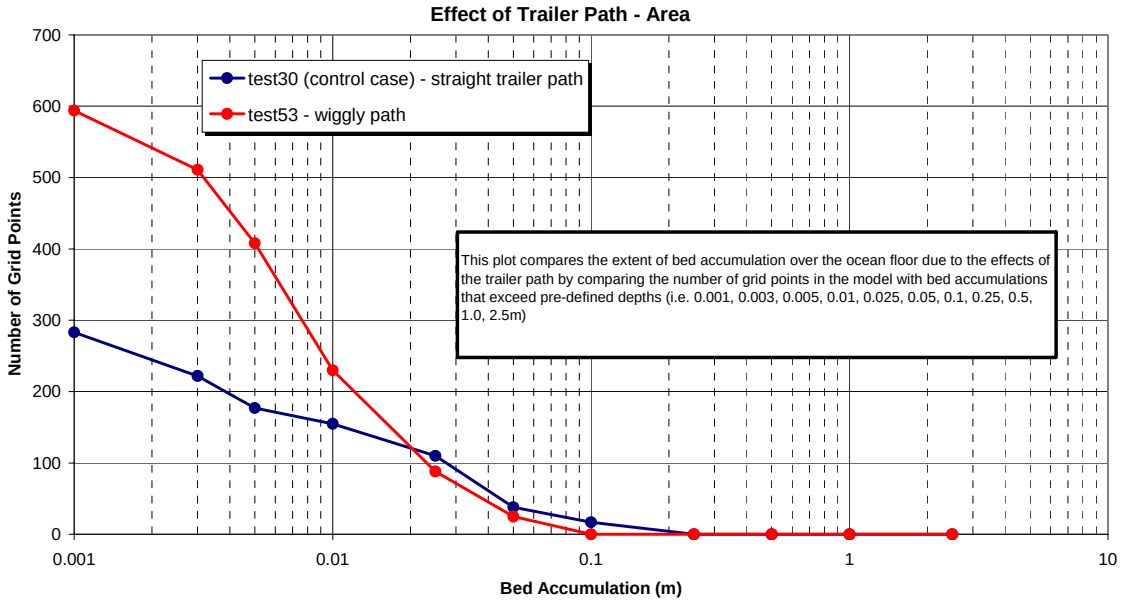

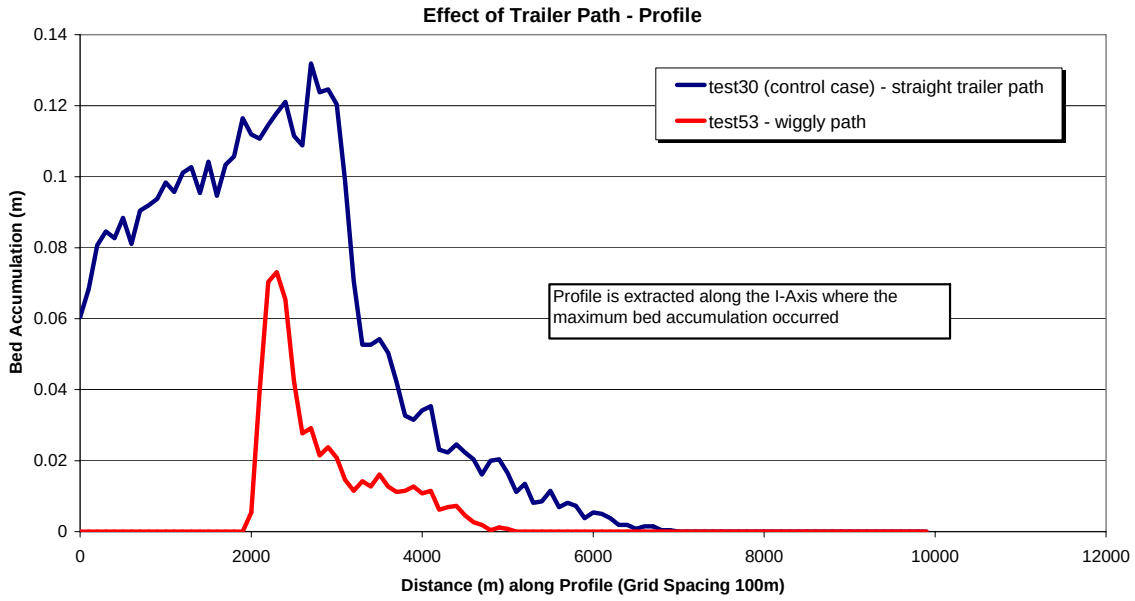

Figure 38. Impact of Trailer Path on Plume Dynamics

Plume Concentration: Horizontal Slice at Surface

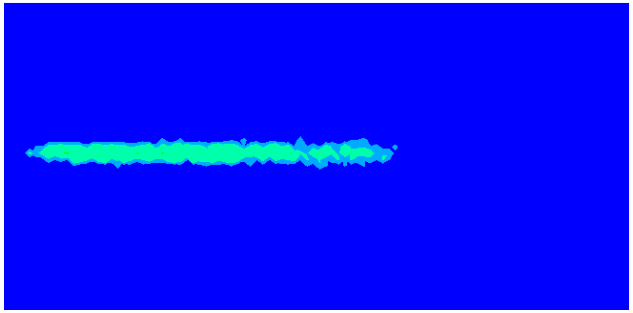

Test30: Straight Trailer Path

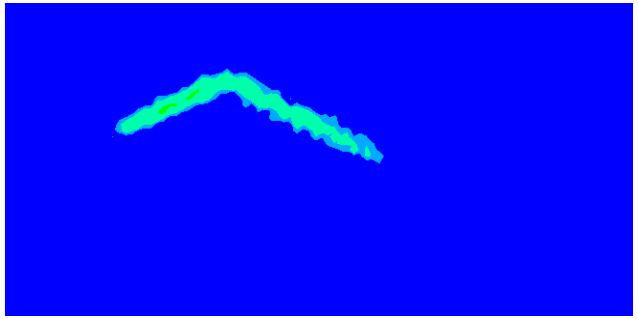

Test53: Wiggly Trailer Path

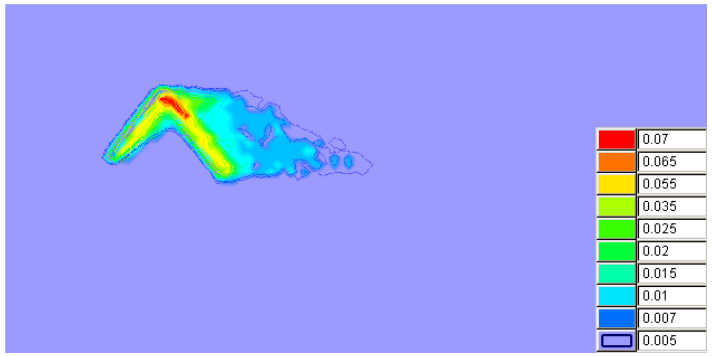

Test53: Bed Accum (m) - Wiggly Trailer Path

10.0 MODEL PERFORMANCE EVALUATION: OWERS BANK

10.1 Introduction

Results from the Process and MMS Plume model were compared with field measurements that were carried out on May 11th and August 19th, 1995 at the Owers Bank Site for the ARCO "S" Class (Severn) Trailing Suction Hopper Dredger (TSHD). In 1995, a comprehensive field program was undertaken at the Owers Bank site in order to understand the overall impact of benthic and surface plumes associated with marine aggregate mining on local ecological systems. The investigation included monitoring the dredger overflow (i.e. flow rates and grain size analysis), discrete measurements of plume concentrations using grab bag sampling methods and the use of an Acoustic Doppler Current Profile (ADCP) to provide visualization and concentration measurements by trailing the dredger in a survey vessel and performing ADCP transects across the plume field. Various datasets from the field program were compared with model results in order to examine the model's ability to simulate operational conditions of the dredger and the plume dynamics in the surrounding coastal regions. The structure for this section of the report can be divided into the following

1) May 11, 1995: Dredging at Owers Bank Site 124/1 - The Process Model was used to simulate the dredging performance of the ARCO Severn. Details such as ship specifications, dredging depth, and the in-situ grain size distribution are discussed in this section along with a brief discussion of the results.

2) August 19, 1995: Dredging at Owers Bank Site 124/8 – The MMS Plume model was used to simulate the plume dynamics as overflow from the ARCO Severn is discharged back into the coastal environment. A brief overview of tide and current conditions, flow model setup and model set-up along with a brief discussion of the results are included in this section.

This study only considers one dredger, as insufficient data was available in order to complete a proper analysis of the other two dredgers that were also part of the field program in August 1995 (i.e. The City of Rochester and the Geopotes XIV). Other limitations such as gaps in particular datasets and geo-referencing issues with the ADCP data have restricted the ability to provide a detailed comparison of model results. *Therefore it is important to note that the comparisons made in this report do not constitute a full validation of the dredger plume model*.

The details and assumptions regarding the Ower's Bank dredging operations is derived from Coastline Surveys Ltd. (1999), HR Wallingford (1996) and Bray (2003).

10.2 Dredging Process Model Evaluation at the Owers Bank Site (124/1) for May 11, 1995

10.2.1 ARCO Severn Specifications

The dredging operations of the ARCO "S" Class (Severn) were simulated using the Process model and the results were compared with field data collected on May 11, 1995. Overspill flow rates were measured using current meters and measuring gauges while the particle size distribution of the overspill was determined from sampling and laboratory testing. May 11, 1995 was chosen as the most ideal date as it contained the most comprehensive dataset, other potential dates such as August 19, 20 and 21, 1995 were dismissed due to gaps in the data (i.e. missing overspill flow rates). The dredging that occurred on May 11th, 1995 at the Owers Bank License Area (124/1) involved an "ALL-IN" (no screening) cargo type and the time required to load the ARCO Severn vessel was three hours.

The specifications used to define the ARCO Severn in the Process model are summarized below in Table 5. The data was obtained from various sources and used as input for the Process model.

TABLE 5. Ship Specifications for the ARCO "S" Class (Severn) Dredger.

Items	ARCO "S" Class (Severn)
Hopper Capacity (m^3)	1300***
Hopper Tonnage (tonnes)	2200**
Hopper Length (m)	30.35*
Hopper Width (m)	8.5*
Hopper Depth (m)	5*
Draft Light Fore	2.32*
Draft Light Aft	3.5*
No. Trailing Arms	One*
Suction Pipe Diameter (mm)	700**
Suction Pipe Velocity (m/s)	2.345 (approximation)
Type of Dredging	Trailing Suction Hopper Dredging**
Path Length of Dredger	1400m***
Trailer Speed (knots)	1.3 (approximation)

*Nick Bray at Dredging Research Ltd (June 13, 2003)
** Coastline Surveys Limited (1999)
*** HR Wallingford (1996)

No actual data were available for trailer speed; therefore, the assumed value of 1.3 knots may be considered a potential source of error. A mixture density of 1165 kg/m^3 was defined in the model. This value was factored to represent dredging inefficiencies, and was slightly less than the average of 1197 kg/m^3 determined for "S" class vessels in the by Coastline Surveys Limited (1999). The suction pipe velocity was based on the average loading performance of 4500 m^3/hr for "S" Class vessels as described in the 1999 Coastline Survey report.

10.2.2 Owers Bank Site Characteristics

The bathymetric features of the Owers Bank Site can be described as relatively uniform. A dredging depth of 19 meters was defined in the Process model and the in-situ grain size distribution specified in the model is described below in Figure 39.

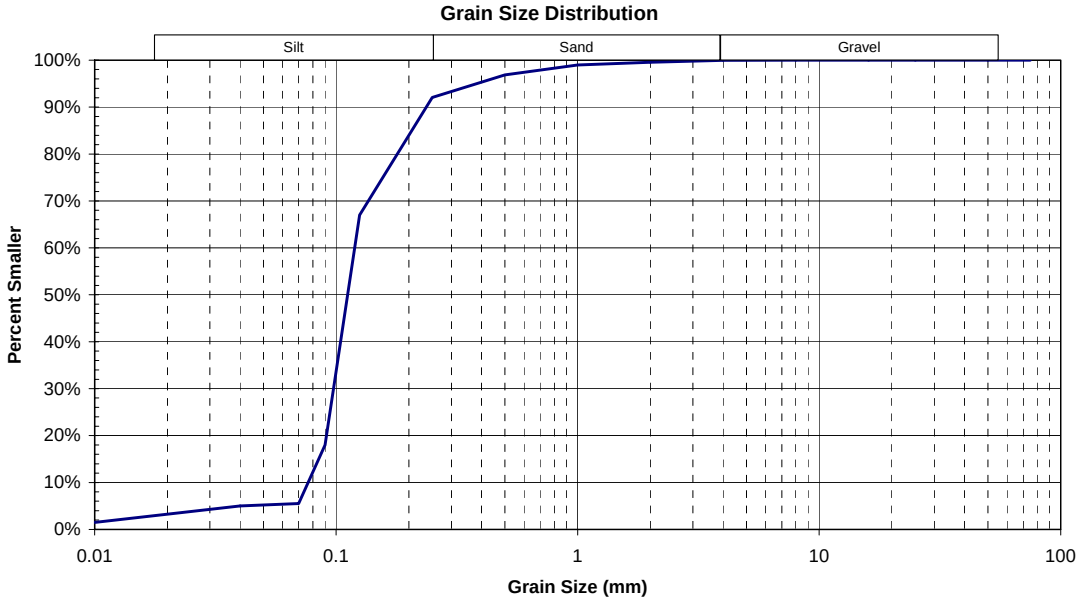

FIGURE 39. Assumed In-Situ Grain Size Distribution at the Owers bank Site (124/1)

10.2.3 Discussion of the Results

A summary of the measured and modeled results is presented in Table 6. The model simulated the overall dredging time very well.

TABLE 6. Compares Measured and Modeled Results For Dredging carried out at Owers Bank Site on May 11, 1995 (ARCO Seven)

	Dredging Time (min)	Overspill Rate (m3/s)	Total Mass Rate (kg/s)
Measured Data	180	0.93*	23
Modelled Results	184	0.90	22

* 0.3 m^3/s per spillway based on flow observations (coastline 1999)

Figure 40 below compares the proportion of materials that were discharged shipside during the dredging cycle. The modeled results compare well with the measured data; however, it is important to recognize that the particle size distribution defined in the Process model was adjusted slightly from the average measured grain size sample in the Owers Bank area in order to provide an optimal fit.

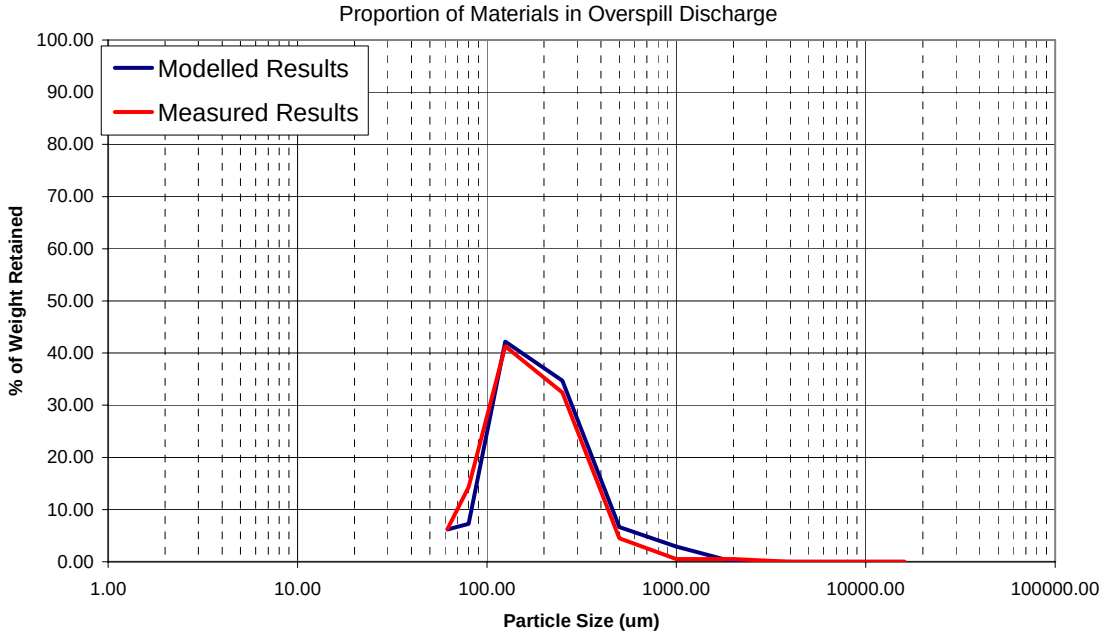

FIGURE 40. Particle Distribution of Material Discharged Ship Side During the Dredging Cycle.

Results from the Process model simulations suggest that the model is capable of reproducing overflow conditions on the ARCO Severn for the period of May 11, 1995. However, it is difficult to substantiate the model's performance with any certainty based on the analysis undertaken as assumptions had to made for several key parameters, such as mixture density, particle distribution, trailer speed and pipe velocity. A more comprehensive field program focused on simultaneous measurements of various components of the dredging operation is recommended.

10.3 Plume Model Evaluation at Owers Bank Site (124/8) for August 19, 1995

The MMS Plume model was compared with field measurements that were carried out on August 19, 1995 for the ARCO Severn dredger. Due to the limited availability of data regarding the dredging process, overflow conditions were defined based on the grain size analysis of the overspill undertaken at the Owers Bank site (124/1/8) for "S" class ships with "ALL-IN" cargo. Table 7 summarizes the grain size distribution of the overflow.

TABLE 7. Proportion of Materials in Overspill Discharge for "S" Class Dredgers

Particle Size	Area 124/1/8
< 0.063 mm	48.0%
0.063 - 0.125 mm	10.6%
0.125 - 0.250 mm	19.0%
0.250 - 0.500 mm	19.7%
0.5 - 1.0 mm	1.8%
1.0 - 2.0 mm	0.5%
> 2.0 mm	0.3%

The vessel was dredging along a NE-SW track approximately 1400 m in length between locations 506200m E, 85800m N and 507400m E, 86500m N (UTM assumed). Dredging began around 2:25pm on August 19, 1995 and terminated approximately 3 hours and 30 minutes later at 5:55pm. It was unclear as to the start location of the dredger (i.e. did dredging commence against or with the tides). For this study, the location 507400m E, 865000m N was assumed to be the starting point.

10.3.1 Tides and Currents

As part of the objectives defined for the field investigation in 1995, measurements were carried out during a neap tide period when dispersion would be smaller, resulting in higher measurable suspended sediment concentrations. Figure 41 shows the predicted tide levels for August 1995 at Portsmouth (Identifier P008).

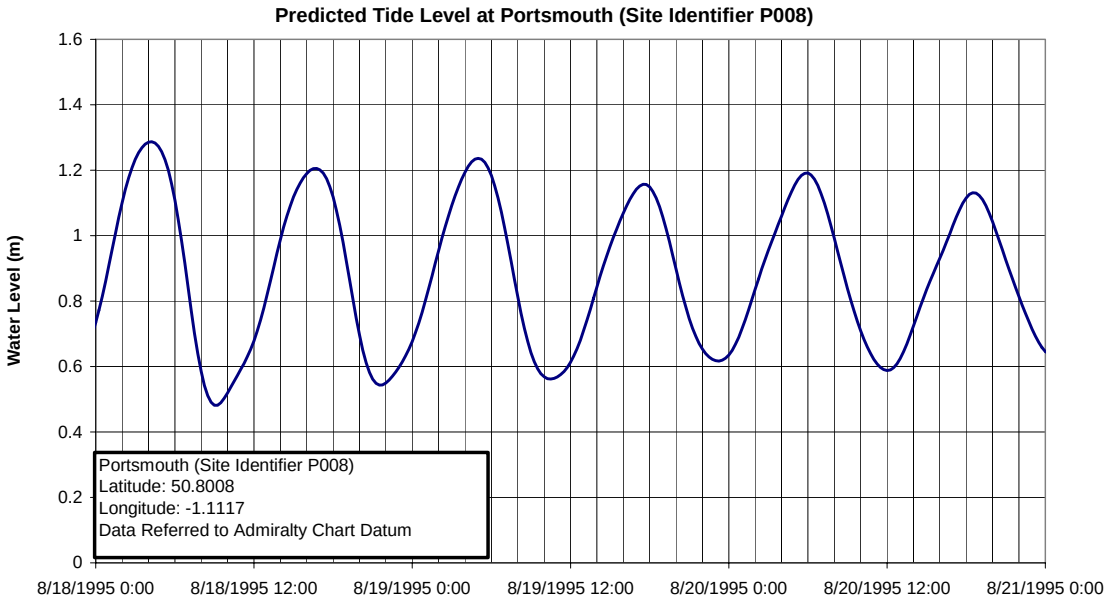

FIGURE 41. Predicted Tide Levels at Portsmouth for August 19, 1995

Numerically modeled tidal currents, including speed and direction, were provided by HR Wallingford for a twelve hour period at location 506698m E, 86306m N (UTM assumed). The time frame provided with the data was in decimal hours from high water without indication as to a specific date or time. It was assumed for this study that these measurements were representative of the coastal conditions on August 19, 1995 where the first high tide period occurred at 5:30 am (see Figure 42).

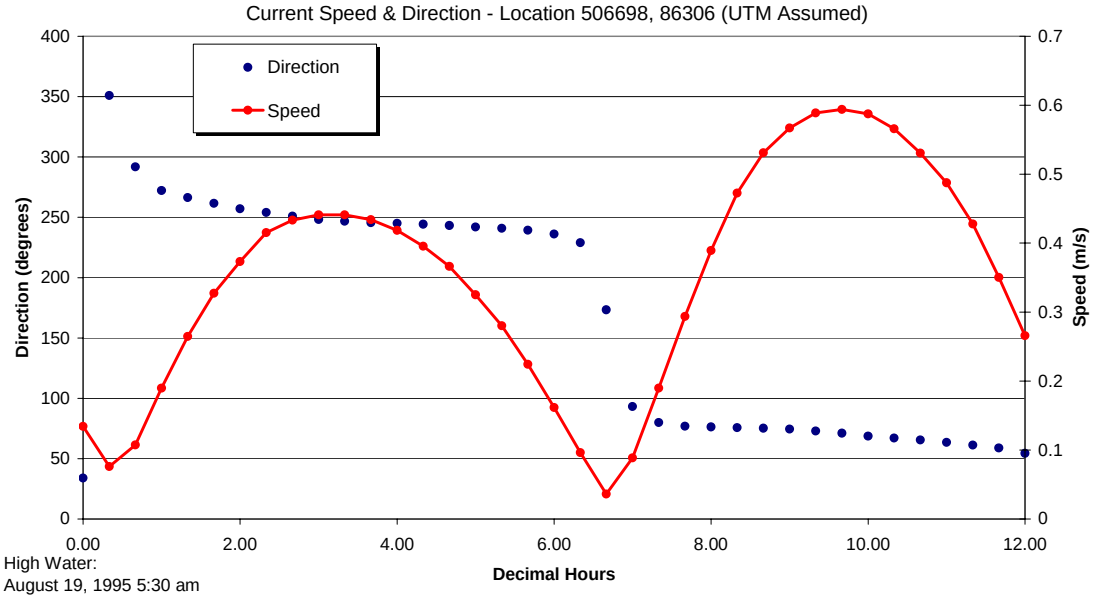

FIGURE 42. Modeled Current Speed and Direction at the Owers Bank Site

10.3.2 Flow Model Setup

Due to the relatively uniform bathymetric features that are evident at the Owers Bank site, the flow model grid was simplified by defining a consistent water depth of 19 m. The 2D hydrodynamic model ADCIRC was utilized to develop a depth averaged current field based on the data discussed in the previous section. These currents were then converted to a three-dimensional flow field by applying a logarithmic velocity profile that was determined based on bed roughness coefficient of 0.05.

10.3.3 MMS Plume Model Setup

Concentration levels of suspended sediment were determined from sampling that was carried out astern of the vessel at various distances and depths, these results were then compared with results generated from the MMS Plume model.

No information regarding mass release rates and overspill flow rates (for various particle sizes) were available on August 19, therefore a detailed comparative analyses would be difficult to carry out. For this study the MMS Plume model was used to simulate the plume dynamics for three grain sizes: 1) Silts (i.e. Particles < 0.063 mm); 2) Very Fine Sand (i.e. Particles = 0.070 mm) and 3) fine sand (i.e. Particles = 0.125 mm). The concentration increases resulting from the release of these different fractions were added together and compared with the observations. Coarser particles were found to be confined to layers very near the bed or to deposit rapidly onto the bed. The purpose was to evaluate the Plume model's response at a basic level and to try to draw any inferences and/or conclusions based on trends observed.

Other key model parameters included a 60 second time step, a simulation period of 210 minutes (i.e. 3.5 hours) and 50 m uniform grid spacing.

10.3.4 Observations and Trends

Table 8 below compares measured data collected on August 19, 1995 with the data generated by the MMS plume model.

TABLE 8 A Comparison of Concentration Levels Measured on August 19, 1995 with Model Results

Distance astern (m)	Water depth (m)	Measured total concentration (mg/l)	Distance astern (m)	Water depth (m)	Predicted total concentration (mg/l)
138	12	1170	175m	18	1100-1300
156	16	1171			
178	18	1346			
194	18	1225			
248	12	582	250m	18	500-1100
259	18	613			
500-700m	0-4 8-12 18	10-46 13-26 18-38	500m	4 10 18	10-35 40-80 70-100

Coastline Surveys (1999) notes that the measurements around 150-200m and 200m-250m were made during the dynamic plume phase while the measurements more than 400m away were more likely to be from the resulting passive plume. The model results displayed have been, therefore, taken from both the dynamic and passive plumes where relevant, although it should be noted that the standard output from the model system is the concentration increases resulting from the passive plume only.

Note that there is considerable uncertainty regarding the direction and speed of the dredger and therefore of the time elapsed between release from the dredger of a sediment "parcel" and the measurement of the same (diluted) sediment parcel at some point later. This is why Table 10.4 presents a wide range of predicted concentration increases.

Based on Table 8, the following observations were noted:

- At the water surface, the measured data showed that concentration levels steeply decrease over the first 300-400m and then become of the order of background conditions with a much slower decline after this point.

- A similar trend was observed for the model results although, notwithstanding the uncertainty about the data, it appears as though the decline in the model prediction of concentration with distance is slower.

The comparisons carried out in this section provide limited information into the model's ability to predict the plume dynamics due to dredging operations within a coastal region, owing to the limited data available about the detail of the field exercise. Having said this exercise provides confidence that the model is reproducing results, which resemble those observed in the field. Limited data required several assumptions to be

made, reducing the likelihood of possibly validating the dredger plume model. It was evident that a simple comparative analysis of model results with available field data was the most ideal approach. It is suggested that for proper validation of the dredger plume model the following field investigations should be carried out simultaneously:

- Detailed measurement of overflow rates and overflow grain size distribution
- The operational efficiency of the draghead should be monitored
- GPS measurement of dredger and survey vessel location over time
- More collection of water samples and use of calibrated ADCP to provide a better assessment of the plume growth for comparison with the model
- Grab samples of the bed using GPS to determine the geographical location of the bed source term

Moreover, it would be ideal for the field program to be carried out under very simple conditions such as constant tidal and current conditions as well as a straight dredger path (i.e. no turning).

HR Wallingford and DRL recently led an international project into the establishment of protocols for trailer hopper suction dredger calibration measurements (HR Wallingford, 2003). It is advised that anyone interested in conducting future measurements of this type inspect these guidelines.

11.0 CONCLUSIONS AND RECOMMENDATIONS

A numerical modeling tool capable of simulating the sedimentation processes associated with a Trailing Suction Hopper Dredger (TSHD) has been developed in this study. This modeling system contains a number of unique features making it far more comprehensive than other models of its type. Unique features include:

- A Process model that reproduces the complete sedimentation processes occurring within a TSHD from sediment uptake to overspill. This model can simulate oversize or undersize screening, as required, and the effects of either Constant Volume or Constant Tonnage systems.

- The ability to simulate plumes created by draghead disturbance.

- A Plume model that can simulate three distinct phases of the overspill sedimentation phases:

    - The Dynamic Phase in which the overspill descends through the water column as a density plume.

    - The Passive Phase in which the plume is advected and dispersed through the ambient waters.

    - The Bed Re-suspension Phase in which sediment already deposited on the bed may become re-suspended by the ambient currents.

- Dredgers are simulated along user-defined pathways which may be linear or variable in speed and direction.

- The model allows for the simulation of multiple releases from multiple dredgers (as well as incorporating the facility for multiple additional point source releases).

- Linkages to the widely-used ADCIRC hydrodynamic model supported by the U.S. Army Corps of Engineers as well as the TELEMAC system developed by LNHE in France. The model interfaces have been prepared in such a way that the model can be readily adapted to many other types of hydrodynamic models in the future.

- Development of a Graphical User Interface which facilitates use of the model and binds together the various model modules.

- Creation of a tool for three-dimensional, animated displays of the plume model, to aid in use and interpretation of the model results.

The ability to properly simulate all of the plume sedimentation phases is a unique characteristic of the MMS Plume Model not found in any of the currently available models in use.

A large series of sensitivity and validation tests were performed on the Dynamic Plume model to assess its behavior and confirm its accuracy. Excellent agreement was achieved with available laboratory test results.

An extensive sensitivity testing program was conducted to evaluate the variation in the sediment footprint predicted by the model when key parameters were varied. The model results largely conformed to the anticipated results for the various tests that were performed.

An attempt was made to validate the MMS Plume Model against measured data from the Owers Bank 1995 field campaign. Reasonable comparisons could be achieved for the TSHD Process model; however, comparisons of suspended sediment concentrations proved difficult to achieve due to limitations in the available datasets. The model validation process showed the importance of collecting simultaneous datasets that include grain size sampling of the overspill, continuous measurements of overspill flow rates and grain size sampling of suspended sediment samples. It is recommended that for proper validation of the dredger plume model, the following field investigations be carried out simultaneously:

- Detailed measurement of overflow rates and overflow grain size distribution.
- The operational efficiency of the draghead should be monitored.
- GPS measurement of dredger and survey vessel location over time.
- Collection of water samples and use of calibrated ADCP to provide a better assessment of the plume growth for comparison with the model.
- Grab samples of the bed using GPS to determine the geographical location of the bed source term.

Future enhancements to the MMS plume model could include:

- The ability to simulate multiple grain sizes simultaneously. Presently, the passive dispersion model is limited to a single grain size fraction.
- The ability to account for various inefficiencies in the dredging process.
- The ability to address bed slope effects during bed collapse of the dynamic plume. This effect can be important when assessing dredge plume effects at locations with steep bed slopes.
- The Plume Animator Software for three-dimensional display of results can be significantly enhanced with tools to allow detailed querying of results.

12.0 REFERENCES

Alavian, V., 1986. Behavior of density currents on an Incline. Journal of Hydraulic Engineering, 112, 1.

Akar, P.J. and G.H. Jirka, 1994. Buoyant spreading processes in Pollutant Transport and Mixing, Part 1: Lateral spreading with Ambient Current Advection, Journal of Hydraulic Research, 32, 6.

Bonnecaze, R.T., H.E. Huppert, and J.R. Lister, 1996. Patterns of Sedimentation from polydispersed turbidity currents, Proceedings of the Royal Society of London, 452: 2247-2261.

Brandsma M.G. and D.J. Divoky, 1976. Development of models for prediction of short-term fate of dredged material discharged in the estuarine environment, Contract Report D-76-5, US Army Engineer Waterways Experiment Station, Vicksburg, MS, prepared by Tetra Tech, Inc., Pasadena, CA.

Camp T.R. 1946, Sedimentation and the design of settling tanks, ASCE Trans p. 895.

Coastline Surveys Ltd., 1999. Marine Aggregate Mining Benthic and Surface Plume Study. Report to U.S. Department of the Interior, Minerals Management Service.

Chu, V.H., and M. B. Goldberg, 1974. Buoyant Forced Plumes in a Cross Flow. J. Hydraulic Div., ASCE, 100: 1203-1214.

Chu, V.H., 1975. Turbulent Dense Plumes in a Laminar Cross Flow. Journal of Hydraulic Research, 13, 3.

Dearnaley M.P., 1996. Direct measurements of settling velocities in the Owen Tube: A comparison with gravimetric analysis, Journal of Sea Research, 36, September 1996: 41-47.

Dimou K.N. and E.E. Adams, 1993, A random-walk particle tracking model for well-mixed Estuaries and Coastal waters, Estuarine, Coastal and Shelf Science, 37: 99-110.

Dyer K.R., A.J. Bale, M.C. Christie, N. Feates, S. Jones, and A.J. Manning 2000. The turbidity maximum in a mesotidal estuary, The Tamar Estuary, UK: II. The floc properties, *In* Fine Sediment Dynamics in the Marine Environment, Proceedings of Marine Science 5,Winterwerp J.C. and C. Kranenburg (Eds), pp.219-232, Elsevier.

Eisma D., A.J. Bake, M.P. Dearnaley, M.J. Fennessy, W. Van Leussen, M.A. Maldiney, A. Pfeiffer, and J.T. Wells, 1996. Intercomparison of in situ suspended matter (floc) size measurements, Netherlands Journal of Sea Research, 36: 3-14.

Fischer H.B., E.J. List, R.C.Y. Koh, J. Imberger, and N.H. Brooks, 1979. Mixing in Inland and Coastal Waters. Academic, New York, 483 pp.

Frick W.E., 1984. Non-empirical closure of the plume equations, Atmospheric Environment, 18, 4: 653-662.

Hallworth M.A., A.J. Hogg, H.E. Huppert, 1998. Effects of external flow on compositional and particle gravity currents, Journal Fluid Mechanics, 359: 109-142.

Hoerner S.F., 1965. Fluid-dynamic drag, Practical information on aerodynamic drag and hydrodynamic resistance, Published by the Author.

Hogg A.J. and A.W. Woods, 2001. The transition from inertia- to bottom-drag-dominated motion of turbulent gravity currents, Journal of fluid mechanics, 449: 201-224.

HR Wallingford, 1996. Dispersion Studies at Ower's Bank. Report EX 3335. February 1996.

HR Wallingford, 1991. Port and Airport Development Strategy - Enhancement of the WAHMO Mathematical Models. Testing of the North West New Territories Coastal Waters Mud Transport Model for Storm Wave Conditions in the Wet Season. Report EX 2267, January 1991.

HR Wallingford, 2003. Protocol for the Field Measurement of Sediment Release from Dredgers. Report produced by HR Wallingford and Dredging Research Ltd. for Vereniging van Waterbouwers in Bagger-Kust en Oeverwerken (VBKO), Issue 1, August.

Jirka G.H., 1999. Five aymptotic regimes of a round buoyant jet in stratified crossflow, XXVII IAHR Congress Proceedings, Graz.

Johnson B,H,, D.N. McComas, D.C. McVan, and M.J. Trawle, 1993. Development and verification of numerical models for predicting the initial fate of dredged material disposed in open water, Report 1: Physical model tests of dredged material disposal from a split-hull barge and a multiple bin vessel, Dredging Research Program Technical Report DRP-93-1, Waterways Experiment Station, US Army Corps of Engineers, Vicksburg, Mississippi, USA.

Koh R.C.Y. and Y.C. Chang, 1973. Mathematical model for barged ocean disposal of waste, Technical Series EPA 660/2-73-029, US Environment Protection Agency, Washington D.C., December 1973.

Land J. and R.N. Bray, 1998. Acoustic measurement of suspended solids for monitoring of dredging and dredged material disposal, Proceedings of the 15th World Dredging Congress, June 28 to July 2, Las Vegas, USA, 1: 105-120.

Lee J.H.W and V. Cheung, 1990. Generalized lagrangian model for Buoyant Jets in Current, Journal of Environmental Engineering, 116, 6, November/December 1990.

Legg B.J. and M.R. Raupach, 1982. Markov-chain simulation of particle dispersion in inhomogeneous flows: the mean drift velocity induced in a gradient in Eulerian velocity variance, Boundary Layer Meteorology, 24: 3-13.

Leuttich, R.A. and J.J. Westerink, 2003. Formulation and Numerical Implementation of the 2D/3D ADCIRC Finite Element Model Version 43.XX. Online Document: http://www.marine.unc.edu/C_CATS/adcirc/adcirc.htm.

Leuttich, R.A. and J.J. Westerink, 2000. ADCIRC: An ADvanced CIRCulation Model for Oceanic, Coastal and Estuarine Waters. Online Document: http://www.marine.unc.edu/C_CATS/adcirc/adcirc.htm.

Mukai A.Y., J.J. Westerink, R.A. Luettich Jr., and D. Mark, 2002. Eastcoast 2001: A tidal constituent database for the western North Atlantic, Gulf of Mexico and Caribbean Sea, US Army Engineer Research and Development Center, Coastal and Hydraulics Laboratory, Technical Report, ERDC/CHL TR-02-24, September 2002, 201pp.

Maxworthy T., J. Leilich, J.E. Simpson, and E.H. Meiburg, 2002. The propagation of a gravity current into a linearly stratified fluid, Journal of Fluid Mechanics, 453: 371-394.

Monin A.S. and A.M. Yaglom, 1971. Statistical Fluid Mechanics, MIT Press, Cambridge, Massachusetts.

Odd N.V.M. and J.G. Rodger, 1978. Vertical Mixing in Stratified Tidal Flows, Journal of the Hydraulics Division, ASCE, 104, HY3: 337-351.

Prych, E.A., 1970. Effects of Density Differences on Lateral Mixing in Open Channel Flows. Report No. KH-R-21. California Institute of Technology. Pasadena, California.

Rottman J.W. and J.E. Simpson, 1983. Gravity currents produced by instantaneous releases of a heavy fluid in a rectangular channel, Journal of fluid mechanics, 135: 95-110.

Schatzmann, M., 1979. An Integral Model of Plume Rise. Atmos. Environ., 13: 721–731.

Schatzmann, M., 1981. Mathematical modeling of submerged discharges into coastal waters, Proc. 19th IAHR Congress, New Delhi, 3: 239-246.

Schiller E.J. and W.W. Sayre, 1973. Vertical Mixing of Heated Effluents in Open-channel Flow. Iowa Institute of Hydraulic Research. Report No. 148.

Soulsby R.L., and R.J.S. Whitehouse, 1997. Threshold of sediment motion in coastal environments. Proceedings of Pacific Coasts and Ports '97 Conference, Centre for Advanced Engineering, Christchurch, NZ, pp. 149-154.

Soulsby R.L., 1997. Dynamics of Marine Sands. Thomas Telford, London. ISBN 0 7277 2584 X.

Tompson A.F.B. and L.W. Gelhar L.W., 1990. Numerical simulation of solute transport in three-dimensional randomly heterogeneous porous media, Water Resources Research, 26, October 1990: 2541-2562.

Turner, J.S., 1973. Buoyancy Effects in Fluids. Cambridge University Press, London.

Wright S.J., 1984. Buoyant jets in density-stratified crossflow, Journal Hydraulic Engineering, 110, 5, May 1984: 643.

Vasbloom W.J. and S.A. Miedema S.A., 1995. A theory of determining sedimentation and overflow losses in hoppers, Proc. WODCON XIV, Amsterdam.

13.0 NOTATION

Vessel Characteristics

B = hopper width, m
B_d = width of draghead, m
D_b = bow thrust propeller diameter, mm
D_p = main propeller diameter, mm
D_s = diameter of suction pipe(s), m
D_{wt} = deadweight of vessel, t
f_b = buoyancy factor, m/t
H_h = depth of water in hopper above settled material, m
H_o = notional hopper depth, m
h = depth of draghead immersion, m
L = hopper length, m
L_d = length of draghead, m
P_b = power on bow thrust, kW
P_t = power on main engines, kW
T_h = maximum tonnage in hopper, t
v_{dr} = speed of raising and lowering draghead, m/s
V_h = hopper capacity, m^3
Z_{vo} = light draft, m

Site Characteristics

ρ = dry density in upper sea bed, kg/m^3
ν = water kinematic viscosity, m^2/s
γ_n = average *in situ* density, Mg/m^3
γ_s = particle density, Mg/m^3
γ_u = average density of upper sea bed, Mg/m^3
γ_w = water density, Mg/m^3
d = particle diameter, microns
DI = soil disaggregation index
L = length of trail run, m
Z_o = dredging depth, m

Operating Characteristics

γ_a = LMOB density setting, Mg/m^3
γ_h = density of material settled in hopper, Mg/m^3
γ_m = mixture density, Mg/m^3
h = depth of draghead immersion, m
K = trailing speed, knots
S = number of suction pipes in use

t_c = time to sail to disposal, dispose and return to dredging site, min
t_t = turning time, min
V_p = pre-load volume of water in hopper, m^3
v_s = velocity in suction pipe, m/s

Computational Symbols

T_o = bed shear stress, N/m
C_v = volumetric concentration of mixture entering hopper
f_{dr} = draghead factor
f_h = hindrance factor
f_s = scour area factor
g = acceleratioin due to gravity, m/s^2
n = number of complete trail runs
Q = mixture flow into hopper, m^3/min
r_h = hindered settling efficiency
t_a = period of operation of LMOB, min
t_f = time to fill hopper, min
t_o = time from start until overflow begins, min
t_p = time loading during last trail run, min
t_r = trailing run time, min
U_{bo} = velocity of bow thrust propeller stream
U_{max} = maximum jet velocity at sea bed, m/s
U_{po} = velocity of main propeller stream, m/s
v = standard settling velocity, m/s
v_{en} = critical erosional velocity below upper layers, m/s
v_{eu} = critical erosional velocity in upper layers, m/s
v_h = hindered settling velocity, m/s
W_a = total LMOB solids discharged, kg
W_m = weight of solids entering hopper, t/min
W_s = total load of solids in hopper, t
W_{s1} = weight of solids in hopper at time increment 1, t
W_w = weight of water entering hopper, t/min
W_{w1} = weight of water in hopper at time increment 1, t
Z_{bs} = distance from propeller axis to sea bed (bow thrust)
Z_I = depth of zone of influence, m
Z_{ps} = distance from propeller axis to sea bed (main propeller), m
Z_u = underkeel clearance, m

Oversize Screening

α_o = Screen angle with horizontal (rising in the direction of flow), degrees
a_o = Screen length, m
b_o = Screen width, m
r_o = Ratio of void to total area
S_o = Aperture size, micron

Undersize Screening

α_u = Screen angle with horizontal (rising in the direction of flow), degrees
a_u = Screen length, m
b_u = Screen width, m
r_u = Ratio of void to total area
S_u = Aperture size, micron

Screening Model Variables

C_o = Mixture loss constant (oversize)
C_u = Mixture loss constant (undersize)
Q_m = Mixture flow, m^3/s
V_m = Mixture velocity, m/s
W = Size index
x = Fraction index
y = Flow index
z = Density index

Screening Computational Variables

γ_o = Density of mixture after oversize screening, Mg/m^3
γ_u = Density of mixture after undersize screening, Mg/m^3
d_{m1} = % of size d_1 material in mixture
d_1% = Percentage of material of size d_1 remaining in stream as a % of the total stream
I_{o1}%= Percentage of in-situ material coming up the suction pipe
I_u% =
m_o = Fraction of material larger than the oversize screen size
m_u = Fraction of material larger than the under size screen
Q_o = Mixture flow after oversize screening, m^3/s
O_1%= Percentage of material of size d_1 rejected by oversize or undersize screen
Q_u = Mixture flow after undersize screening, m^3/s
W_o = Mixture loss in oversize screen, m^3/s
W_o%= Percentage mixture loss in oversize screen
W_u = Mixture loss in undersize screen, m^3/s
W_u%= Percentage mixture loss in undersize screen

Plume Model Notation

ρ_{amb} = density of ambient fluid
ρ_k = plume density at time step, k
$\Delta\rho_k$ = difference in density between plume and the ambient fluid
ρ_{part} = density of particulate plume
ϕ_k = angle of plume path with the horizontal plane
θ_k = angle of plume path with the ambient current plane projected onto the horizontal
φ_{i0} = initial volume of ith sediment fraction expressed as proportion of A
Δ_{sk} =
A = initial cross – sectional area of plume (equal to $l_0 h_0$)
β_i =
b_k = plume radius at time step, k
C = concentration of sediment fraction
C_d = friction coefficient
d = particle diameter
D_* = dimensionless particle size
g' = gravital acceleration modified for buoyancy
E = entrainment coefficient
F = local densimetric Froude number
h_f = thickness of the density current
h_k = plume thickness at time step, k
κ = Von Karman constant of 0.4
l_b = buoyancy length scale
l_f = density current length
M_k = plume mass at time step, k
ΔM_s = increase in plume mass
R_f = Richardson Flux number
t = time
Δt = time step
$\underline{u}_{ambient}$ = Ambient Currents
$\underline{u}_{dredge}$ = Dredger Velocity
u_f = speed of propogation of density current
w_s = particle settling velocity
$\underline{x}$ = Cartesian Coordinate System
x' = Coordinate System moving with the Dredger
x_f = density current travel distance